PERFORMANCE EVALUATION AND CFD ANALYSIS OF A POSITIVE DISPLACEMENT DIAPHRAGM PUMP

A THESIS SUBMITTED TO
THE GRADUATE SCHOOL OF NATURAL AND APPLIED SCIENCES
OF
MIDDLE EAST TECHNICAL UNIVERSITY

BY

GÖKAY GÖKÇE

IN PARTIAL FULFILLMENT OF THE REQUIREMENTS
FOR
THE DEGREE OF MASTER OF SCIENCE
IN
MECHANICAL ENGINEERING

SEPTEMBER 2011

Approval of the Thesis:

PERFORMANCE EVALUATION AND CFD ANALYSIS OF A POSITIVE DISPLACEMENT DIAPHRAGM PUMP

submitted by **GÖKAY GÖKÇE** in partial fulfillment of the requirements for the degree of **Master of Science in Mechanical Engineering Department, Middle East Technical University** by,

Prof. Dr. Canan Özgen
Dean, Graduate School of **Natural and Applied Sciences** _____

Prof. Dr. Süha Oral
Head of Department, **Mechanical Engineering** _____

Prof. Dr. Kahraman Albayrak
Supervisor, **Mechanical Engineering Dept., METU** _____

Dr. Serkan Kayılı
Co-Supervisor, **Mechanical Engineering Dept., METU** _____

Examining Committee Members:

Prof. Dr. Haluk Aksel
Mechanical Engineering Dept., METU _____

Prof. Dr. Kahraman Albayrak
Mechanical Engineering Dept., METU _____

Assist. Prof. Dr. M. Metin Yavuz
Mechanical Engineering Dept., METU _____

Dr. Serkan Kayılı
Mechanical Engineering Dept., METU _____

Dr. Ertuğrul Başeşme,
General Manager, Punto Engineering _____

Date: 13.09.2011

I hereby declare that all information in this document has been obtained and presented in accordance with academic rules and ethical conduct. I also declare that, as required by these rules and conduct, I have fully cited and referenced all material and results that are not original to this work.

Name, Last name: Gökay Gökçe

Signature:

ABSTRACT

"PERFORMANCE EVALUATION AND CFD ANALYSIS OF A POSITIVE DISPLACEMENT DIAPHRAGM PUMP"

Gökçe, Gökay
M.Sc., Department of Mechanical Engineering
Supervisor: Prof. Dr. Kahraman Albayrak
September 2011, 102 Pages

In order to understand flow characteristics inside a positive displacement pump, every point in the flow field must be carefully observed. Such observations are difficult, expensive and usually time consuming to achieve with physical testing. During tests one can observe flow characteristics only at the locations where the instrument device is attached, not the whole flow domain.

This thesis mainly focuses on the evaluation of design and performance characteristics of a positive displacement triplex diaphragm pump. For this purpose not only numerical investigations but also experimental studies were conducted using a positive displacement pump which is supplied by the pump manufacturer and is available in the fluid mechanics laboratory of Middle East Technical University.

The effect of valve characteristics on the pump efficiency such as valve spring stiffness, valve displacement, mass of the check valves, and diaphragm shape are investigated in this thesis by using CFD (Computational Fluid Dynamics) technique. The pump performance is analyzed in terms of its volumetric and hydraulic efficiencies. The effect of the valve closure delay is also discussed.

After the CFD and experimental results of the current pump model are compared and it is seen that they are in close agreement with each other, parametric studies are performed in computer environment. From analysis results it is observed that using stiffer springs reduces valve closing time and tend to decrease flow reversal effects. Secondly, using heavier check valves increases valve closing and opening times and also increases the stresses on the components of the pump with the increased pressure drop through discharge valve. As a result of this condition, hydraulic and volumetric efficiency reduce. Thirdly, with the longer valve displacement arrangement, more time is required for opening and closing of the check valves therefore efficiency of the pump reduces.

Keywords: Diaphragm pump, CFD analysis, pump performance tests, flow ripple.

ÖZ

"POZİTİF DEPLASMANLI DİYAFRAM POMPA PERFORMANSININ HAD ANALİZLERİYLE BELİRLENMESİ"

Gökçe, Gökay
Yüksek Lisans, Makina Mühendisliği Bölümü
Tez Yöneticisi: Prof. Dr. Kahraman Albayrak
Eylül 2011, 102 Sayfa

Pozitif deplasmanlı pompa içi akış yapısını anlamak için, akış alanı içindeki her nokta detaylı olarak gözlemlenmelidir. Bu gözlemlemelerin deneysel metodlarla yapılması çoğu zaman zor, pahalı ve uzun süreli olmaktadır. Ayrıca deneysel metodlarla akış olaylarının bütünü görülememekte, sadece ölçüm yapılan noktalardaki parametreler belirlenebilmektedir.

Bu tez çalışması pozitif deplasmanlı üç silindirli bir diyafram pompanın tasarım ve performans karakteristiğinin belirlenmesine odaklanmaktadır. Bu amaçla bir pompa imalatçısı tarafından sağlanan pompa modeli üzerinde ODTÜ akışkanlar mekaniği laboratuarında deneysel ve nümerik çalışmalar yapılmıştır.

Çalışma kapsamında kontol valflerinde kullanılan yayların sertliği, kontrol valflerinin deplasmanı, valflerin kütleleri gibi valf karakteristiklerinin ve diyafram şeklinin verim üzerindeki etkisi HAD (Hesaplamalı Akışkanlar Dinamiği) yöntemiyle incelenmiştir. Pompa performansı hacimsel ve hidrolik verimler cinsinden ifade edilmiştir. Ayrıca valflerin kapanma sürelerindeki gecikmelerin etkisi de bu çalışmada incelenmiştir.

Deney sonucunda elde edilen sonuçlar ile HAD analizleri sonunda elde edilen sonuçlar karşılaştırılıp, bunların birbiriyle uyum içinde olduğu gözlemlendikten

sonra bilgisayar ortamında parametrik çalışmalar yapılmıştır. Parametrik çalışmaların sonuçlarından sert yayların kullanılmasıyla kontrol valflerinin kapanma sürelerinin dolayısıyla valflerde gerçekleşen ters akışların azaldığı görülmektedir. Kontrol valflerinin kütleleri arttıkça, valf açılma ve kapanma sürelerinin arttığı ayrıca pompa elemanları üzerindeki gerilmelerin ve valf boyunca gerçekleşen basınç kaybının arttığı, buna bağlı olarak pompanın hidrolik ve hacimsel veriminin düştüğü tesbit edilmiştir. Valf deplasmanının artırılmasının yine valflerin açılma ve kapanma sürelerini olumsuz yönde etkilediği ve buna bağlı olarak pompa veriminin düştüğü gözlemlenmiştir.

Anahtar Kelimeler: Diyafram pompa, HAD analizleri, pompa performans testleri, akış dalgalanması

To My Mother

ACKNOWLEDGMENTS

I express my deepest gratitude to my supervisor Prof. Dr. Kahraman Albayrak for his guidance, advice, criticism, encouragements and insight throughout the research. Working with him has been an enjoyable, unique and valuable learning experience.

I would like to thank to Dr. Ertuğrul Başeşme for his motivation and encouragement. Dr. Başeşme is the one who truly made a difference in my life. It was under his tutelage that I developed a focus and became interested in computational fluid dynamics. He provided me with direction, technical support and became more of a mentor than a teacher. With his persistence, understanding and kindness I completed my graduate degree. I doubt that I will ever be able to convey my appreciation fully, but I owe him my eternal gratitude.

I would like to thank to Dr. Serkan Kayılı for his assistance in writing thesis, answering my questions and his valuable comments throughout my graduate program. In critical times, his assistance helped me along the way. Also thanks to Şahika Pulur for her support and help during the experiments.

I would also like to thank my friend Emrah Erden for our engineering debates and exchange of knowledge during the graduate program. Also thanks to Mahmut M. Göçmen and Enis Dönmez for their motivation before MS jury presentation.

Finally, I would like to thank my mother for the support she provided me through my entire life.

TABLE OF CONTENTS

LIST OF TABLES

TABLES

LIST OF FIGURES

FIGURES

LIST OF SYMBOLS

d	valve displacement (mm)
d_i	pipe inside diameter (mm)
d_o	pipe outside diameter (mm)
E	Young's modulus of elasticity of the pipe (N/m^2)
F	force (N)
g	gravitational acceleration (m/s^2)
k	spring stiffness (N/cm)
l	connecting rod length (mm)
L	pipe length (m)
m	mass (kg)
n	rotational speed of the pump (rpm)
p	pressure (Pa)
P	power (W)
Q	volume flow rate (m^3/s)
r	crank radius (mm)
t_r	reflection time (s)
T	torque (Nm)
u	x-component of velocity (m/s)
v	y-component of velocity (m/s)
V	velocity of the piston (m/s)
w	z-component of velocity (m/s)
x	piston displacement (mm)
a	acoustic speed (m/s)

β	ratio of crank radius to connecting rod length
Δp	pressure difference (Pa)
η	overall efficiency of the pump
η_h	hydraulic efficiency of the pump
η_m	mechanical efficiency of the pump
η_v	volumetric efficiency of the pump
θ	crank angle (degree)
ρ	density (kg/m^3)
τ	time required for one stroke (s)
ω	angular velocity (rad/s)

CHAPTER 1

INTRODUCTION

According to research done by Hydraulic Institute [1], pumping systems consume nearly 20 % of the world's electrical energy and between 25-50 % of the energy usage in certain industrial plant operations. Pumping systems are commonly used in industry; they provide domestic services, commercial and agricultural services, municipal water/waste water services and industrial services for food processing, chemical, petro-chemical and many other mechanical industries. The energy and materials used by a system depend on the design of the pump, the design of the installation and the way of the system is operated. These factors are related with each other. Moreover, they should be matched to each other and must work on operating conditions to ensure the lowest energy and maintenance costs, longer equipment life, and other benefits. The initial purchase cost of a pump is small for high usage pumps as compared with the operating costs [2]. Understanding the operating principles of all the components in the pump and how they affect each other will provide an opportunity to reduce energy, operational and maintenance costs.

In order to increase the efficiency of a positive displacement pump, flow characteristics inside the pump must be carefully observed. Such observations are difficult, expensive and time consuming to achieve with physical testing. So, after experimental procedure is applied to a current pump model, parametric studies (numerical experiments) are done in computer environment using commercial CFD code known as Autodesk Simulation CFD v2012.

The theory of the thesis which covers positive displacement pumps especially diaphragm pumps. Their main components and operating principles, sources of pressure pulsations and literature survey are mentioned in this chapter.

The experimental set-up and instrumentation, CFD analysis of the pump, results and conclusion are given in the following chapters.

1.1 Positive Displacement Pumps

Positive displacement pumps can be divided into two main categories as;

- Rotary pumps
- Reciprocating pumps.

Rotary pumps transfer liquids with the help of the rotating pump elements [3]. This rotation creates a vacuum that draws fluid into its casing. These pumps are easy to design and can be very effective for many applications. They are also used with viscous fluids but the pump should be operated at lower speeds to achieve higher efficiencies. Unlike centrifugal pumps, rotary positive displacement pumps provide a flow that is not affected by the pressure head of the system. So, in applications where large pressure differences occur between the inlet and outlet of the system, these pumps should be preferred.

In reciprocating pumps (given in figure 1.1), check valves are placed to the suction and discharge sides. Fluid is expelled into the cylinder through the suction valve by the plunger, piston or diaphragm. At the end of the stroke, when the suction valve closes the plunger moves forward into the cylinder, forcing the fluid to flow out through discharge valve.

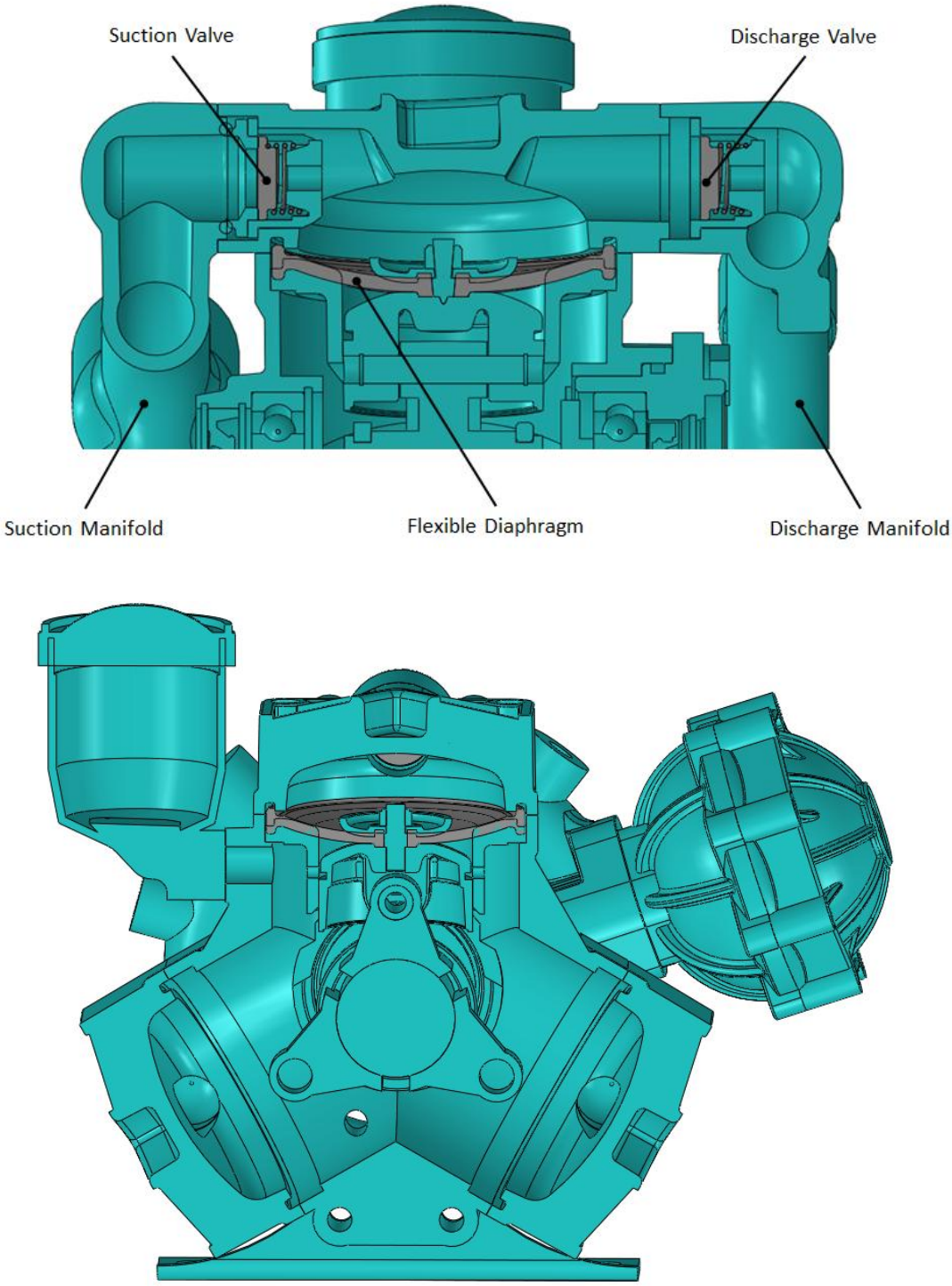

Figure 1.1 Components of Reciprocating Pump

A positive displacement pump produces the same flow rate at the specific rotational speed independent from the discharge pressure. These pumps cannot be operated against a closed valve on the discharge side of the pump, unlike centrifugal pumps. If the discharge is closed, pump will continue to produce flow until the pressure in

the discharge line bursts or the pump is damaged. For this reason relief valve can be used to avoid this type of problems.

In reciprocating design there is always a small amount of leakage in the pump. That leakage is caused by the movement of the check valves (non-return valves), the small amount of back (reverse) flow that occurs before a check valve closes. In piston operated pumps (unlike the diaphragm operated pumps) there is a negligible leakage through the piston. Because of this phenomenon, the characteristic curve of real pump is different from the ideal one. At the high pump head the volume flow rate of the pump does not remain constant. Actually, it decreases. The flow rate at which liquid leaks from the pump discharge to its suction is called slippage [4]. The system curve of a positive displacement pump is shown in figure 1.2.

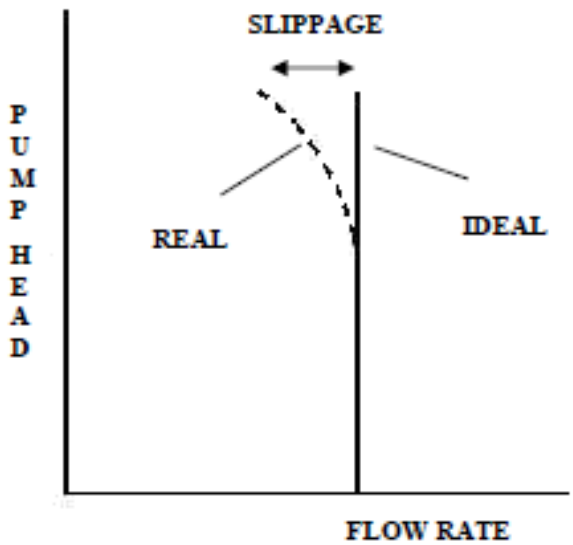

Figure 1.2 Positive Displacement Pump Characteristics [4]

1.1.1 Main Components of a Positive Displacement Pump

In this section, the main components that are used in analysis of a positive displacement pump are given.

Suction manifold or inlet manifold is the part of a pump that supplies fluid to the cylinders.

Discharge manifold is the part of a system that collects the fluid from multiple cylinders into the discharge pipe. In figure 1.3 the manifold of a sample pump is shown.

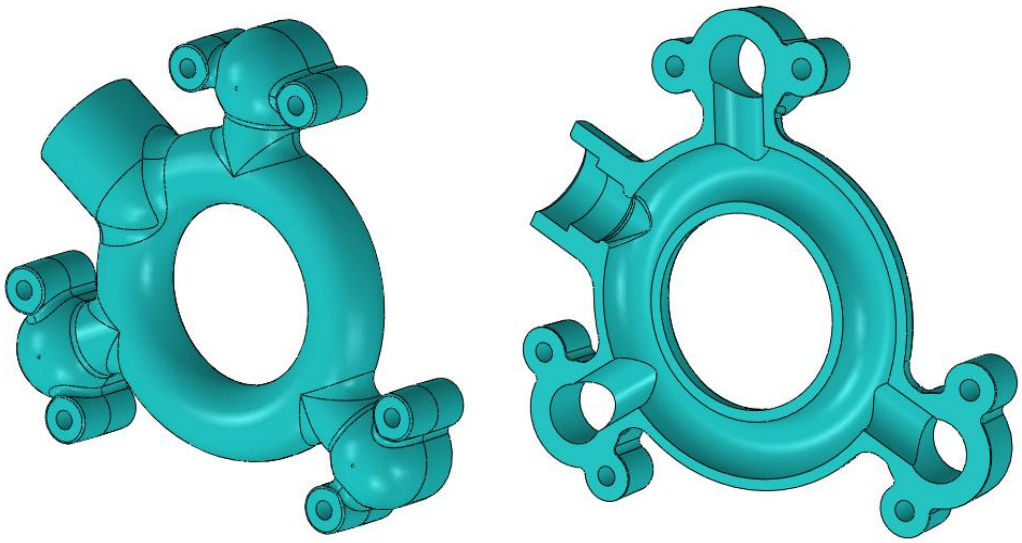

Figure 1.3 Suction Manifold

Check valves (non-return valves) are installed to a positive displacement pump in order to prevent back flow of fluid. There are different types of valves available in industry. Such as swing type, ball type etc. [5]

Working principle of a check valve is quite simple; the pressure on upstream of the valves tend to open them, and fluid flow forces hold the valves open, when that pressure reduces, valves start to close because of the spring force. (Figure 1.4)

There is finite time required for closing process. As a result of this phenomenon always certain amount of leakage (backflow) exists through the valves.

This leakage becomes important especially at high flow rates; the valve is closed by the spring, the spring applies a force to the valve and valve accelerates proportional to its mass. At high speeds there is insufficient time for valve to close unless stronger spring is attached [6]. Stronger springs reduce the closing time of check valves. But stronger springs bring some disadvantages to a system. When stronger spring is attached to the system large pressure drop through the check valves may be observed. And sudden closure can cause large pressure surges

downstream of the valves. This pressure surges may damage to the hydraulic equipment in the system [7]. (Water hammer effect)

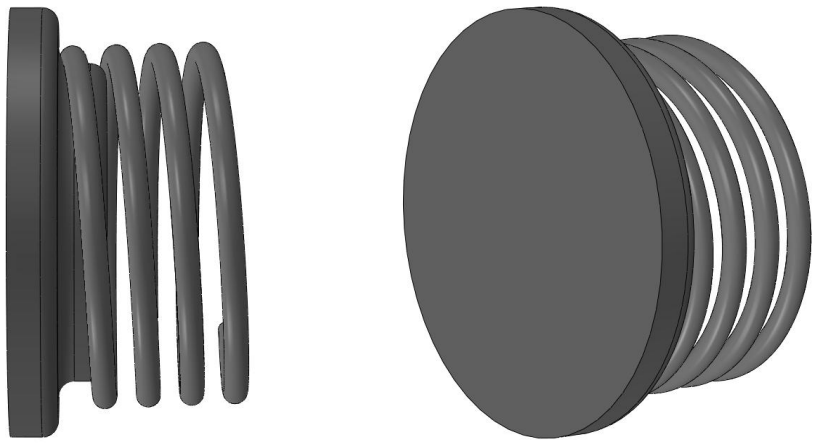

Figure 1.4 Check Valve

Due to the reasons that are mentioned above check valves must be designed and selected carefully.

In reciprocating pumps, piston or diaphragm is doing harmonic motion. They are driven by a rotating crank and connecting rod so that flow is in a pulsating regime [8].

To better understand the kinematics of reciprocating pump, the schematic diagram of the piston elements are in figure 1.5, where crank radius is “r”, crank angle is “θ”, connecting rod length is “l” and displacement of the piston is “x”.

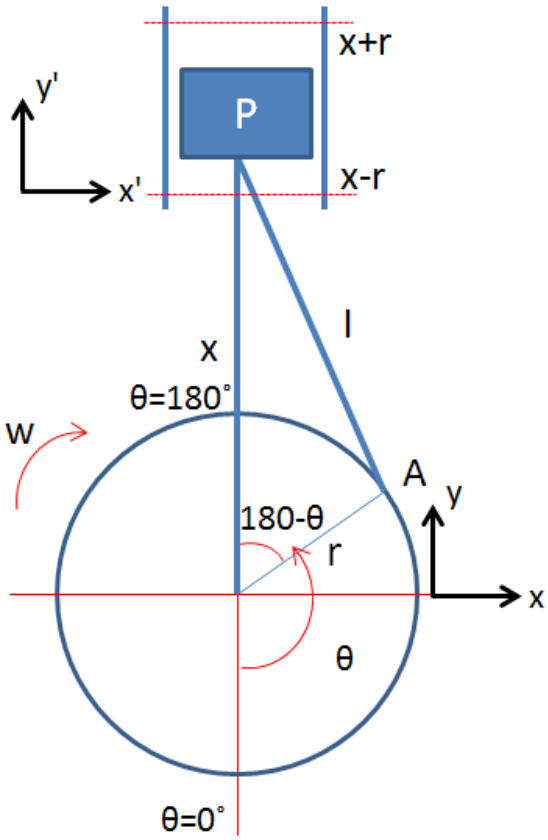

Figure 1.5 Piston Displacement

Using Cosine theorem for $\widehat{POA}$,

$$l^2 = r^2 + x^2 - 2xrcos(180 - \theta) \tag{1.1}$$

Where, $cos(180 - \theta) = -cos\theta$ (1.2)

Adding, $r^2[(cos^2\theta + sin^2\theta) - 1]$ to right side of the equation 1.1 and re-arranging the terms,

$$l^2 - r^2 = x^2 + 2xr\cos\theta + r^2[(cos^2\theta + sin^2\theta) - 1] \tag{1.3}$$

$$l^2 - r^2 + r^2 - r^2sin^2\theta = x^2 + 2xr\cos\theta + r^2cos^2\theta \tag{1.4}$$

$$l^2 - r^2sin^2\theta = (x + rcos\theta)^2 \tag{1.5}$$

$$x = -rcos\theta + \sqrt{l^2 - r^2sin^2\theta} \tag{1.6}$$

In order to transform coordinate axis from xy to x'y' "r-l" must be added to right hand side of the equation. Then equation 1.6 becomes,

$$x = -l + r\,(1 - cos\theta) + \sqrt{l^2 - r^2 sin^2\theta} \tag{1.7}$$

Introducing dimensionless parameter β,

$$\beta = \frac{r}{l}$$

Writing equation 1.7 in terms of β,

$$x = r\,(1 - cos\theta) + l(-1 + \sqrt{1 - \beta^2 sin^2\theta}) \tag{1.8}$$

Similarly, the velocity of the piston can be formulated by taking the derivative of position with respect to time.

$$V = \frac{dx}{dt} = \frac{dx}{d\theta} x \frac{d\theta}{dt} \tag{1.9}$$

Where $\frac{d\theta}{dt}$ is the angular velocity ω (rad/s)

$$V = \omega r\left(\sin(\theta) - \frac{\beta \sin(\theta)\cos(\theta)}{\sqrt{1 - \beta^2 sin^2\theta}}\right) \tag{1.10}$$

Because of the triplex pump arrangement there is a constant phase shift between the pistons (120˚). In figure 1.6 piston displacement versus crank angle and piston velocity versus crank angle are shown.

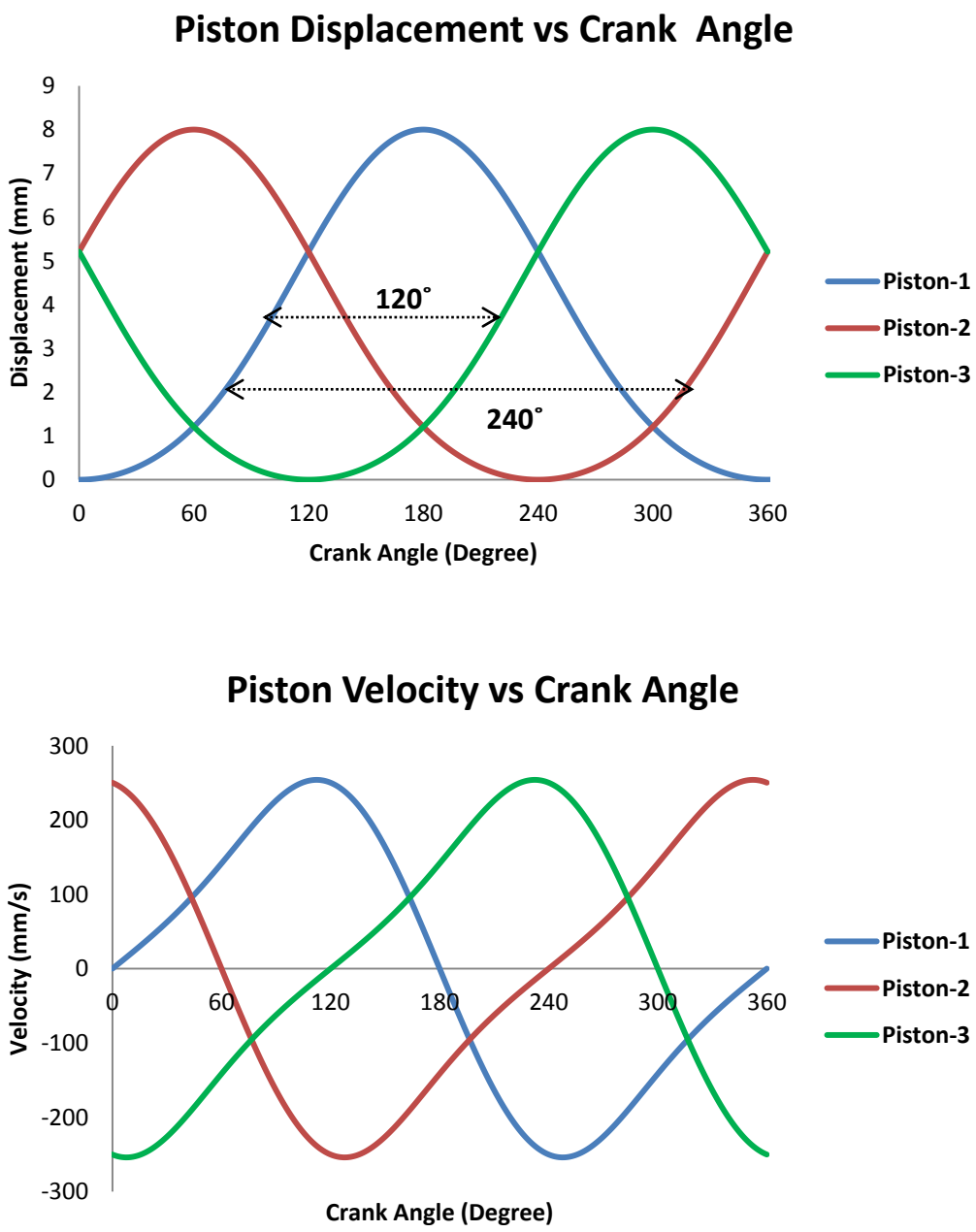

Figure 1.6 Piston Displacement and Piston Velocity vs. Crank Angle

From equation 1.8, it can be observed that shape of flow pattern is affected by the design of the pump (e.g. the ratio (β) of crank radius (r) to connecting rod length (l) and number of pistons, triplex, nonuplex etc.)

In figure 1.7 discharge volume flow rate vs. crank angle for triplex pump (3-piston) is given for different crank radius/connecting length ratios. (*)

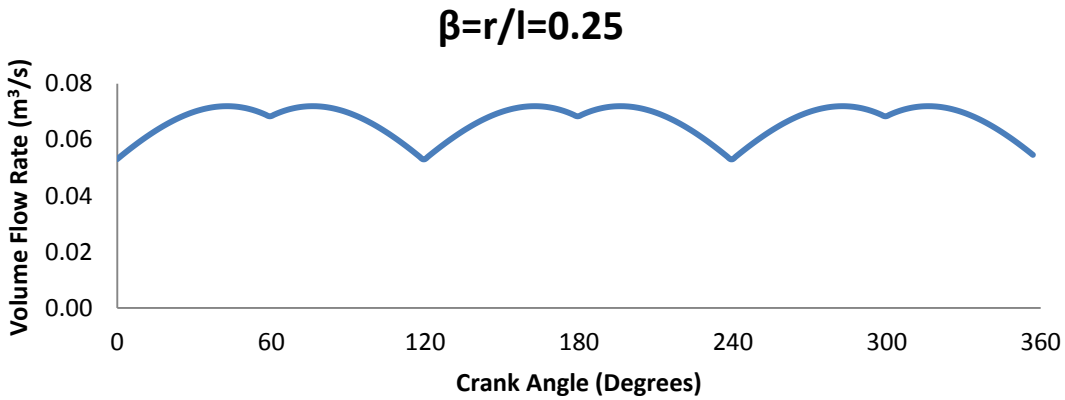

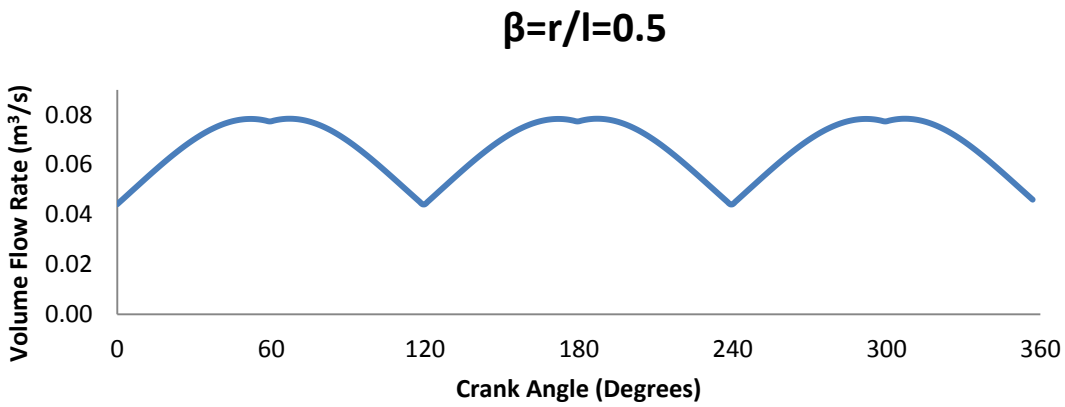

Figure 1.7 Volume Flow Rate vs. Crank Angle for different r/l ratios

From the figure 1.7, it can be observed that reducing r/l ratio will provide more uniform distribution at the discharge.

*** These graphs are drawn for ideal flow. Leakage at the valves is not taken into account.**

1.1.2 Diaphragm Pump

Diaphragm pumps are kind of positive displacement pumps which are mechanically or hydraulically actuated. Their operating principles are very similar to piston pumps and only difference is instead of rigid piston, deformable elastic diaphragm is used in their arrangements. The diaphragm pump uses check-valves to prevent the backflow inside the system and relief valves may be installed to the system to avoid excess pressure.

Diaphragm pump uses either a flapper valve or a ball valve to transfer liquids. Diaphragm pump is also called as a membrane pump. They are ideal for viscous liquids. Most models are available in electric, engine, manual, air operated or hydraulic configurations. [9]

Diaphragm pumps offer smooth flow, reliable operation, and the ability to pump a wide variety of viscous, chemically aggressive, abrasive and impure liquids. They are used in many industries such as mining, petro-chemical, pulp and paper and others. [10]

In figure 1.8 the diaphragm pump is shown. The operating principle is as follows: Fluid is transferred to the outlet of the system with an elastic diaphragm which is doing harmonic motion. As the diaphragm moves backward, vacuum is created inside the cylinder that draws fluid into the cylinder. This process is called “suction process”. During the suction process, discharge valve remains closed and suction valve is opened. These valves are regulating the flow direction and used to prevent back flow inside the system. As the diaphragm moves reverse direction and suction valve is closed, discharge process begins. During the discharge process, discharge valve stays open. The trapped fluid inside the cylinder is transferred to the exit of the pump.

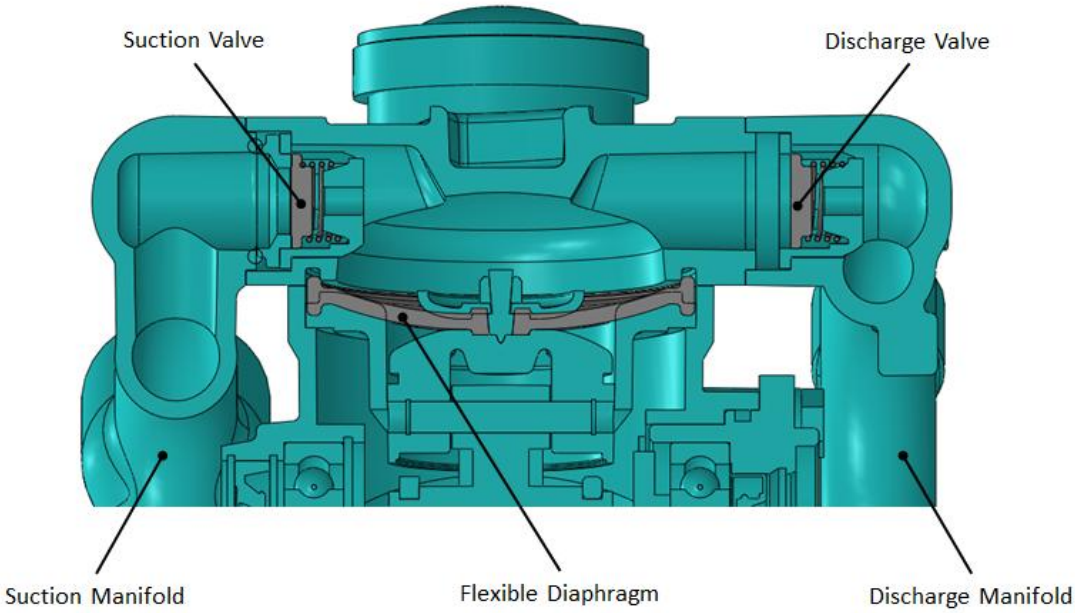

Figure 1.8 Diaphragm Pump

The main advantages of the diaphragm pumps are given below,

- Easy to install and portable.
- Can transfer fluids which have high viscosity.
- Have good suction lift characteristics, can work with both high and low flow rates. High pressure types are capable of higher flow rates, depending on the effective working diameter of the diaphragm and its stroke.[11]
- Diaphragm pumps transfer almost any kind of slurry, food processing residual, liquid, stones, sticks, sugar, oil sludge, refinery waste, mud, clay pharmaceutical, industrial fluids and much more. [11]
- Pumping chambers and the material being pumped are not in contact with any close fitting rotary or sliding seals. This makes double diaphragm pumps ideal to be used with abrasives, slurries or even run dry. [12]
- The arrangement of diaphragm eliminates the wear and leakage between a moving piston and liner.

1.2 Pressure Pulsations

There are several sources of dynamic pressure pulsations generated by the pump [8]; firstly, the pistons are doing simple harmonic motion; the fluid is unable to follow piston dynamics due to inertia. The fluid accelerates and decelerates faster than the piston, causing pressure pulsations. Liquid flow variations and pressure pulsations caused by reciprocating pumps cannot be determined easily because they are function of a whole system.

Secondly, at the end of the discharge stroke, the fluid inside the cylinder is at discharge pressure. In order to open suction valve it is necessary to decompress the fluid. This means a sudden drop in suction intake pressure. Similarly one may encounter with the similar problem at the discharge since the fluid must be compressed to discharge pressure before the discharge valve opens. If the discharge pressure is increased, the pressure and flow fluctuations increase.

Thirdly, the number of pistons in the pump also affects the flow field inside the pump and pressure pulsations. If the pump has several pistons, the magnitudes of overall pulsations are decreased. And this condition can be seen in figure 1.9 [13]

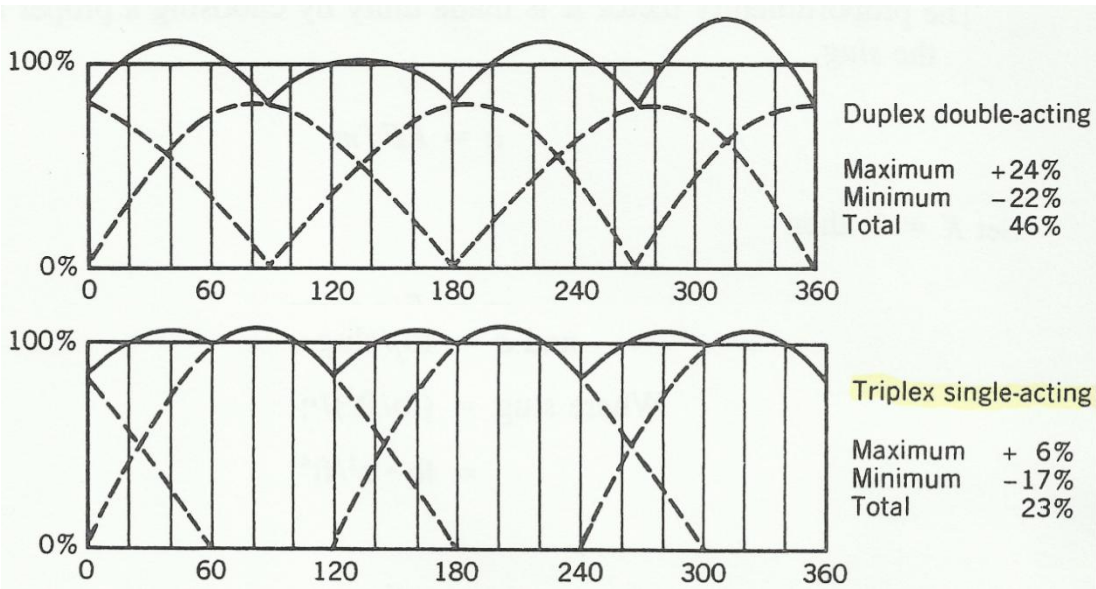

Figure 1.9 Flow Ripple for Different Pump Arrangements [13]

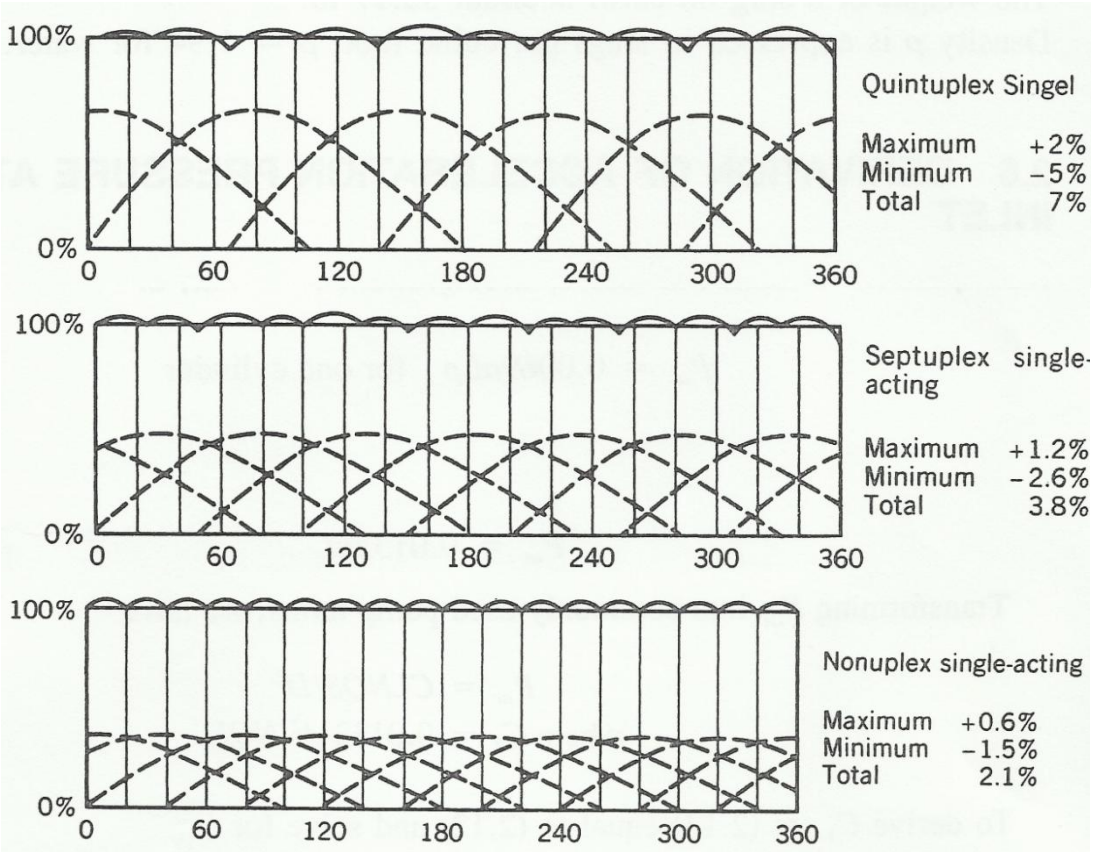

Figure 1.9 Flow Ripple for Different Pump Arrangements (Cont.) [13]

According to reference [14], if the difference between mean flow rate and maximum flow rate is more than 20 % and mean flow rate is coincide with the operating point which gives the maximum pump efficiency, the performance of the pump is negatively influenced by this condition.

Finally, **water hammer type** pressure fluctuations occur when the check valves rapidly close. Obviously rapid closure of check valves prevents back flow and increases volumetric efficiency. But it causes pressure increase in front of the valve. This pressure increase means a pressure wave, which propagates at acoustic speed “a”. (This phenomenon may cause pipeline to burst or may damage the mechanical parts of the system).

Water has an acoustic speed approximately 1450 m/s in ideal conditions. But in real conditions flexibility of wall reduces the acoustic speed. The wall effect on the acoustic speed is given by equation (1.11) [15]

$$a = \sqrt{\frac{\frac{g}{w}}{\frac{1}{K} + \frac{1}{8E}(d_0^4 - d_i^4)}} \tag{1.11}$$

Where,

a = wave speed (m/s)

g = gravitational acceleration (m/s^2)

w= specific weight (N/m^3)

E= Young's modulus of elasticity of the pipe (N/m^2)

d_o= pipe outside diameter (m)

d_i= pipe inside diameter (m)

The valve is not affected by the pressure wave before it is reflected from the end of the pipe and returned to the valve. The time required called reflection time given by "t_r". [16]

$$t_r = \frac{2L}{a} \tag{1.12}$$

Where,

t_r= reflection time (s)

L=pipe length (m)

a= wave speed (m/s)

If pressure fluctuations occur at the suction side of the pump, they may cause **cavitation** and incomplete filling of the cylinders. [17]

Cavitation occurs, when fluid velocity increases, it causes the local hydrostatic pressure to drop to a critical value which corresponds to the vapor pressure of the fluid. This phenomenon creates small bubbles filled with vapor. These bubbles finally collapse when they reach the high-pressure areas as they are carried along by the fluid flow. In the final phase of bubble implosion, high pressure peaks are generated inside the bubbles and in their surroundings. These pressure peaks lead to mechanical vibrations, noise and material erosion of surfaces [18]. If cavitation

intensity is high, the hydraulic valve coefficients as well as the fluid properties may change. Cavitation also decreases volumetric efficiency of the pump.

To avoid pressure pulsations and cavitation;

- Suction pressure may be increased.
- A flexible hose may be added at the pump discharge with flow control valve. The flexible hose acts as a capacitor to store the pressure fluctuations originated from the pump while the valve is shifting directions from one chamber to the other. [18]

In this part of the thesis, the literature survey is summarized. Although there are several numerical studies regarding pump analysis, most of them are related to gear pumps, axial pumps, centrifugal pumps etc. no reference are made to numerical studies of positive displacement pumps since no significant studies could be found related to positive displacement pumps. Also theoretical studies given in literature are very approximate and exclude important parameters that affect the system. Many of them are based on incompressible flow assumption and neglect the back flow through check valves. Obviously, in real systems there is always a certain amount of backflow and real fluids are compressible. Due to these reasons, theoretical studies may not be useful for designing or performance evaluation of pumping systems. [14]

Rob Broberg [19] analyzed a special class of internal rotary pump which utilizes cyclical gear profiles which means that the gear profile is generated by rolling, without slippage in commercial CFD program known as CFX. He investigated the effect of inlet to outlet pressure ratio on the efficiency of the pump and his results showed that larger pressure gradient causes the fluid to flow in reverse direction resulting in leakage; therefore the efficiency of the pump reduces.

John E. Miller [8] built a test set up to find the parameters that affect performance of single-acting triplex piston pump, such as the valve characteristics (valve spring stiffness, mass of valves), suction pressure and suction pipe length. At first, author observed the valve spring POSIVA effect. He defined a POSIVA (Pounds per Square Inch of Valve Area) definition for valve springs as spring force (lb) acting

per unit valve through area (in^2). Author stated that using stiffer springs on the valves (high POSIVA) causes valves to close faster and tend to increase volumetric efficiency on condition that suction pressure is increased. In addition, it is also observed that on the same cylinder pressure and valve weight at 360 rpm, the volumetric efficiency calculated at 4 POSIVA is greater than calculated at 8 POSIVA. However, on the same conditions but at 625 rpm the volumetric efficiency calculated at 8 POSIVA is greater than calculated at 4 POSIVA.

At 325 rpm on the same cylinder pressure and on the same POSIVA, the volumetric efficiency calculated with 3 oz. valve weight is greater than calculated with 2.75 oz. However, at 625 rpm the volumetric efficiency calculated with 2.75 oz. is greater than calculated with 3 oz.

According to test results [8], using 6 in long suction pipe instead of 4 in pipe under the same operating conditions reduces the pressure fluctuations and increases the volumetric efficiency.

From Miller results, one can understand that the parameters that affect the performance characteristics of the positive displacement pumps are highly non-linear. As a result there is no general rule that can be followed in designing reciprocating pumps.

Terry Henshaw [20] stated that improper design of valve dynamics contributes pulsation and vibrations problems in the pump and tends to reduce the pump efficiency. He also observed that many reciprocating pumps in industry attached with too weak suction and discharge springs. Weak springs (have lower stiffness) do not close the valves soon enough. Stiffer springs close faster the valves but fast closing valves may cause hydraulic shocks inside the pump. These shocks may damage to the valves also the other pump components. Increasing valve spring stiffness also brings higher net positive suction head requirement (NPSH). A late closing suction valve contributes to the reverse flow through valve.

The suction valve is closed by the fluid which is pushed by the pistons or diaphragms then the instantaneous stopping of the flow occurs when the valve hits the seat as a result of this condition hydraulic shock at the pump inlet and inlet manifold may arises. Such valve action may also bring a valve flutter, shorter life of pump components such as gaskets, gears, crankshafts, manifolds, etc.

CHAPTER 2

EXPERIMENTAL PROCEDURE AND INSTRUMENTATION

2.1 Experimental Setup

Some experiments are conducted to evaluate the performance characteristics of a positive displacement diaphragm pump. The pump that is used in this study is tested in the Fluid Mechanics Laboratory of Middle East Technical University. In this study not only the pump efficiency but also exit pressure fluctuations are measured during the tests.

Test setup is shown in figure 2.2. The system is fed by tank, a filter is attached to the tank to avoid unwanted particles in the system. Water is used as working fluid. The outlet pressure of the pump is controlled by the discharge valve. The main control panel is attached to system in order to start and stop the electric motor (18.5 kW) which drives the pump. The pump operates at 540 rpm. In order to maintain this rotational speed frequency converter is used. The technical specifications of the electric motor are given in appendix A. Cole-Parmers optical tachometer is used to measure the rotational speed of the pump. The suction pressure is measured by a gage and discharge pressure is measured by a pressure transmitter. The pressure transmitter is connected to datalogger which is used to collect data coming from transmitter and send them to computer. Then the output voltage data is converted to pressure value in computer environment using calibration curve which is obtained from dead weight tester. Technical specifications of datalogger are given in appendix A.

The calibration formula is given by equation 2.1;

$$p_{exit} = \frac{60}{(4.4-0.8)}(V-0.8) \tag{2.1}$$

The calibration curve is given in figure 2.1

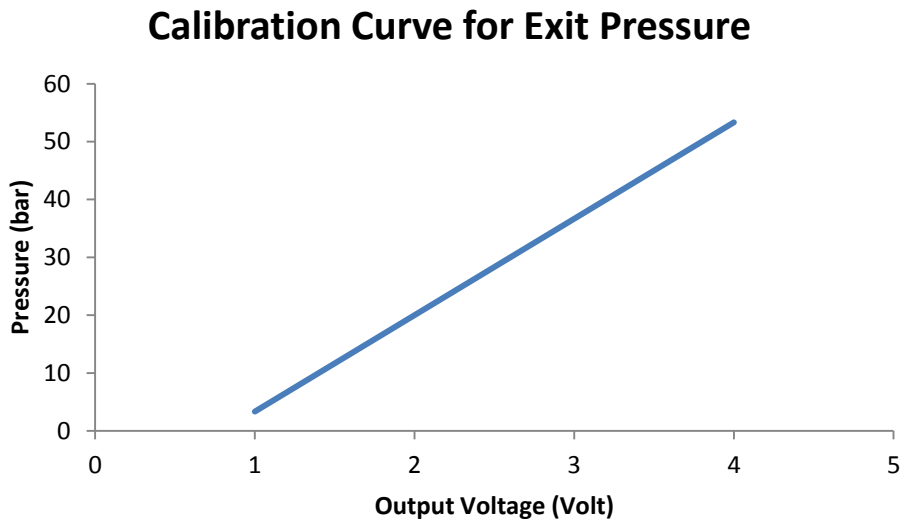

Figure 2.1 Calibration Curve for Pressure Sensor

Electrical variables of the system are measured by current transformer system. The power input to the system is directly read by this system. The reason why the current transformer system is used in experiments instead of a voltmeter and clampmeter is that the electrical power calculated with voltmeter and clampmeter is not correct because they have some inaccuracies at the studied frequency range (27 Hz). Hedland digital flowmeter with a measurement range of 20-190 l/min is installed on the discharge pipe and used to measure the discharge volume flow rate of the system. All connections are made with flange connections which are fastened with bolts and nuts to each other. The experimental setup is shown in figure 2.2.

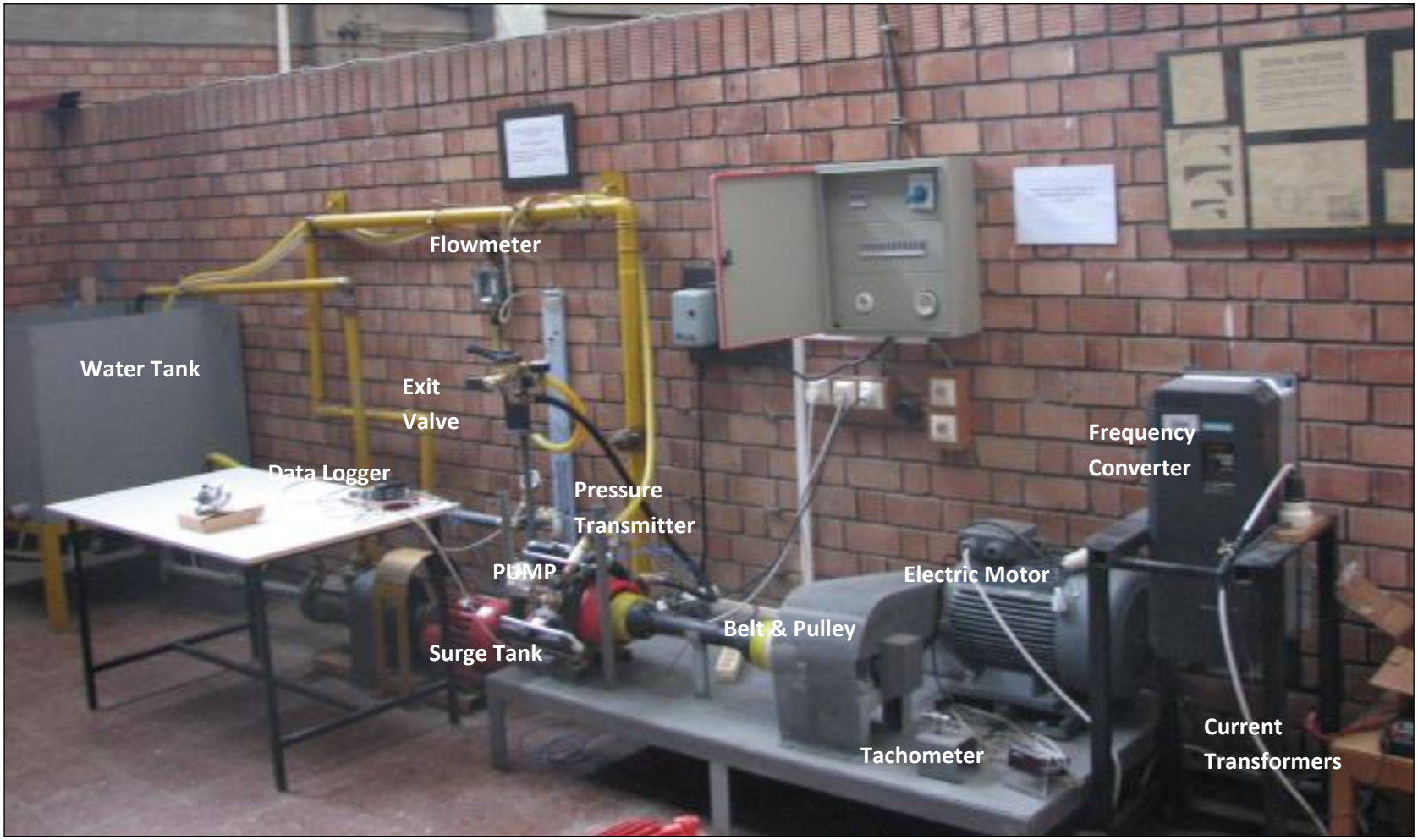

Figure 2.2 Experimental Setup

2.2 Experimental Procedure

The procedure followed during the testing of positive displacement diaphragm pump is given below.

1. All connections such as frequency converter, electric motor, datalogger are plugged into the electrical energy source.

2. The tank (water reservoir) is filled with water.

3. All connections are controlled before starting the pump to make sure that there is no fluid leakage from these connections.

4. Labjack U12 datalogger is connected to a computer and controlled if the output signal is coming to the computer.

5. Pressure transmitter is attached to the discharge side of the pump in order to get pressure fluctuations and pressure gage is attached to a suction side of the pump.

6. The pump is started to operate at 0 bar discharge gage pressure (atmospheric) and frequency converter is adjusted in order to get a desired rotational speed (540 rpm).

7. The system is run approximately for 5 minutes until the system reaches steady state then discharge pressure is set to desired value (40 bar) by using discharge valve.

8. The system is run approximately for another 5 minutes until the system reaches equilibrium. Then the pressure, flow rate and input power data are collected and transferred to computer environment.
9. The discharge pressure is set to 0 bar then the pump is stopped. All electrical connections are unplugged and safety regulations are followed.

2.3 Experimental Results

During the experiments, the suction and discharge pressures, volumetric flow rate of the pump, power consumption of the system and rotational speed of the pump are measured. By using these data the performance characteristics of the pump and pump efficiency is obtained.

The pressure difference of the pump is;

$$\Delta p = p_2 - p_1 \tag{2.2}$$

Where P_2 is the discharge pressure and P_1 is the suction pressure, ΔP is calculated during the experiments as;

$$\Delta p = 40 \text{ bar}$$

The rotational speed of the pump is measured as;

$$n = 540 \text{ rpm} = \frac{540\,[\text{rpm}]}{60\,[\text{s}]} \times 2\pi = 56.55 \text{ rad/s}$$

The volume flow rate is read from flowmeter and determined as;

$$Q = 86\,[\text{l/min}] = \frac{86 \times 0.001}{60} = 0.00143\,[\text{m}^3/\text{s}]$$

The overall efficiency is defined as the ratio of actual power gained by the fluid to the power consumption of the system.

$$\eta = \frac{\text{Hydraulic Power}}{\text{Power Consumption of the System}} = \frac{\Delta p \times Q}{P_{system}} \tag{2.3}$$

Power consumption of the system at the 40 bar pressure difference and 540 rpm is measured by current transformer system as 8251 W.

Using these values the overall efficiency of the pump is calculated as;

$$\eta = \frac{\Delta p \times Q}{P_{system}} = \frac{40 \times 10^5\,[\text{Pa}] \times 0.00143\,[\text{m}^3/\text{s}]}{8251\,[\text{W}]} = 0.69$$

Overall efficiency is also defined as;

$$\eta = \eta_m \eta_h \eta_v \tag{2.4}$$

Where η_m is the mechanical efficiency of the system, η_v is the volumetric efficiency of the system and η_h is the hydraulic efficiency of the system.

Mechanical components inside the system such as, bearings, motor, belt and pulley system and frequency converter generates mechanical losses that increase the power consumption of the system. In order to take into account these losses the definition of mechanical efficiency is introduced.

The mechanical efficiency of the system η_m is calculated using the following parameters;

- The efficiency of the belt and pulley system is taken as 0.94 [21]
- The efficiency of the frequency converter is taken as 0.97 [22]
- The efficiency of the electric motor is taken as 0.93 at the rated power [23]

So the mechanical efficiency of the system becomes;

$$\eta_m = \eta_b \eta_f \eta_e = 0.94 \times 0.97 \times 0.93 \cong 0.85$$

The volumetric efficiency of the system is defined as the ratio of actual flow rate of the pump to piston displacement.

$$\eta_v = \frac{\text{Actual Flow Rate of the pump}}{\text{Piston Displacement}} = \frac{Q_{actual}}{Q_{\text{piston displacement}}} \tag{2.5}$$

Because of the sampling rate of the flowmeter, volumetric efficiency could not measured directly during the experiments. So the volumetric efficiency is taken from the manufacturers brochures as 0.98

Hydraulic efficiency of the pump is found from equation 2.4;

$$\eta_h = \frac{\eta}{\eta_m \eta_v} = \frac{0.69}{0.85 \times 0.98} = 0.83 \tag{2.6}$$

The pressure vs. time history at the discharge is measured with pressure transmitter collected data is converted from voltage domain to pressure domain using equation (2.1) pressure time history is given in figure 2.3

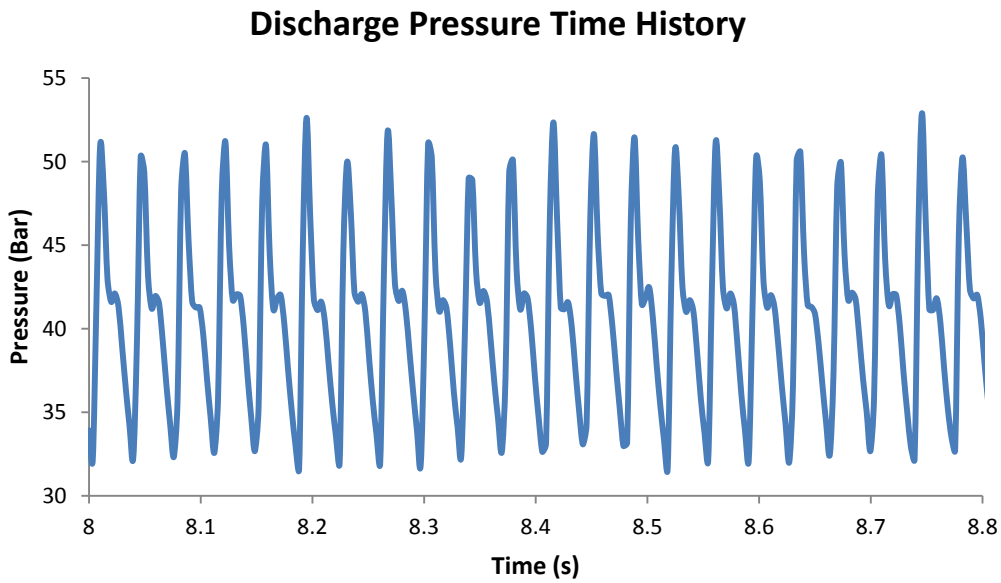

Figure 2.3 Discharge Pressure Time History

From Figure 2.3 it is observed that discharge pressure fluctuates between 35-50 bar. The pressure fluctuations are effective parameters on the pump efficiency. It is important to keep pressure values in narrow range.

CHAPTER 3

CFD ANALYSIS OF THE PUMP

3.1 Introduction

Due to the difficulties and limitations of experimental procedure, CFD analysis is applied to the positive displacement triplex pump in this thesis.

In order to reduce the manufacturing and test costs and shorten design periods, commercial CFD programs can be used in any design process. Similarly a commercial CFD program is used in this study.

The aim of this thesis is investigating the performance characteristics of a positive displacement diaphragm pump by means of applying numerical experimentations in computer environment without producing a prototype. The commercial CFD code known as Autodesk Simulation CFD v2012 is used for this purpose. Using Autodesk Simulation, internal flow parameters such as suction and discharge pressures, flow rates, pressure fluctuations inside the pump are observed in order to obtain better performance characteristics from the current pump. For this purpose velocity and pressure distributions, traces and velocity vectors in the flow field are investigated. These distributions are given in the following sections.

3.2 History

The usage of modern computational fluid dynamics (CFD) began with the development of the digital computer in the early 1950s. There are two different basic methods which are used in the discretization of partial differential equations; finite element methods (FEM) and finite difference methods (FDM). They have different origins. [24]

In 1910, at the Royal Society of London, Richardson presented a paper on the first finite difference solution for the stress analysis of a masonry dam. However, the first finite element work was published in the Aeronautical Science Journal by Turner, Clough, Martin, and Topp for applications to aircraft stress analysis in 1956. Since then, both methods have been developed in fluid dynamics, heat transfer and related areas. [25]

Many valuable textbooks can be found in literature related to finite difference method such as; Patankar (1980), Peyret and Taylor (1983), (1984, 1997), Hoffman (1989), Anderson (1995), Tannehill, and Pletcher (1997), Ferziger and Peric (1999), Roache (1999).

With the knowledge of FDM and FEM there is a new method developed known as finite volume method (FVM) which is very popular in recent years because of its simplicity.

Historically, finite difference methods were dominant in CFD community due to their simplicity in formulations and computations [26]. On the other hand, finite element method's calculations and formulations are more complicated and time consuming.

3.3 Computational Fluid Dynamics

Computational Fluid Dynamics or CFD is analyzing of systems involving fluid flow, heat transfer and associated phenomena such as chemical reactions and diffusion by means of computer-based simulation. Using CFD, a model may be constructed that permits a better comprehension of a physical problem. Generally, CFD user is interested in velocity, pressure, and temperature distributions in the flow field. The technique is widely used in industry. Some examples are [27]:

- Chemical Engineering (Mixing)
- Aerodynamics
- Hydrodynamics
- HVAC

- Biomedical Engineering
- Meteorology (Weather prediction)
- Turbomachinery

CFD principle which is common to all commercial programs is that the computational domain is divided into a three dimensional grid of data points. This grid may be “structured” or “unstructured” depending on the numerical scheme and solver method used.

Structured grids are the simplest types and were used in the earliest forms of numerical solution techniques. These grids contain uniform distributions of grid points in all coordinate directions. This is made less restrictive by the use of numerical mapping schemes that allow the generation of so-called body fitted meshes to fit complex curved surfaces at domain boundaries. There are some difficulties coming with this restriction. One can overcome these difficulties by using multi-block techniques. Using these techniques, more complex volume geometries can be generated by joining great numbers of hexahedral blocks together. Therefore structured multi-block method was the most commonly used approach in applications of CFD until present time [26].

When using unstructured meshes computational domain can be discontinuous or arbitrary shape on condition that there will be no gaps or disconnection between volumes. There are various grid volume shapes in the commercial CFD programs (such as FLUENT, CFX, STAR CD, Autodesk Simulation CFD) which use unstructured grids e.g. hexahedral, tetrahedral, prisms, etc. and unstructured mesh method is rapidly becoming the most common approach in industrial CFD applications, with the development of methods for automatic grid generation.

Transforming a partial differential equation to linear algebraic set of equations is called numerical discretization. In this discretization process each term within a partial differential equation must be converted into an algebraic equation that the computer can be programmed to calculate. To apply this numerical discretization various techniques can be used and each technique is based on a different set of

principles. Most commonly used discretization techniques in literature are given in the following section.

3.4 Discretization Methods

The most common methods used in discretization of partial differential equations are finite difference method, finite element method, finite volume method and spectral methods. Since finite element method is used in the analyses, only this method is explained in detail.

3.4.1 Finite Element Method

Finite element method (FEM) is a numerical method for solving a differential or integral equation. As long as the governing differential equations are available, the method can be applied any physical problem. [28]

At the beginning the method was used as a procedure for constructing matrix solutions to displacement and stress calculations in structural analysis. Finite element method uses piecewise polynomial functions on the elements in computational domain to describe the variations of the unknown variables.

When the piecewise polynomial functions are substituted into the governing equations, there are errors occurred and concept of residual is defined to measure that errors.

The residuals can be minimized in such a way that multiplying by a set of weighting functions and then integrating. This results in a set of algebraic equations for the unknown terms of the approximating functions and hence the flow solution can be found.

There are a number of finite element codes are available, both research and commercial based. (e.g. Autodesk Simulation CFD) Finite element methods bring a high degree of accuracy to the mathematical model. But generally this method requires more computational resources and CPU time as compared with the other methods. Like finite volume and spectral methods. [26]

3.5 Performed Analyses

Due to the limitations and difficulties of experimental study, CFD analyses are conducted to obtain performance characteristics of positive displacement pump.

Different CFD models are prepared in order to evaluate the effect of valve spring stiffness, valve displacement, shape of the piston and mass of the check valves on the pump efficiency.

These models are mentioned in this section.

- Model #1-3 Flat Pistons (k_{spring}=3.66 N/cm, ρ_{valve}=8000 kg/m^3, d_v=3.1 mm)
- Model #2-1 Flat Piston (k_{spring}=3.66 N/cm, ρ_{valve}=8000 kg/m^3, d_v=3.1 mm)

To investigate the effect of valve spring stiffness

- Model #3-1 Flat Piston (**k_{spring}=7.32 N/cm**, ρ_{valve}=8000 kg/m^3, d_v=3.1 mm)
- Model #4-1 Flat Piston (**k_{spring}=14.64 N/cm**, ρ_{valve}=8000 kg/m^3, d_v=3.1 mm)
- Model #5-1 Flat Piston (**k_{spring}=29.28 N/cm**, ρ_{valve}=8000 kg/m^3, d_v=3.1 mm)
- Model #6-1 Flat Piston (**k_{spring}=58.56 N/cm**, ρ_{valve}=8000 kg/m^3, d_v=3.1 mm)

To investigate the effect of mass of check valves on the pump efficiency,

- Model #7-1 Flat Piston (k_{spring}=3.66 N/cm, **ρ_{valve}=16000 kg/m^3**, d_v=3.1 mm)
- Model #8-1 Flat Piston (k_{spring}=3.66 N/cm, **ρ_{valve}=32000* kg/m^3**, d_v=3.1 mm) (*There is no material which has 32000 kg/m^3 density in nature this analysis is done to obtain a trend)
- Model #9-1 Flat Piston (k_{spring}=3.66 N/cm, **ρ_{valve}=6000 kg/m^3**, d_v=3.1 mm)
- Model #10-1 Flat Piston (k_{spring}=3.66 N/cm, **ρ_{valve}=4000 kg/m^3**, d_v=3.1 mm)

To investigate the effect of valve displacement on the pump efficiency,

- Model #11-1 Flat Piston (k_{spring}=3.66 N/cm, ρ_{valve}=8000 kg/m^3, **d_v=6.1 mm**)
- Model #12-1 Flat Piston (k_{spring}=3.66 N/cm, ρ_{valve}=8000 kg/m^3, **d_v=9.1 mm**)

To investigate the effect of rounded piston on the pump efficiency,

- Model #13-1 Rounded Piston (k_{spring}=3.66 N/cm, ρ_{valve}=8000 kg/m^3, d_v=3.1 mm)

After investigating the effect of each parameter on the pump efficiency, combined model #14 is prepared in such a way that the best model is selected from each category (among spring stiffness, mass of the check valves, valve displacement) which gives the highest hydraulic and volumetric efficiency.

- Model #14-3 Flat Piston (k_{spring}=29.28 N/cm, ρ_v=6000 kg/m^3, d_v=3.1 mm)

Finally, in order to compare experimental results with CFD results, the pump used in experiments is modeled for the CFD analysis.

- Model#15-3 Flat Pistons, (k_{spring}=3.66 N/cm, ρ_{valve}=8000 kg/m^3, d_v=3.1mm)

In table 3.1, the analyzed models are shown.

Table 3.1 Analyzed Models

Model	Arrangement	Spring Stiffness	Valve Density	Valve Displacement
#1	3-Flat Pistons	3.66 N/cm	8000 kg/m^3	3.1 mm
#2	1-Flat Piston	**3.66 N/cm**	8000 kg/m^3	3.1 mm
#3	1-Flat Piston	**7.32 N/cm**	8000 kg/m^3	3.1 mm
#4	1-Flat Piston	**14.64 N/cm**	8000 kg/m^3	3.1 mm
#5	1-Flat Piston	**29.28 N/cm**	8000 kg/m^3	3.1 mm
#6	1-Flat Piston	**58.56 N/cm**	8000 kg/m^3	3.1 mm
#7	1-Flat Piston	3.66 N/cm	**16000 kg/m^3**	3.1 mm
#8	1-Flat Piston	3.66 N/cm	**32000 kg/m^3**	3.1 mm
#9	1-Flat Piston	3.66 N/cm	**6000 kg/m^3**	3.1 mm
#10	1-Flat Piston	3.66 N/cm	**4000 kg/m^3**	3.1 mm
#11	1-Flat Piston	3.66 N/cm	8000 kg/m^3	**6.1 mm**
#12	1-Flat Piston	3.66 N/cm	8000 kg/m^3	**9.1 mm**
#13	**1-Round Piston**	3.66 N/cm	8000 kg/m^3	3.1 mm
#14	3-Flat Pistons	29.28 N/cm	6000 kg/m^3	3.1 mm
#15*	3-Flat Pistons	3.66 N/cm	8000 kg/m^3	3.1 mm

***** Model #15 seems to be identical with model #1, in fact they are not. Manifold designs are different in these models. (Explained in relevant section)

3.5.1 Model #1

Numerical model (CFD Model) is different from production model, before starting the analysis CAD model must be simplified in order to use the mesh efficiently and reduce the solution time.

The production model may contain assembly clearances or interfering parts which impractically increases the mesh sizes and time required for solution process. The model also consist of unwanted and less important parts which do not affect the flow field such as bolts, nuts, etc. In the figure 3.1 production and CFD model of a positive displacement triplex diaphragm pump is shown which used in this thesis.

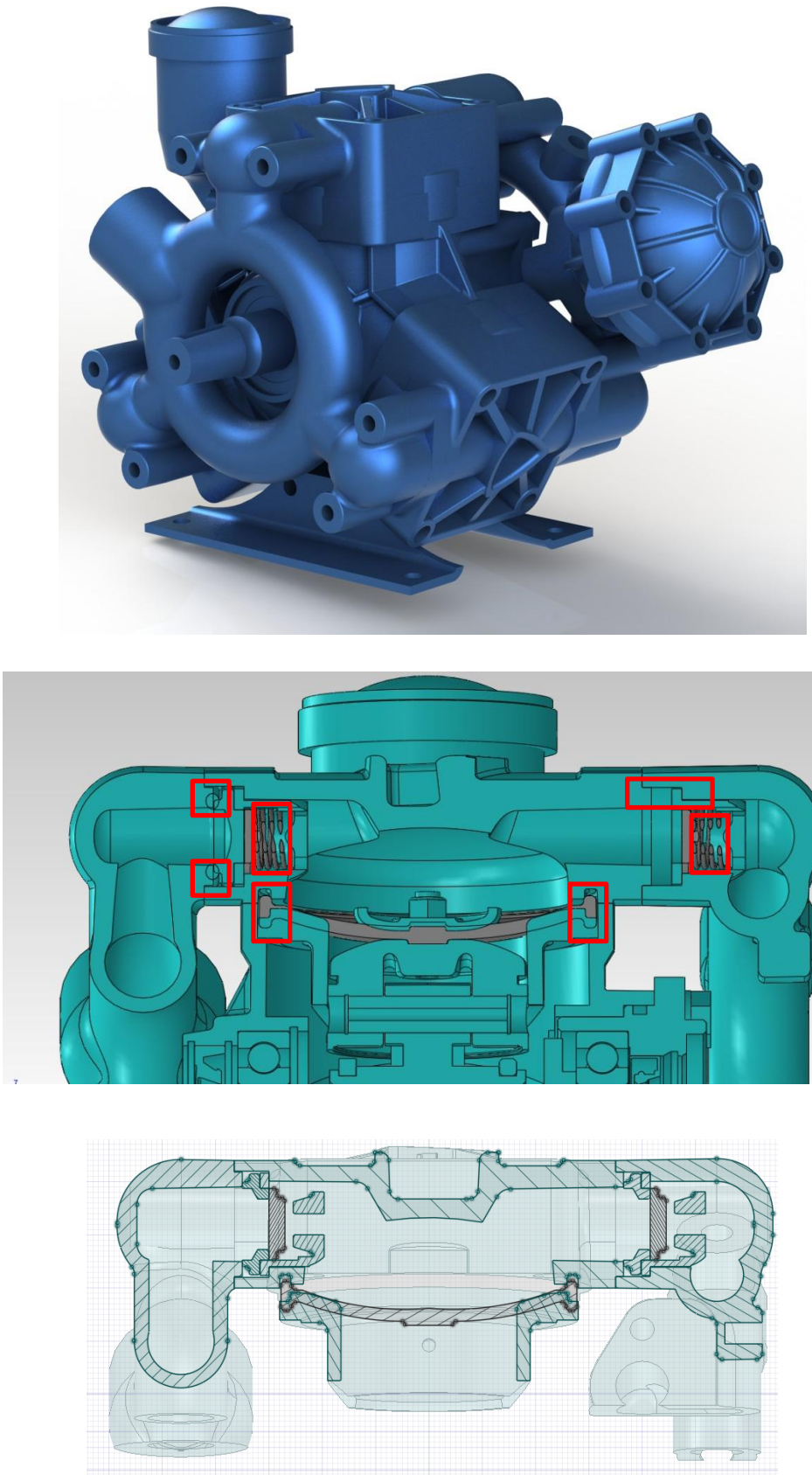

Figure 3.1 Positive Displacement Pump Model #1

In figure 3.1 it can be seen that small fillets, less important parts such as springs, connecting rods and unwanted parts which do not affect flow field are removed. So the model is nearly ready for CFD analysis.

Model is nearly ready because the motion of flexible diaphragm remains unknown. In order to model flexible diaphragm it is necessary to consider how diaphragm shape changes with time. But it is not possible to detect the exact diaphragm shape in time. This problem requires a fluid-solid interaction analysis with deforming bodies. With Autodesk Simulation CFD v2012 one cannot simulate the motion of deforming bodies.

Because of the lack of physical information and capabilities of the CFD program, equivalent piston is used to simulate diaphragm motion in the pump. The equivalent piston stroke must be calculated in such a way that rigid piston delivers the same flow rate with the diaphragm at each stroke (Figure 3.2). To calculate equivalent piston stroke technical specifications of the pump are given in Table 3.2

Table 3.2 Technical specifications of the pump

Technical Specifications of The Pump	
Diaphragm Diameter [mm]	96
Discharge Flow Rate [l/min]	90
Max pressure [bar]	50
Rotational Speed [rpm]	540
Number of Diaphragms	3
Efficiency (%)	76
Size [cm]	35x42x35

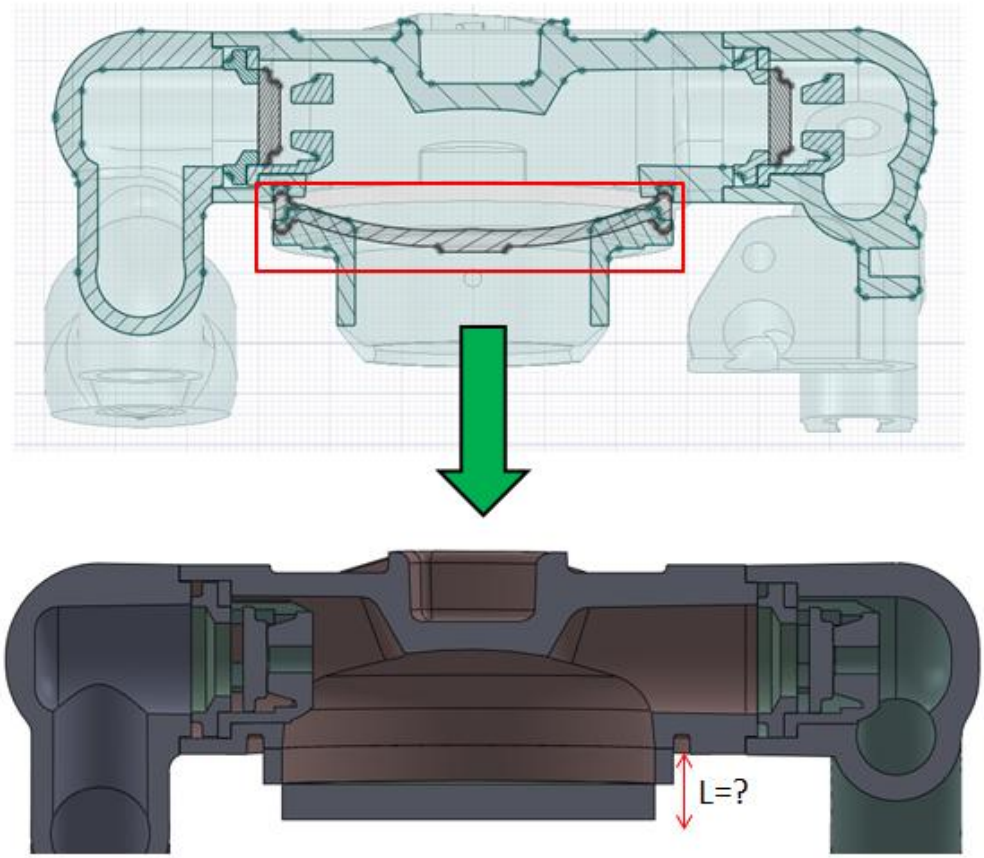

Figure 3.2 Equivalent Rigid Piston

In table 3.2, volumetric flow rate at the discharge is given as 90 l/min and diaphragm diameter is given as 96 mm. Therefore one diaphragm capacity at one stroke can be calculated as;

$$\text{Diaphragm Capacity} = \frac{\text{Volumetric Flow Rate of the Pump } [\text{mm}^3/\text{s}]}{\text{Rotational Velocity[RPM] x Number of Diaphragms}}$$

$$\text{Diaphragm Capacity} = \frac{90\text{x } 10^6[\text{mm}^3/\text{s}]}{540\ [\text{RPM}]\text{ x } 3} \cong 55556\ \text{mm}^3$$

The capacity of single rigid piston is equal to volume which is swept by piston during one stroke;

$$\text{Piston Capacity} = \frac{\pi \text{xD}^2}{4}\text{xL} = \frac{\pi \text{x}96^2}{4}\text{xL}$$

Where, L is the stroke length.

By definition, piston capacity must equal to diaphragm capacity.

$$\frac{\pi x 96^2}{4} xL = 55556 \text{ mm}^3$$

L ≅ 8 mm

Now the CFD model is ready for analysis.

3.5.1.1 Boundary Conditions and Motion Parameters

Boundary conditions are very important in the setup. Without them, analysis cannot be started. Boundary conditions are persistent throughout an analysis, and can be either constant or transient.

This analysis is transient however boundary conditions don't change with time. 0 bar (gage) pressure boundary condition is assigned to the inlet of the pump and 40 bar (gage) pressure is assigned to the outlet of the pump as shown in figure 3.3

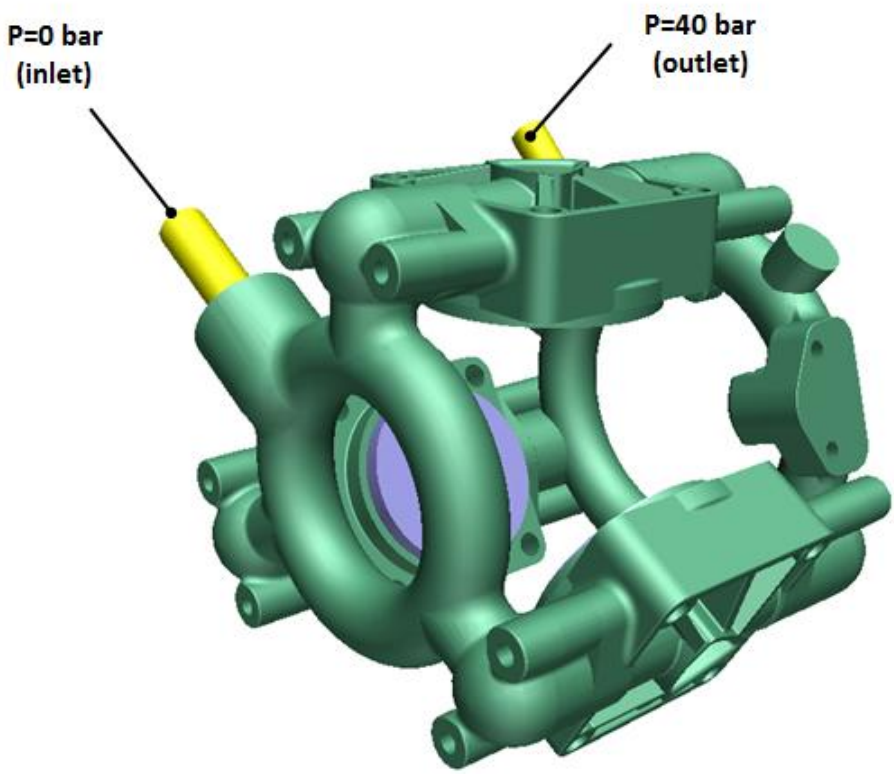

Figure 3.3 Boundary Conditions

The effect of the motion on the fluid medium as well as the flow-induced forces on the check valves are analyzed in Autodesk Simulation CFD v2012.

There are two types of motion in the pump, one is user defined motion, and the other is flow induced motion.

In user defined motion, the object moves according to a fully-prescribed motion, it does not react to the flow. The object will move in the direction and across distances that are explicitly specified by the analyst. In this thesis user defined motion given in figure 1.6 (Chapter-1) is applied to the pistons.

In flow induced motion, objects are influenced by the flow as well as user specified driving and resistive forces. The origins of such forces do not have to be included in the analysis model (springs). The forces act on the object in a user-prescribed manner to either push the object in its prevailing direction or to impede its progress. Flow induced motion is assigned to the check valves in this study. Shown in figure 3.4

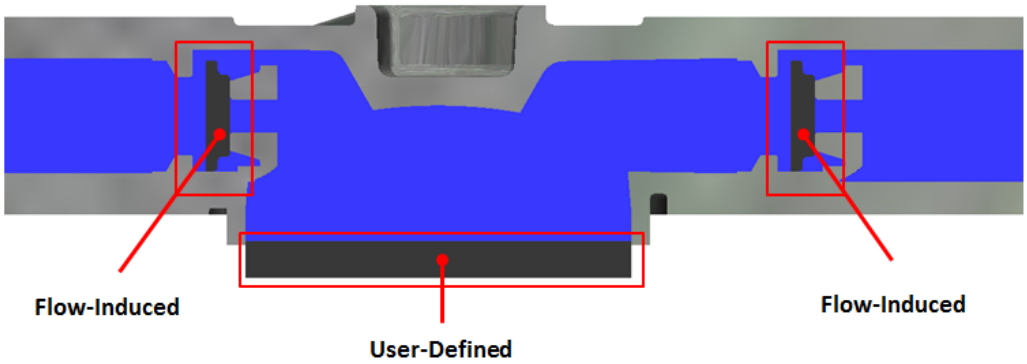

Figure 3.4 Motion Parameters

The initial position of the valves, the limits of travel of the valves, and the spring parameters are defined. In Table 3.3 the valve spring characteristics are given,

Table 3.3 Model #1 Spring Characteristics

Model #1 Spring Characteristics	
Compression Displacement (mm)	3.1 mm
Compression Load (N)	1.14 N
Pre Load (N)	3.3 N
Stiffness	3.66 N/cm

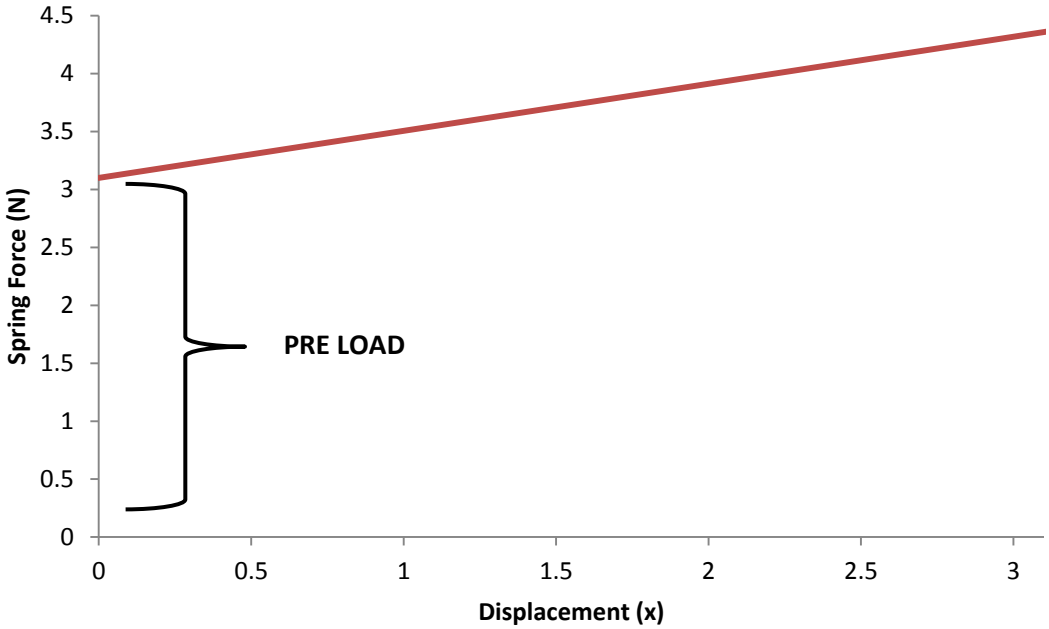

Figure 3.5 Spring Characteristics of Model #1

The springs which are used in check valves are initially pre-loaded as shown in figure 3.5. This pre-loading force and compression force of the spring are defined to the valves in Autodesk Simulation motion module. For this reason springs are not drawn in CFD model.

3.5.1.2 Mesh

In order to prepare the mesh efficiently, the distribution of mesh must be sufficient enough to solve velocity and pressure gradients. If the fluid flows in one direction with a little gradient, coarser mesh may be used at those zones. In the regions where large gradients such as separation, vortex and flow reversal occur, finer mesh is required in this condition.

If high-gradient flow occurs in the model, the mesh must be refined in those regions. For that purpose fluid or solid in which high gradients occur, must be drawn as separate parts in the CAD domain. In this study the path of check valves and pistons are drawn as separate parts and their meshes are locally refined. (shown in figure 3.6)

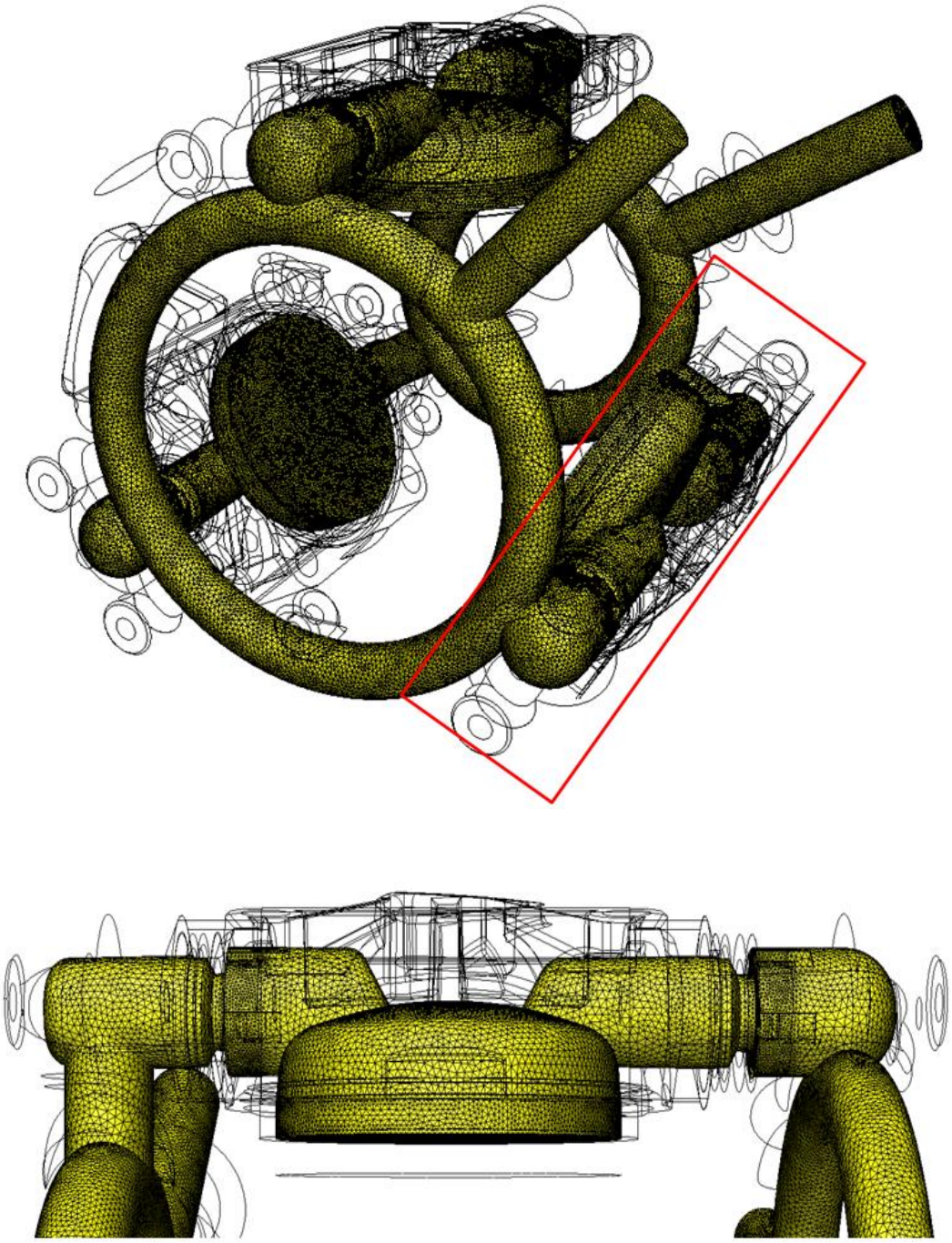

Figure 3.6 Mesh of Model #1

There are 2456987 fluid nodes, 4365412 fluid elements, 451236 solid nodes and 1023651 solid elements in model #1.

The mesh plays an important role on the solution. In CFD investigations, the analyst should use a mesh structure on the domain being examined that allows the

important flow features to be determined while placing minimum demands upon the finite resources of the computer.

If the mesh size is sufficient enough for a given model, the results will not differ even when a finer mesh size is used. The solution which is done by using that sufficient mesh size called “mesh independent solution”.

In order to find mesh independent solution, 4 analyses are made by using different mesh sizes. To show that analysis results do not change with mesh size, volumetric efficiency is chosen as a reference parameter. (Figure 3.7)

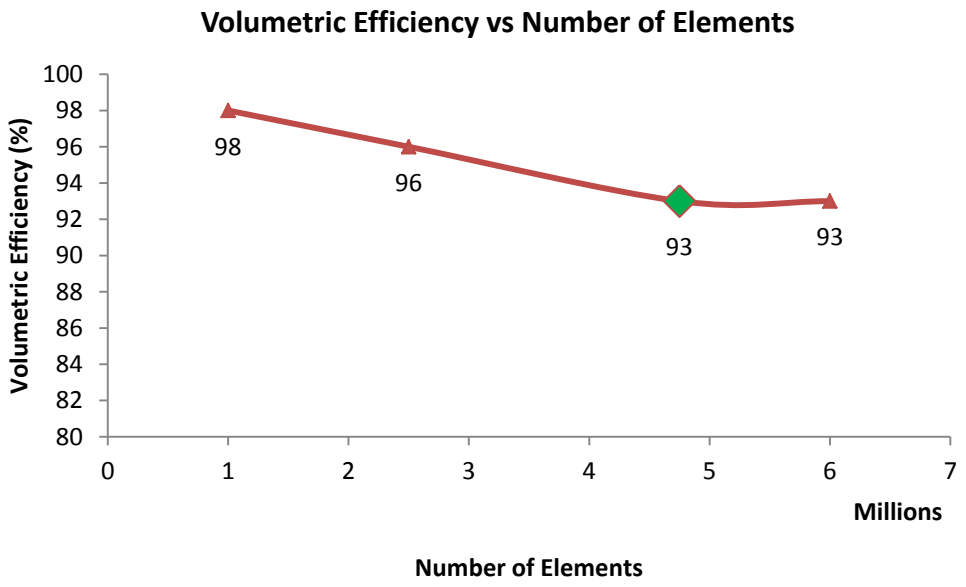

Figure 3.7 Optimum Mesh for Model #1

3.5.1.3 Solution

Autodesk Simulation CFD solves 6 equations which are basic conservation equations.

- Conservation of Mass

$$\frac{\partial \rho}{\partial t}+\frac{\partial \rho u}{\partial x}+\frac{\partial \rho v}{\partial y}+\frac{\partial \rho w}{\partial z}=0 \tag{3.1}$$

- Conservation of Momentum

x-momentum:

$$\begin{aligned}&\rho\frac{\partial u}{\partial t}+\rho u\frac{\partial u}{\partial x}+\rho v\frac{\partial u}{\partial y}+\rho w\frac{\partial u}{\partial z}=\rho g_x-\frac{\partial P}{\partial x}+\frac{\partial}{\partial x}\left[2\mu\frac{\partial u}{\partial x}\right]\\&+\frac{\partial}{\partial y}\left[\mu\left(\frac{\partial u}{\partial y}+\frac{\partial v}{\partial x}\right)\right]+\frac{\partial}{\partial z}\left[\mu\left(\frac{\partial u}{\partial z}+\frac{\partial w}{\partial x}\right)\right]+S_w+S_{DR}\end{aligned} \tag{3.2}$$

y-momentum:

$$\begin{aligned}&\rho\frac{\partial v}{\partial t}+\rho u\frac{\partial v}{\partial x}+\rho v\frac{\partial v}{\partial y}+\rho w\frac{\partial v}{\partial z}=\rho g_y-\frac{\partial P}{\partial y}+\frac{\partial}{\partial x}\left[\mu\left(\frac{\partial u}{\partial y}+\frac{\partial v}{\partial x}\right)\right]\\&+\frac{\partial}{\partial y}\left[2\mu\frac{\partial v}{\partial y}\right]+\frac{\partial}{\partial z}\left[\mu\left(\frac{\partial v}{\partial z}+\frac{\partial w}{\partial x}\right)\right]+S_w+S_{DR}\end{aligned} \tag{3.3}$$

z-momentum:

$$\begin{aligned}&\rho\frac{\partial w}{\partial t}+\rho u\frac{\partial w}{\partial x}+\rho v\frac{\partial w}{\partial y}+\rho w\frac{\partial w}{\partial z}=\rho g_z-\frac{\partial P}{\partial z}+\frac{\partial}{\partial x}\left[\mu\left(\frac{\partial u}{\partial z}+\frac{\partial w}{\partial x}\right)\right]\\&+\frac{\partial}{\partial y}\left[\mu\left(\frac{\partial v}{\partial z}+\frac{\partial w}{\partial y}\right)\right]+\frac{\partial}{\partial z}\left[2\mu\frac{\partial w}{\partial z}\right]+S_w+S_{DR}\end{aligned} \tag{3.4}$$

- Energy Equation (For incompressible flow)

$$\begin{aligned}&\rho C_p\frac{\partial T}{\partial t}+\rho C_p u\frac{\partial T}{\partial x}+\rho C_p v\frac{\partial T}{\partial y}+\rho C_p w\frac{\partial T}{\partial z}=\frac{\partial}{\partial x}\left[k\frac{\partial T}{\partial x}\right]\\&+\frac{\partial}{\partial y}\left[k\frac{\partial T}{\partial y}\right]+\frac{\partial}{\partial z}\left[k\frac{\partial T}{\partial z}\right]+q_V\end{aligned} \tag{3.5}$$

- Turbulent Kinetic Energy (TKE) and Turbulent Energy Dissipation (TED)

TKE:

$$\rho\frac{\partial K}{\partial t}+\rho u\frac{\partial K}{\partial x}+\rho v\frac{\partial K}{\partial y}+\rho w\frac{\partial K}{\partial z}=\frac{\partial}{\partial x}\left[\left(\frac{\mu_t}{\sigma_K}+\mu\right)\frac{\partial K}{\partial x}\right]$$
$$+\frac{\partial}{\partial y}\left[\left(\frac{\mu_t}{\sigma_K}+\mu\right)\frac{\partial K}{\partial y}\right]+\frac{\partial}{\partial z}\left[\left(\frac{\mu_t}{\sigma_K}+\mu\right)\frac{\partial K}{\partial z}\right]-\rho\varepsilon \tag{3.6}$$
$$+\mu_t\left[2\left(\frac{\partial u}{\partial x}\right)^2+2\left(\frac{\partial v}{\partial y}\right)^2+2\left(\frac{\partial w}{\partial z}\right)^2+\left(\frac{\partial u}{\partial y}+\frac{\partial v}{\partial x}\right)^2+\left(\frac{\partial u}{\partial z}+\frac{\partial w}{\partial x}\right)^2+\left(\frac{\partial v}{\partial z}+\frac{\partial w}{\partial y}\right)^2\right]$$

TED:

$$\rho\frac{\partial \varepsilon}{\partial t}+\rho u\frac{\partial \varepsilon}{\partial x}+\rho v\frac{\partial \varepsilon}{\partial y}+\rho w\frac{\partial \varepsilon}{\partial z}=\frac{\partial}{\partial x}\left[\left(\frac{\mu_t}{\sigma_\varepsilon}+\mu\right)\frac{\partial \varepsilon}{\partial x}\right]$$
$$+\frac{\partial}{\partial y}\left[\left(\frac{\mu_t}{\sigma_\varepsilon}+\mu\right)\frac{\partial \varepsilon}{\partial y}\right]+\frac{\partial}{\partial z}\left[\left(\frac{\mu_t}{\sigma_\varepsilon}+\mu\right)\frac{\partial \varepsilon}{\partial z}\right]-C_2\rho\frac{\varepsilon^2}{K} \tag{3.7}$$
$$+C_1\mu_t\frac{\varepsilon}{K}\left[2\left(\frac{\partial u}{\partial x}\right)^2+2\left(\frac{\partial v}{\partial y}\right)^2+2\left(\frac{\partial w}{\partial z}\right)^2+\left(\frac{\partial u}{\partial y}+\frac{\partial v}{\partial x}\right)^2+\left(\frac{\partial u}{\partial z}+\frac{\partial w}{\partial x}\right)^2+\left(\frac{\partial v}{\partial z}+\frac{\partial w}{\partial y}\right)^2\right]$$

To predict performance characteristics and flow field inside the pump, the mentioned discretized equations were solved in three-dimensions using an iterative, segregated solution method where in the equation sets for each dependent variable was solved sequentially.

The Monotone streamline upwind solution algorithm is used to treat the pressure-velocity coupling of the flow field. In solving the transport equations, no-slip boundary condition was imposed on the velocity components at the wall.

The RNG model, low Reynolds k-epsilon model, k-epsilon model and Eddy Viscosity models are available in Autodesk Simulation CFD v2012. The k-epsilon model is used in this study. The reason of using k-epsilon model is; it is typically more accurate than the constant eddy viscosity and constant eddy viscosity is recommended for lower speed turbulent models.

Since the analysis is transient, time step size must be determined. Time step size should be small enough to maintain solver stability and capture the physics of phenomena.

The pump used in analysis operates at 540 rpm, so time required for one stroke can be calculated as;

$$\tau = \frac{60[\mathrm{s}]}{540[\mathrm{rpm}]} = 0.111\ \mathrm{s}$$

Autodesk Simulation CFD calculated the time step size based on the defined motion parameters and the mesh size as 0.00867s. Using the time step size calculated by Autodesk Simulation, causes solution to diverge. For this reason, first time step size is chosen as 0.0003 s (1/360th of one stroke) then the time step size is reduced to 0.00015 s (1/720th of one stroke) and the results are compared. Since there is a minor difference between two cases the bigger time step size (0.0003 s) is used in analyses. This also captures check valves opening and closing processes.

The analysis is run for 1800 iterations (5 strokes) until the solution stability is maintained. The convergence graph is given in figure 3.8

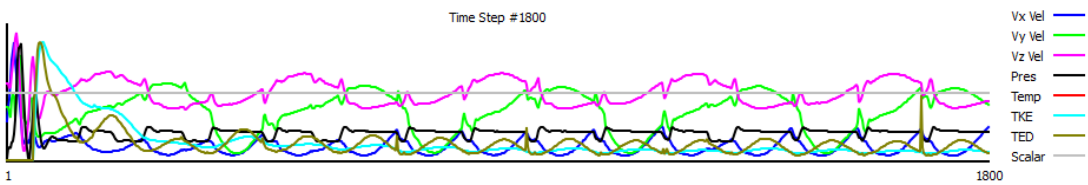

Figure 3.8 Convergence Graph of Model #1

The solution took 76 hours on the computer with the following specifications;

Table 3.4 Computer Specifications

Computer Specifications	
Mainboard	GIGABYTE P67X-UD3-B3 Intel P67 Socket 1155 DDR3 2133MHz (O.C.) SATA 3.0
CPU	INTEL Core i7 2600K Socket 1155 3.4GHz 8MB Cache 32nm
RAM	CORSAIR 16GB (4x4GB) Vengeance DDR3 1600MHz CL9 Dual Kit Ram
Graphics Processor	SAPPHIRE HD6950 GDDR5 2GB 256Bit AMD Radeon DX11

3.5.1.4 Results

In this section velocity distributions and velocity vectors in the discharge manifold for different crank angles are given.

For θ=90˚;

In figure 3.9, it is observed that piston #1 is active at this crank angle, due to the fact that there is 120˚ time shift between the pistons, piston #2 and piston #3 do not contribute to discharge volume flow rate at this instant.

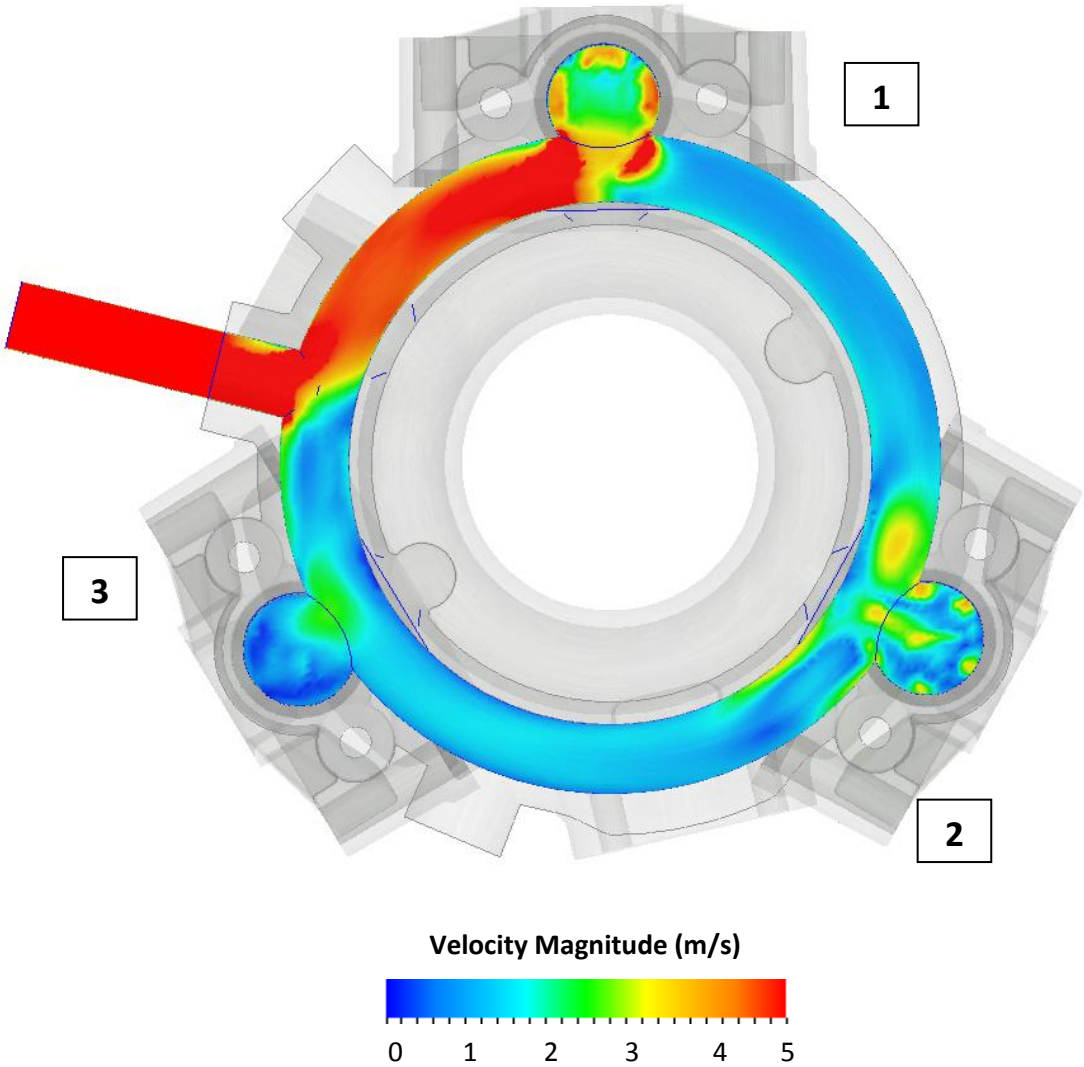

Figure 3.9 Velocity Distribution in the Discharge manifold for 90˚ crank angle

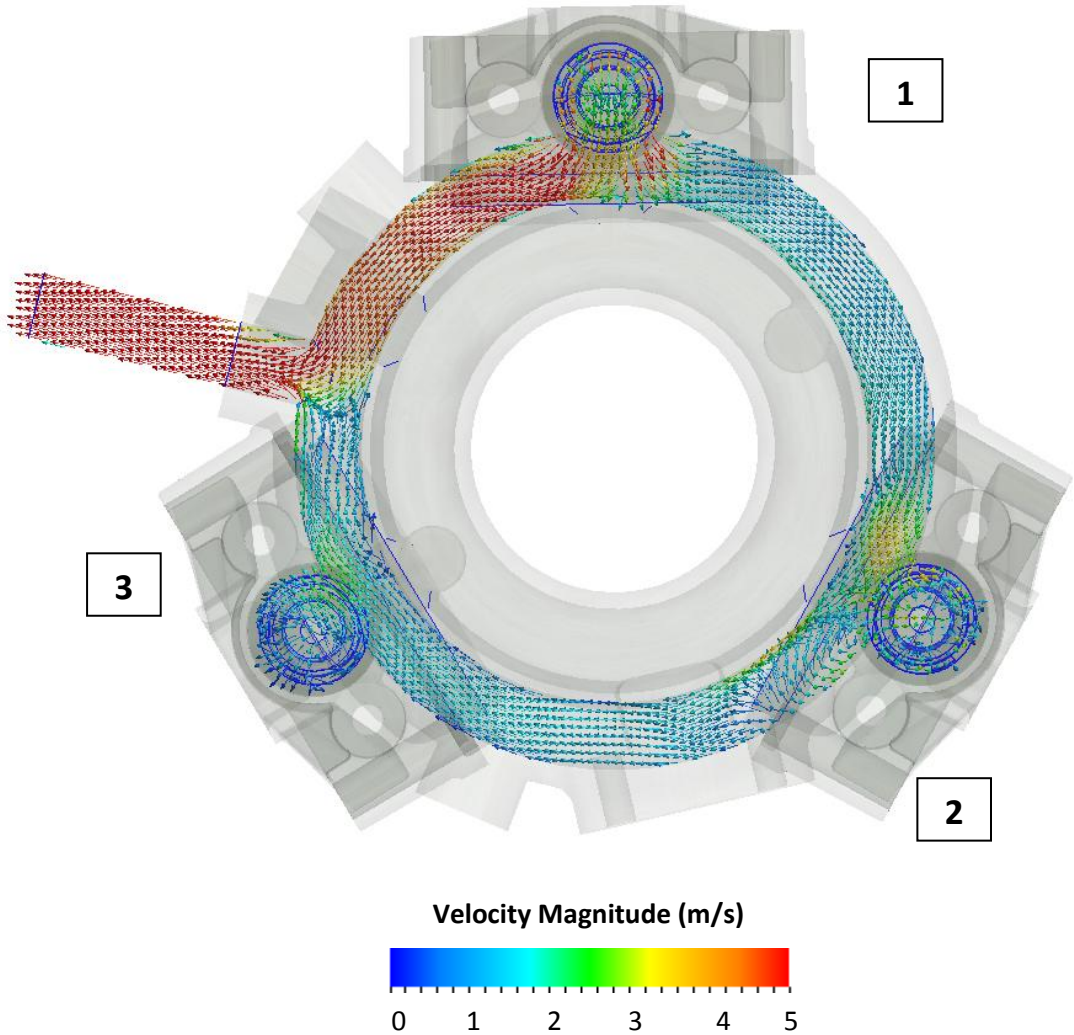

Figure 3.10 Velocity Vectors in the Discharge Manifold for 90° Crank Angle

From velocity vectors (Figure 3.10), it is seen that some of the fluid coming from piston #1 does not head for to the exit of the pump. It prefers to go towards piston #2 direction. This condition causes the pump to work inefficiently. From figure 2.9 it is also seen that the velocity magnitude of the fluid flows through piston #1 to outlet of the pump increases. Since piston #2 and piston #3 are inactive at this crank angle the velocity magnitude through piston #2 and piston #3 decreases.

For θ=180˚;

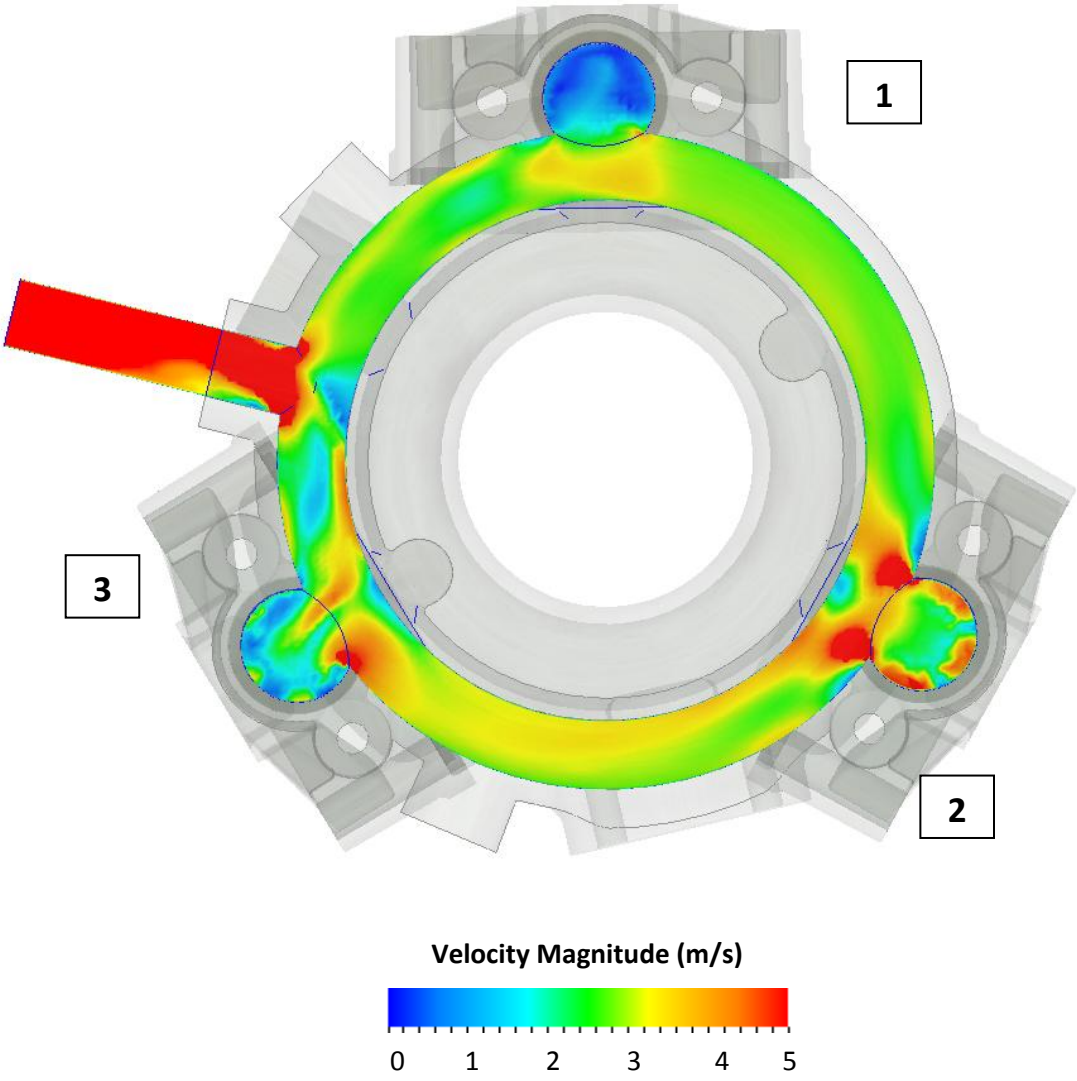

Figure 3.11 Velocity Distribution in the Discharge Manifold for 180˚ Crank Angle

Similar to results obtained for 90˚ crank angle, due to 120˚ time shift between the pistons, piston #1 and piston #3 do not contribute to the discharge flow rate at this instant. Therefore the velocities in the piston #1 and piston #3 reduce.

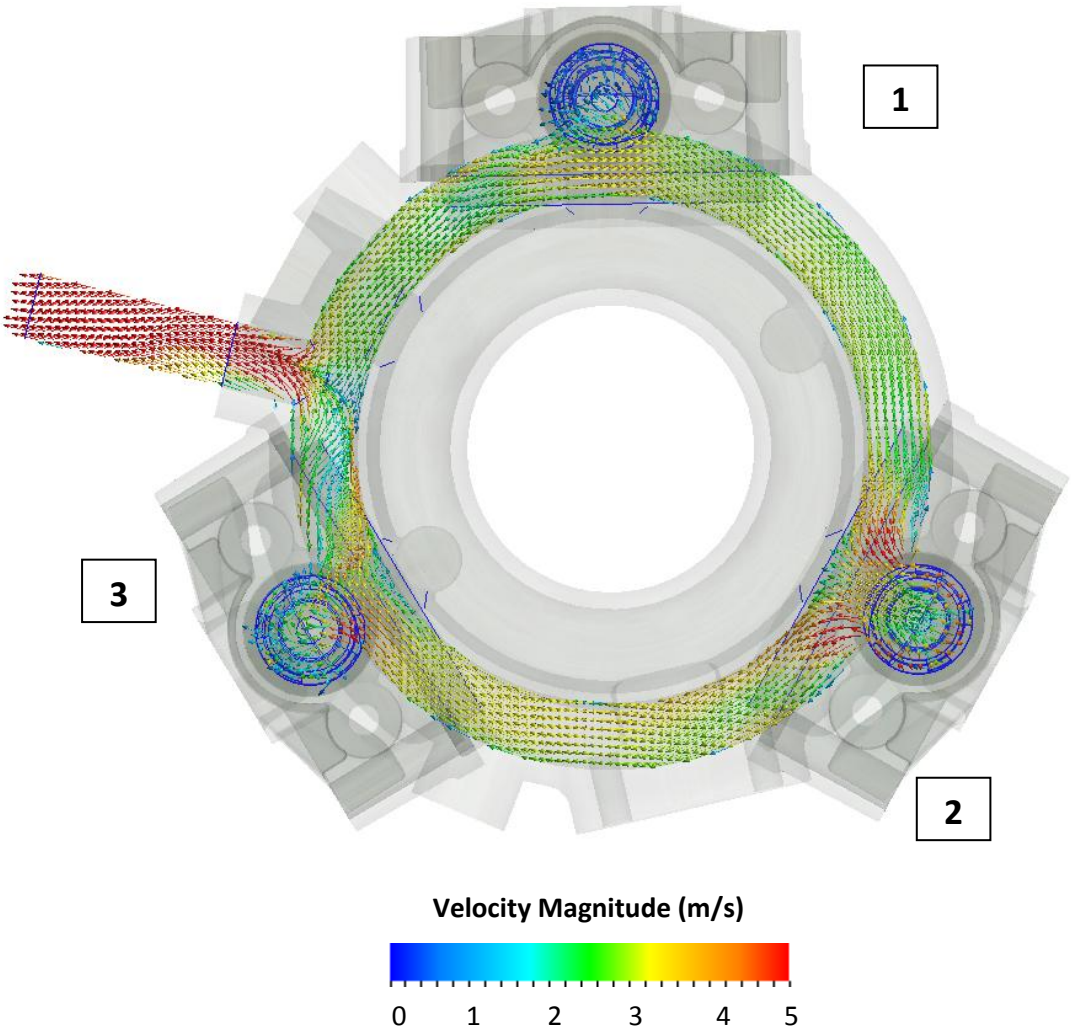

Figure 3.12 Velocity Vectors in the Discharge Manifold for 180° Crank Angle

From figure 3.12 it is observed that fluid flow which is discharged from piston #2 separates into two directions and goes to the outlet of the pump. It is observed that Velocities in the direction of piston #3 are higher than the other direction.

For θ=270˚;

Similar to 180˚ crank angle, due to 120˚ time shift between the pistons, piston #1 does not contribute to the discharge flow rate at this instant. From figure 3.13 it is seen that velocity magnitude of the fluid which is discharged from piston #3 increases, since piston #1 is inactive at this crank angle,

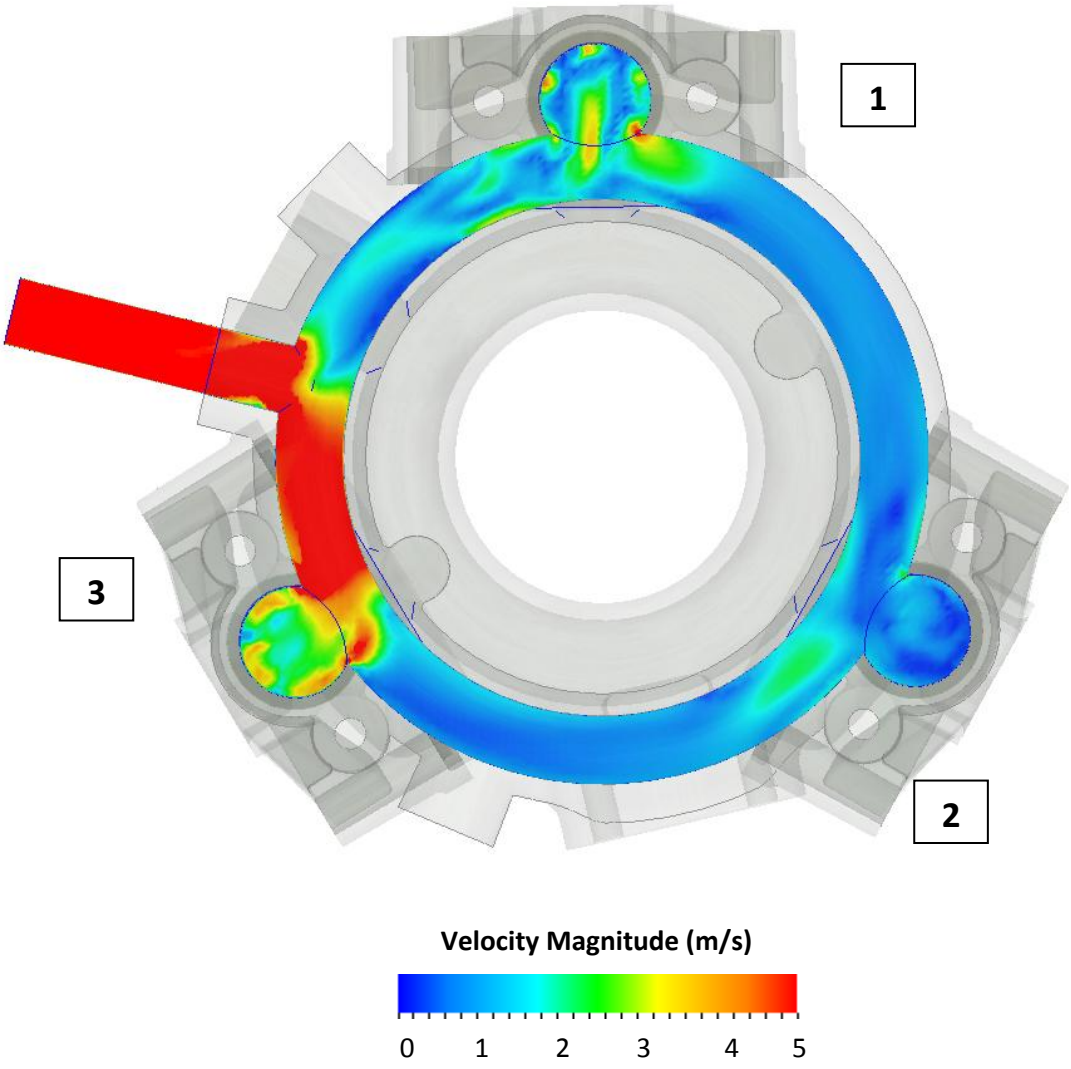

Figure 3.13 Velocity Distribution in the Discharge Manifold for 270˚ Crank Angle

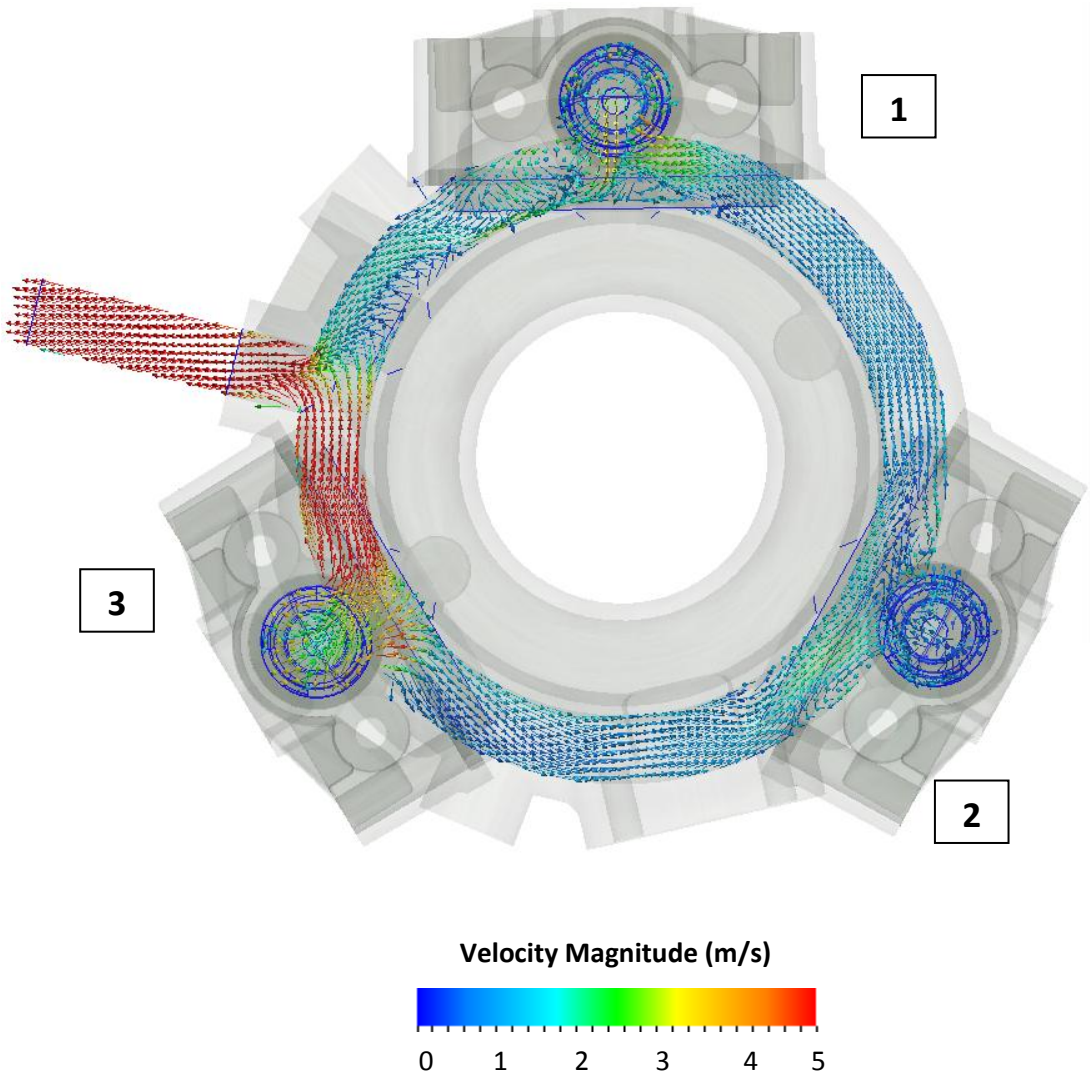

Figure 3.14 Velocity Vectors in the Discharge Manifold for 270° Crank Angle

From velocity vectors (Figure 3.14), it is observed that some of the fluid coming from piston #3 does not head for the exit of the pump. It prefers go through piston #2 direction. This causes the pump to work inefficiently.

The volume flow rate versus crank angle graph is given in figure 3.15

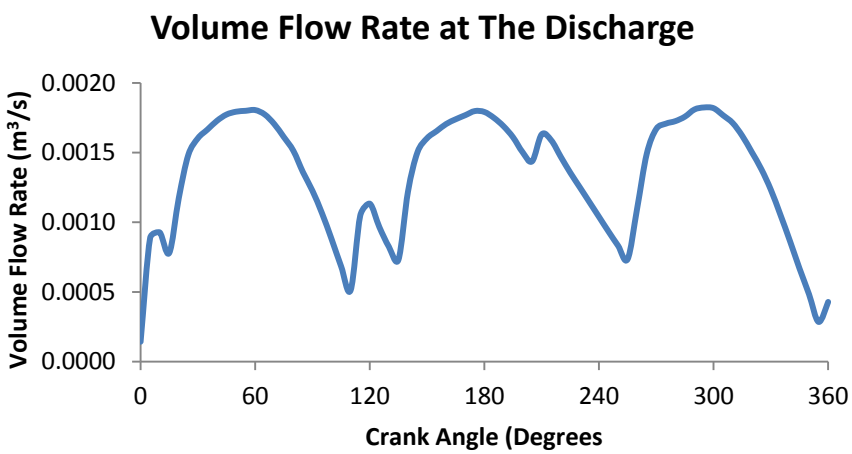

Figure 3.15 Volume Flow Rate of Model #1 at the Exit of the Pump

Volumetric efficiency of the pump can be calculated using equation (2.5)

$$\eta_v = \frac{Q_{actual}}{Q_{theoretical}} \tag{2.5}$$

Hydraulic Efficiency can be calculated using equation (3.8)

$$\eta_h = \frac{P_{hydraulic}}{P_{input}} = \frac{\Delta p x Q_{actual}}{Txn} \tag{3.8}$$

Where;

Δp: Pressure differential between suction and discharge (Pa)

Q_{actual}: Actual displacement of the pump (m^3/s)

$Q_{theoretical}$: Ideal displacement of the pump (m^3/s)

T: Torque (Nm)

n: Rotational velocity of the pump (rad/s)

Due to the fact that connecting rod and shaft are not modeled in CFD analysis, power input cannot be calculated using Txn formula. Input power is calculated using P_{input}= FxV formula. Instead of using P_{input}=Txn.

Where;

F: Force acting on the piston (N)

V: Velocity of the piston (m/s)

So hydraulic efficiency becomes;

$$\eta_h = \frac{P_{hydraulic}}{P_{input}} = \frac{\Delta p x Q_{actual}}{FxV} \tag{3.9}$$

Since the analysis is transient FxV and Q_{actual} are changing in each time step. In order to find average values of FxV and Q_{actual}, time average integral is calculated using numerical integration method known as trapezoidal rule. After calculating the average values the volumetric and hydraulic efficiencies of the pump becomes;

$$\eta_v = \frac{0.00137814[m^3/s]}{0.0015[m^3/s]} = 0.92 \ \ (92\%)$$

$$\eta_h = \frac{40x10^5[Pa]x0.00137814[m^3/s]}{6562.543[W]} = 0.84 \ (84\%)$$

3.5.2 Model # 2

From model #1, it is seen that positive displacement pump analyses are very difficult and time consuming because of the nature of the flow and complexity of the geometry. So a different analysis strategy is developed for investigating the effect of valve characteristics and piston shape on the pump efficiency.

There is a geometrical periodicity in the model. And due to the fact that investigating and improving one part of the model means, improving the whole model, only one part of the pump as shown in figure 3.16 is analyzed.

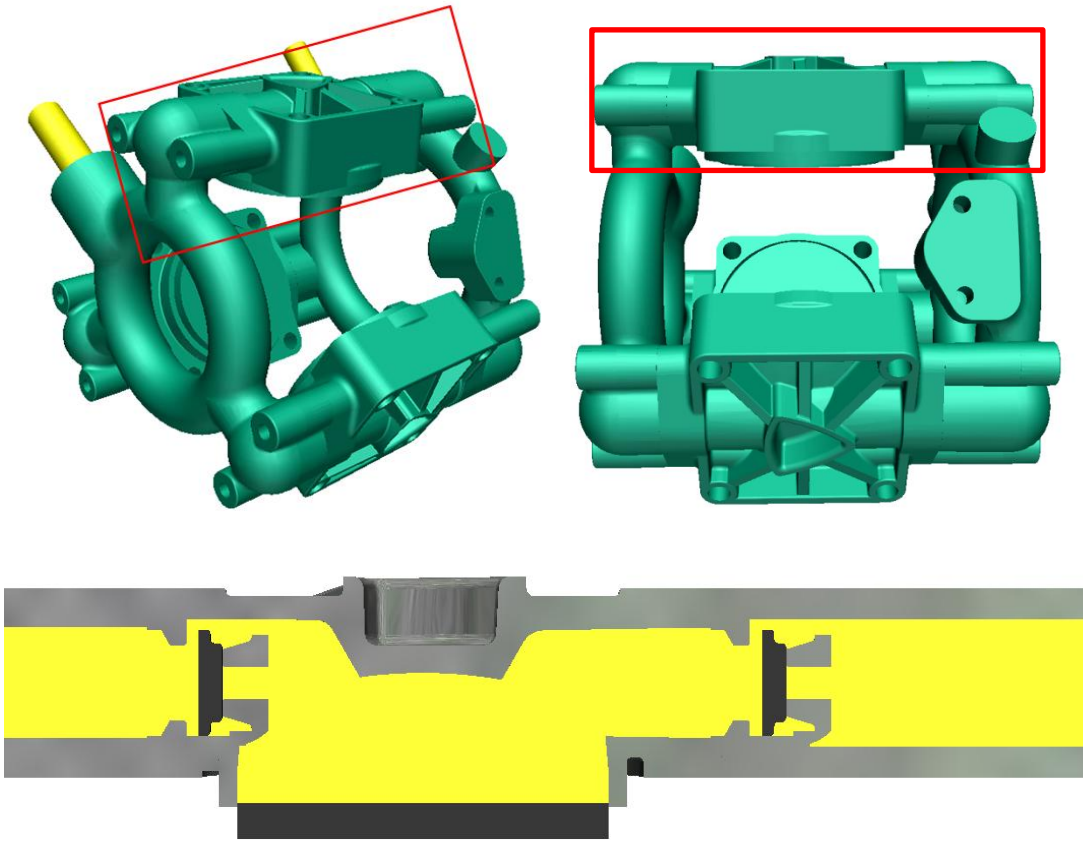

Figure 3.16 Model #2

Since the flow pattern is symmetric inside the 1-piston geometry, only half of the model is analyzed as shown in figure 3.16

After the mesh dependency analyses is applied to model #2, optimum mesh is found and is shown in figure 3.17

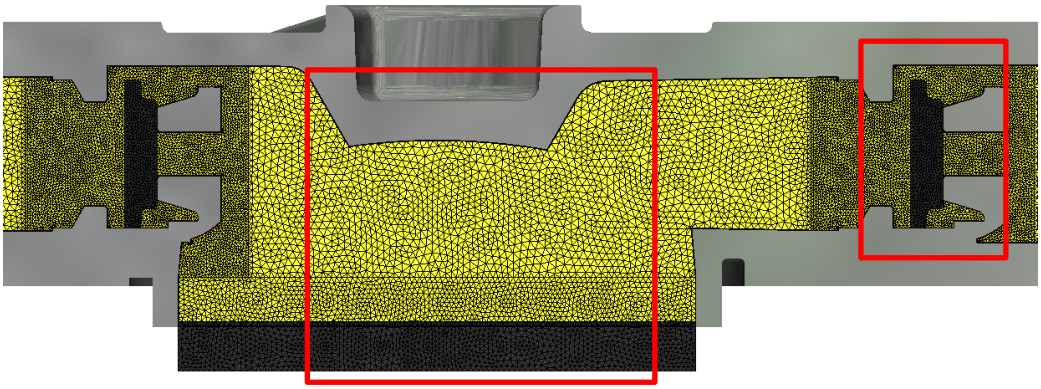

Figure 3.17 Mesh of Model #2

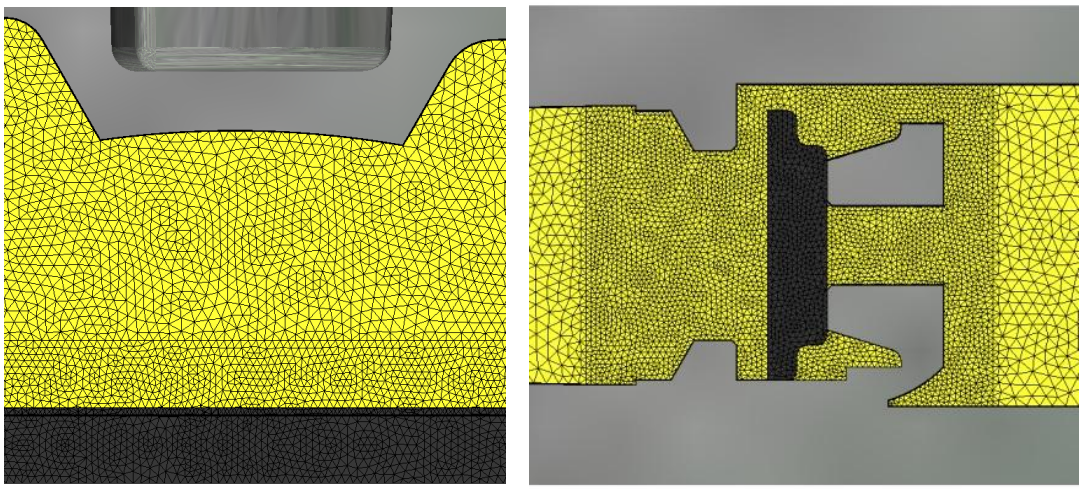

Figure 3.17 Mesh of Model #2 (Cont.)

There are 968745 fluid nodes, 2165845 fluid elements, 198754 solid nodes and 446539 solid elements in model #2. The analysis of model #2 took 35 hours on the same computer whose specifications are mentioned in table 3.4

0 bar pressure (gage) boundary condition and 40 bar pressure (gage) boundary condition are applied to the inlet and outlet of the pump is shown in figure 3.18

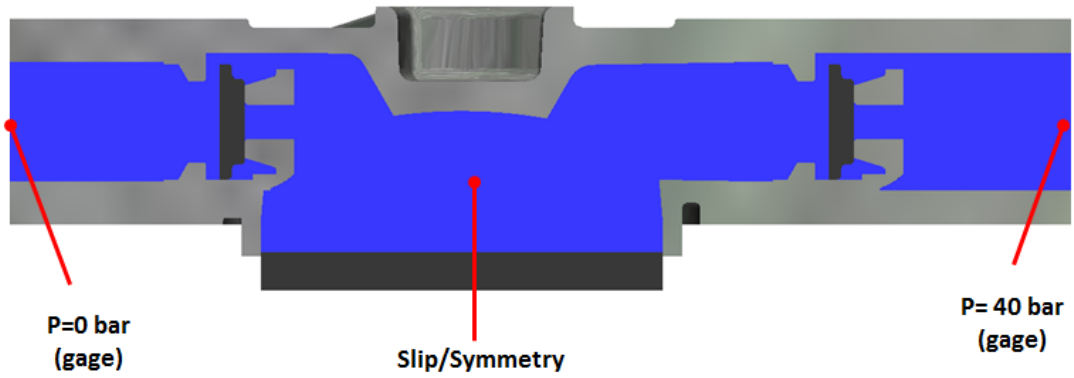

Figure 3.18 Boundary Conditions of Model #2

User defined motion is assigned to the piston (figure 3.19) and flow induced motion is assigned to the check valves.

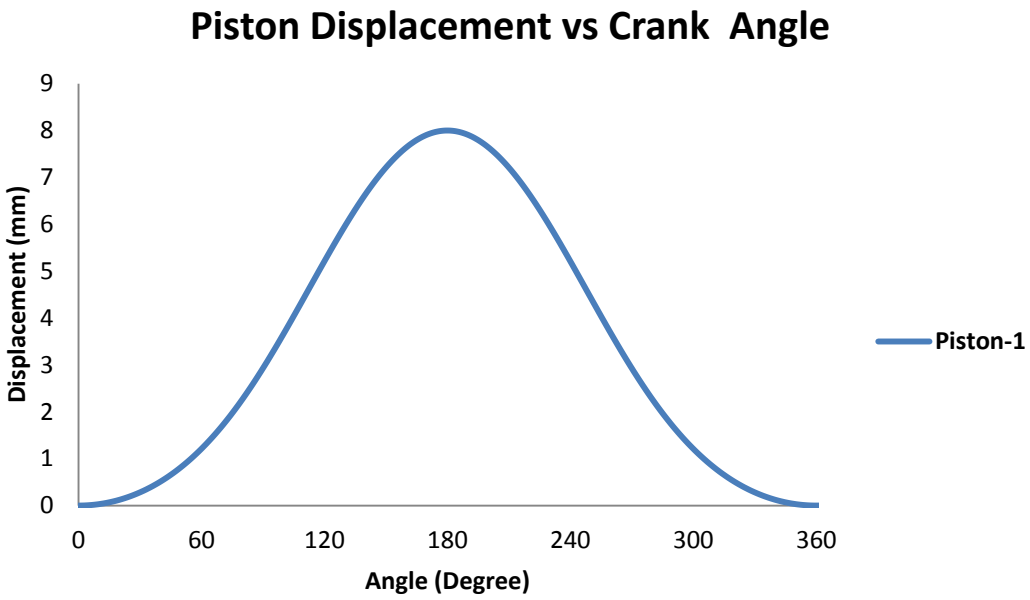

Figure 3.19 Piston Displacement vs. Crank Angle

The analysis is run for 1800 iterations (5 strokes) with time step size 0.0003 s until the solution stability is achieved.

The velocity and pressure distributions for different crank angles are given in the following figures. (First one is velocity and second one is pressure distribution).

For θ=60˚;

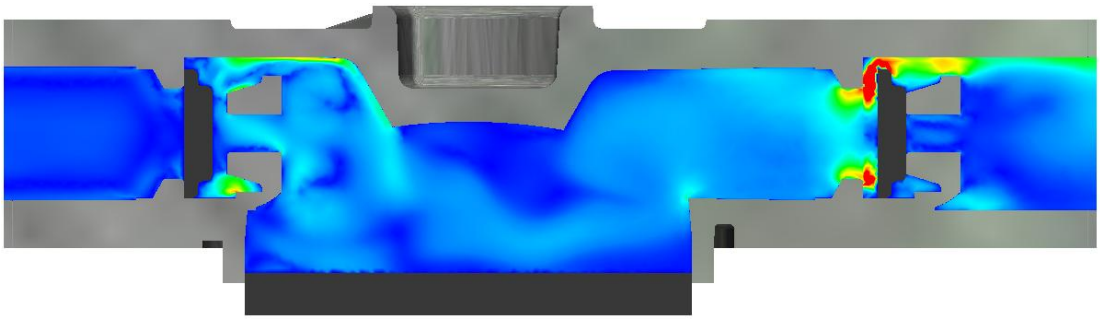

Figure 3.20 Velocity and Pressure Distributions of Model #2 for 60˚ Crank Angle

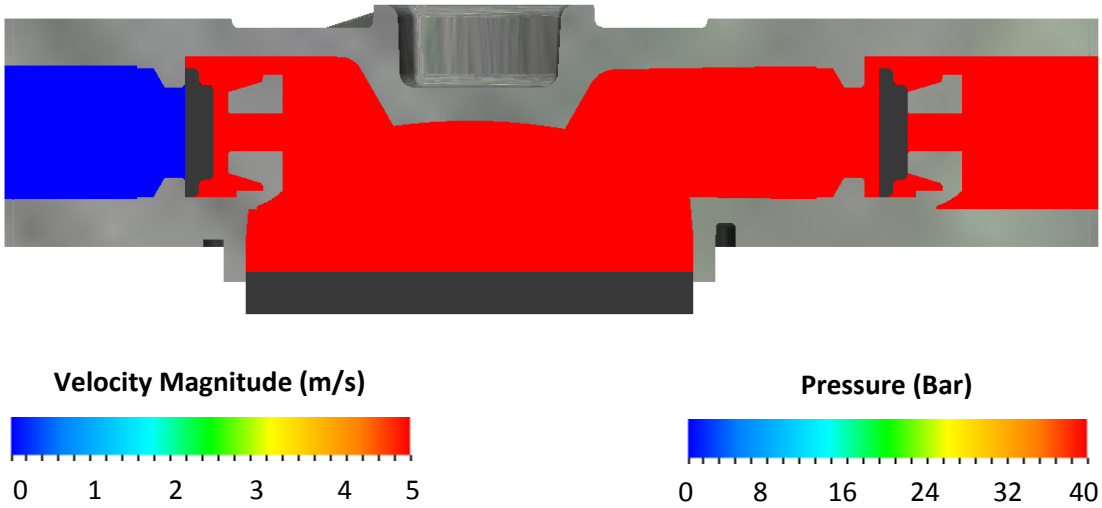

Figure 3.20 Velocity and Pressure Distributions of Model #2 for 60˚ (Cont.)

Beginning of the discharge, it is seen that suction valve closes and discharge valve starts opening. Cylinder pressure is greater than the discharge pressure opens the discharge valve.

For θ=120˚;

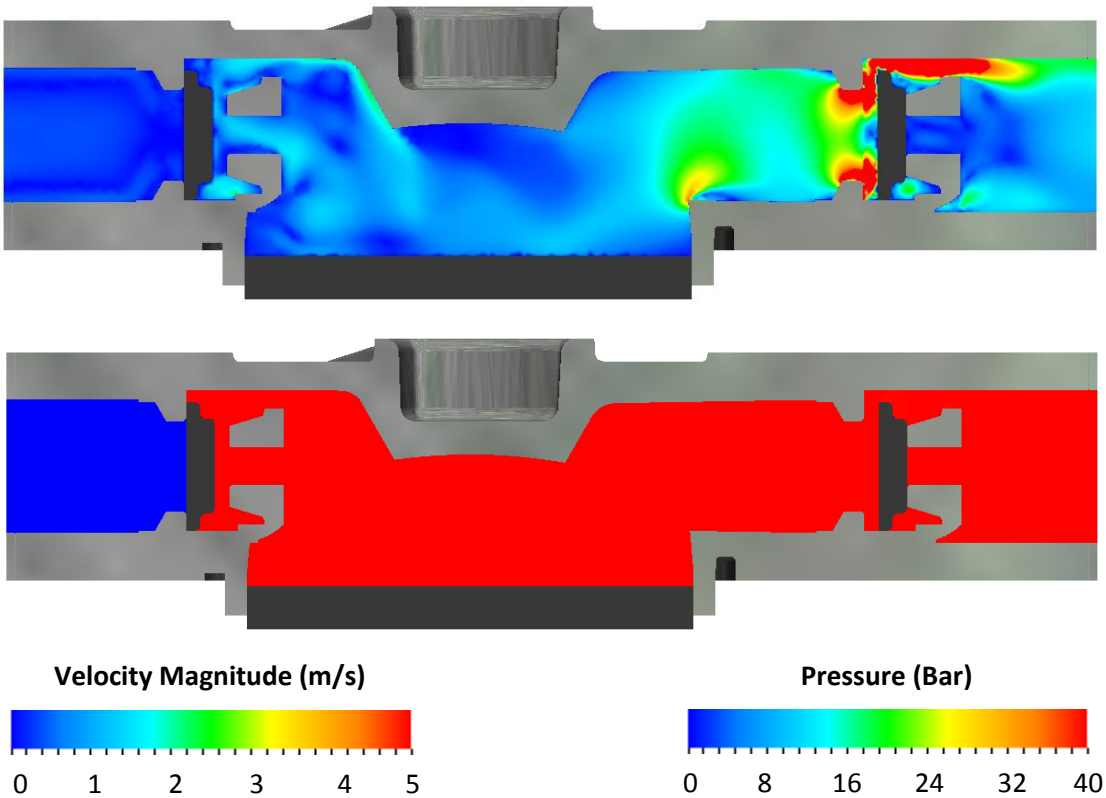

Figure 3.21 Velocity and Pressure Distributions of Model #2 for 120˚ Crank Angle

As discharge process continues velocity through discharge valve increases also cylinder pressure continues to increase. As long as cylinder pressure is greater than discharge pressure, discharge valve remains open.

For θ=180˚;

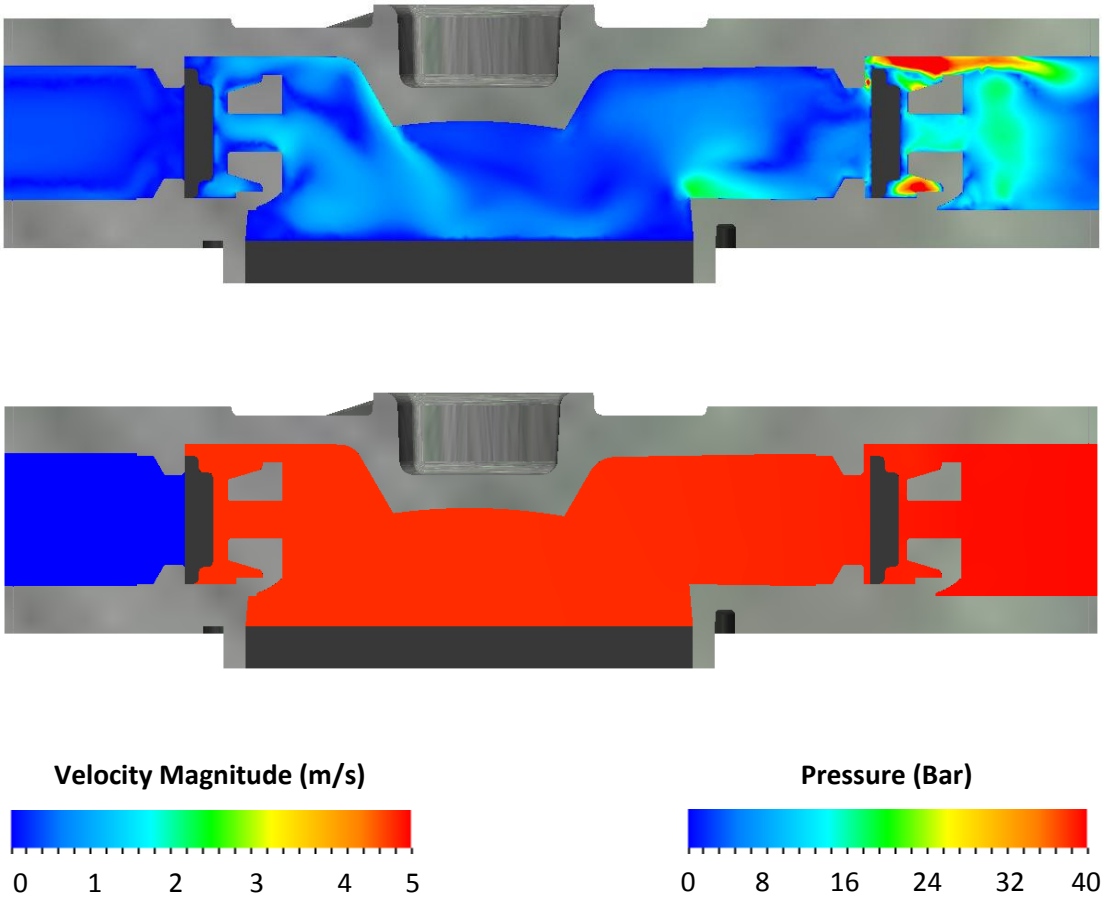

Figure 3.22 Velocity and Pressure Distributions of Model #2 for 180˚ Crank Angle

At the end of the discharge and beginning of the suction process, after this angle, discharge valve starts closing and suction valve starts opening. Velocity magnitude through discharge valve and cylinder pressure reduce.

For θ=240˚;

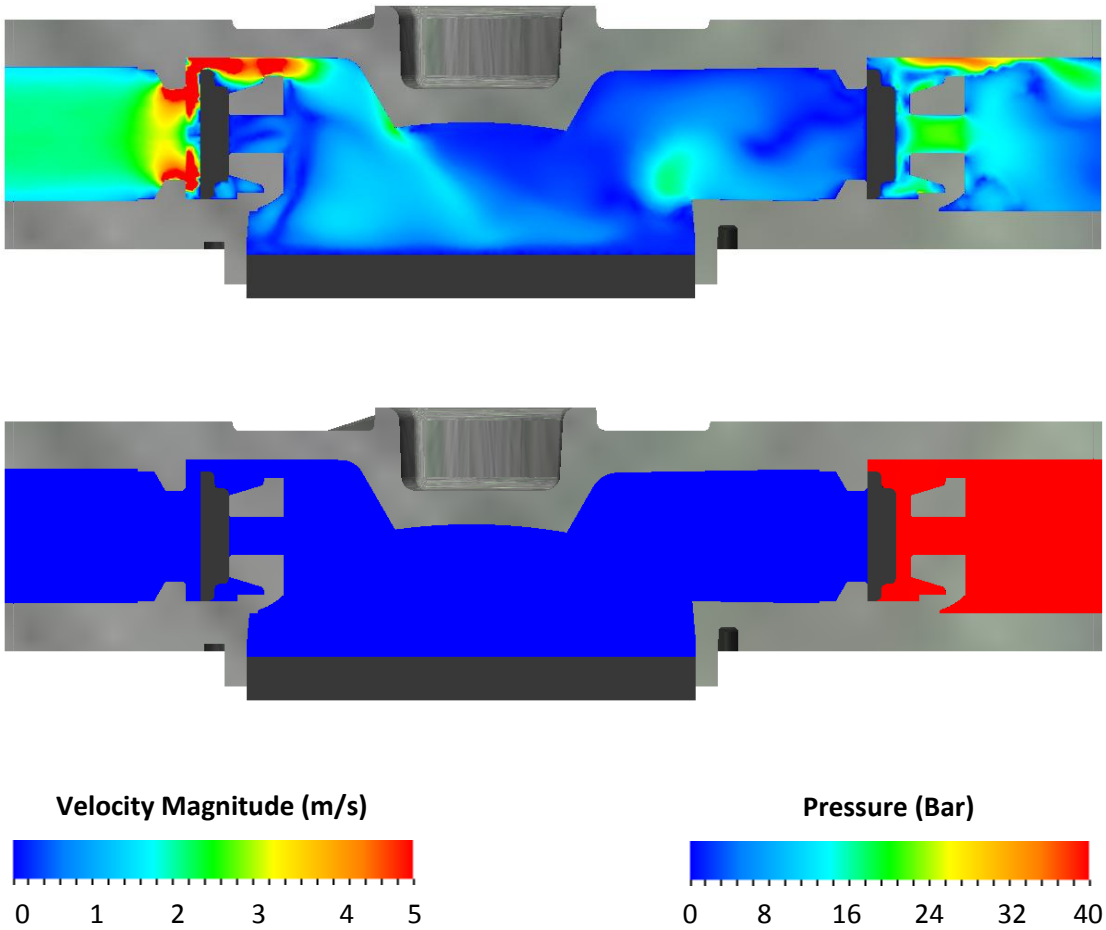

Figure 3.23 Velocity and Pressure Distributions of Model #2 for 240˚ Crank Angle

Suction process continues, discharge valve closes and suction valve opens. Some water escapes inside the cylinder from the discharge side. (Back flow), cylinder pressure continues to reduce. Suction pressure becomes greater than the cylinder pressure as long as suction pressure is greater than cylinder pressure, suction valve remains open.

For θ=300˚;

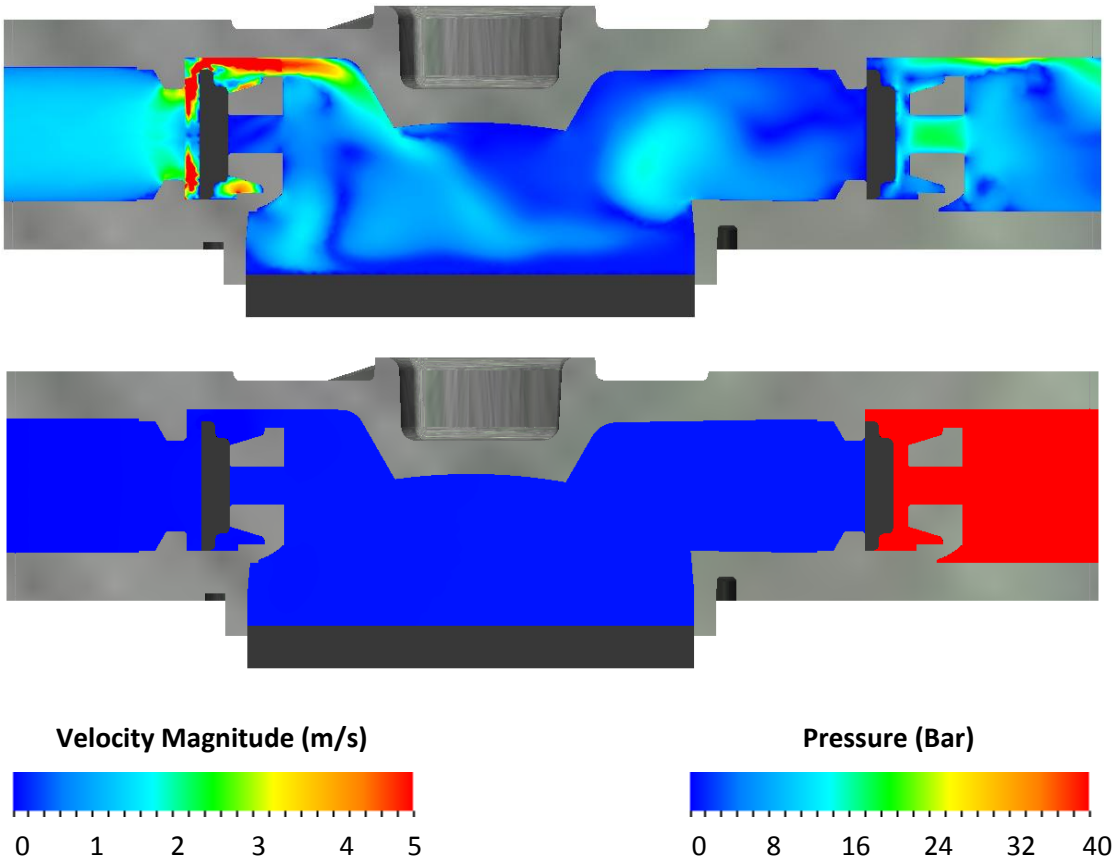

Figure 3.24 Velocity and Pressure Distributions of Model #2 for 300˚ Crank Angle

Suction process continues, suction valve is fully opened. Cylinder pressure continues to reduce. Velocity magnitude through suction valve greatly increases.

For θ=360˚;

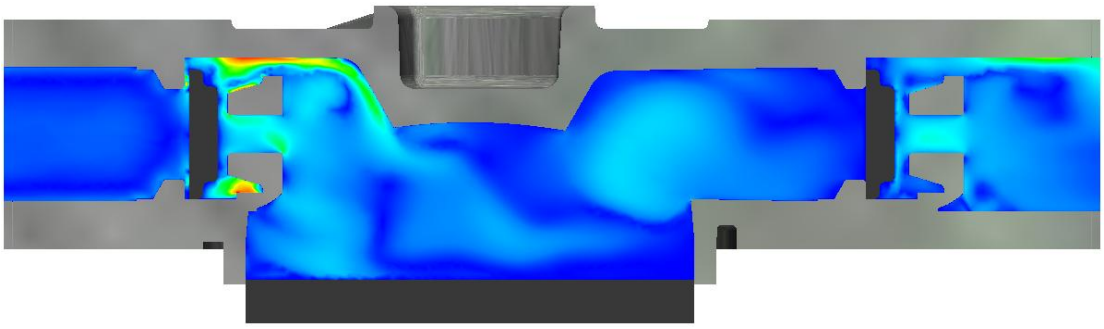

Figure 3.25 Velocity and Pressure Distributions of Model #2 for 360˚ Crank Angle

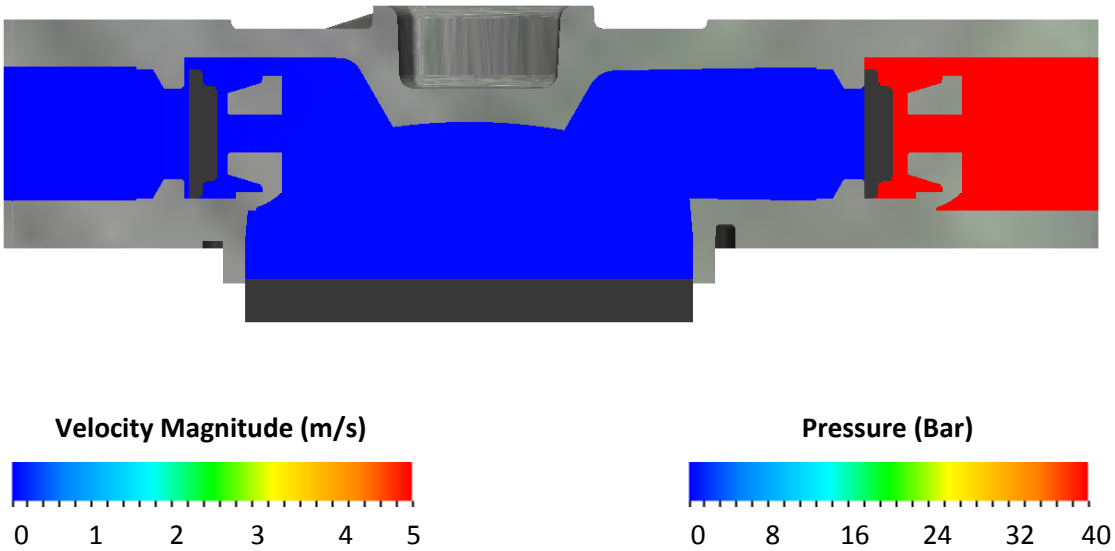

Figure 3.25 Velocity and Pressure Distributions of Model #2 for 360° (Cont.)

At the end of suction process, suction valve starts closing and cylinder pressure increases.

In figure 3.26 volume flow rate at the discharge is given for model #2;

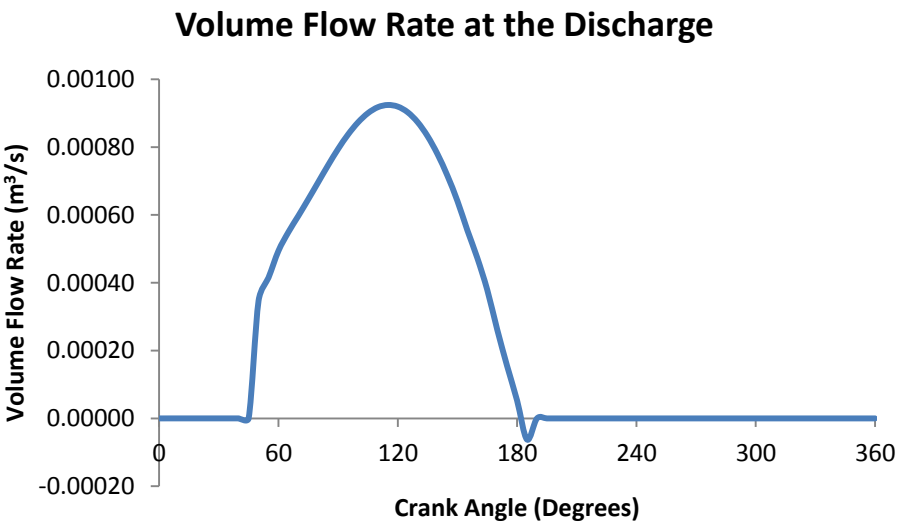

Figure 3.26 Volume Flow Rate of Model #2 at the Exit of the Pump

Since the analysis is transient FxV and Q_{actual} changes in time. In order to find average values of FxV and Q_{actual}, time average integral is calculated using

numerical integration method known as trapezoidal rule. Sample calculation of power input to the system is given in appendix B.

Volumetric efficiency can be calculated using equation (2.5)

$$\eta_v = \frac{Q_{actual}}{Q_{theoretical}} = \frac{0.0004803[m^3/s]}{0.0005[m^3/s]} = 0.96 \ \ (96\%)$$

Hydraulic efficiency can be calculated using equation (3.9)

$$\eta_h = \frac{P_{hydraulic}}{P_{input}} = \frac{\Delta p x Q_{actual}}{FxV} = \frac{40x10^5[Pa]x0.0004803[m^3/s]}{2114.386[W]} = 0.91 \ (91\ \%)$$

3.5.3 Model #3-Model #10

Since model #3-model #10 are constructed for investigating the spring stiffness effect and the effect of masses of the valves on the pump efficiency, mesh, boundary and motion conditions, and time step size are identical with model #2.

In figure 3.27 spring stiffness for model #2 – model #6 are shown.

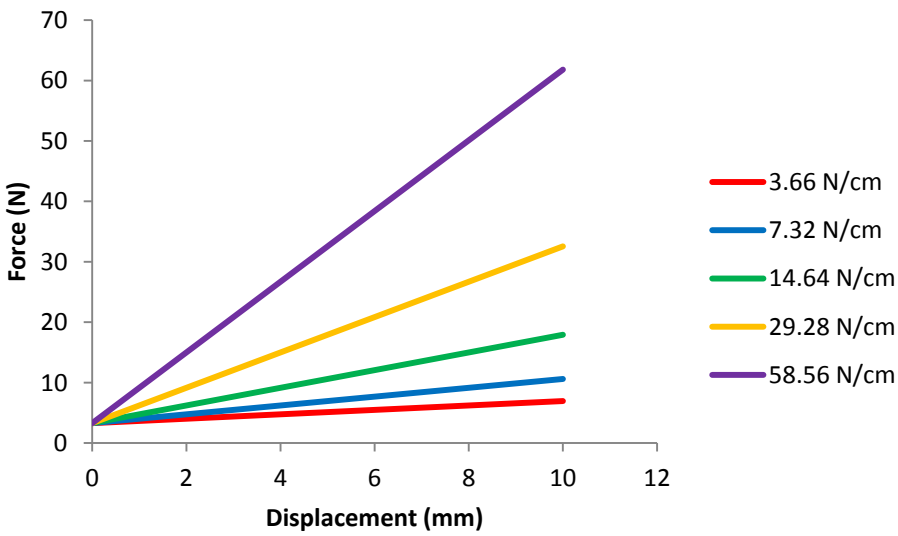

Figure 3.27 Spring Stiffness of Models #2 - #6

3.5.4 Model #11 & Model #12

Since model #11 and model #12 are constructed to investigate the effect of valve displacement on the pump efficiency, boundary conditions motion parameters, and time step size are identical with model #2. In figure 3.28 model #11 and model #12 are given.

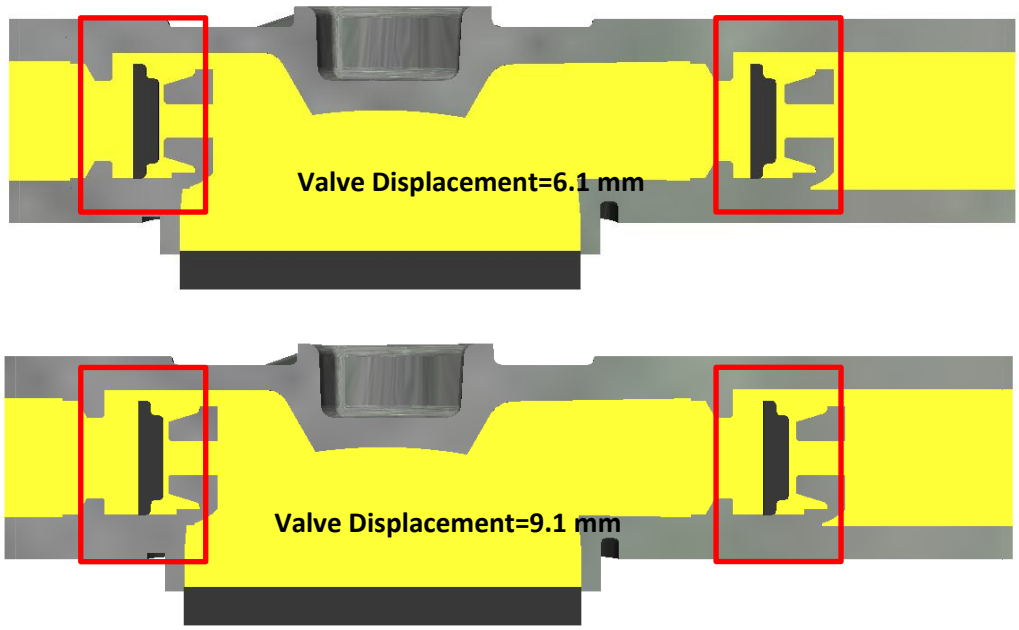

Figure 3.28 Model #11 and Model #12

3.5.5 Model # 13

Since model #13 is constructed for investigating the piston shape effect on the pump efficiency, boundary conditions, motion parameters, and time step size are identical with model #2 except for the shape of piston. Using rounded piston shape, the motion of flexible diaphragm is better represented than using flat piston. In figure 3.29 shape of the piston is given for model #13;

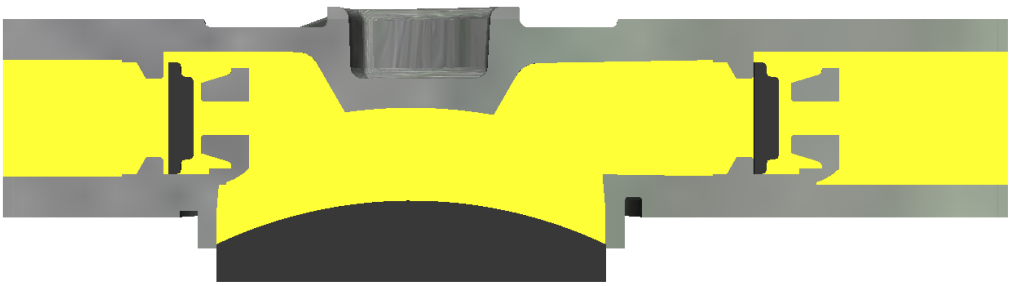

Figure 3.29 Model #13

3.5.6 Model #14

Model #14 is constructed in order to achieve best performance characteristics. For this purpose best result are taken from each category (spring stiffness, mass of the valves, displacement of the valves) and a new combined model is analyzed.

In combined model, springs which have 29.28 N/cm stiffness and valves with 6000 kg/m^3 density and 3.1 mm displacements are used. 91% volumetric efficiency and 83.5% hydraulic efficiency is obtained with this model.

The model gives lower efficiencies than the current model (model #1). Because of these systems are highly non-linear.

3.5.7 Model # 15

Model #15 is constructed for the comparison of experimental results with the CFD results. Model #15 is identical with model #1 except manifold arrangements; suction and discharge manifolds are cut between two pistons, they have U shape unlike model #1. In figure 3.30 model #15 is shown.

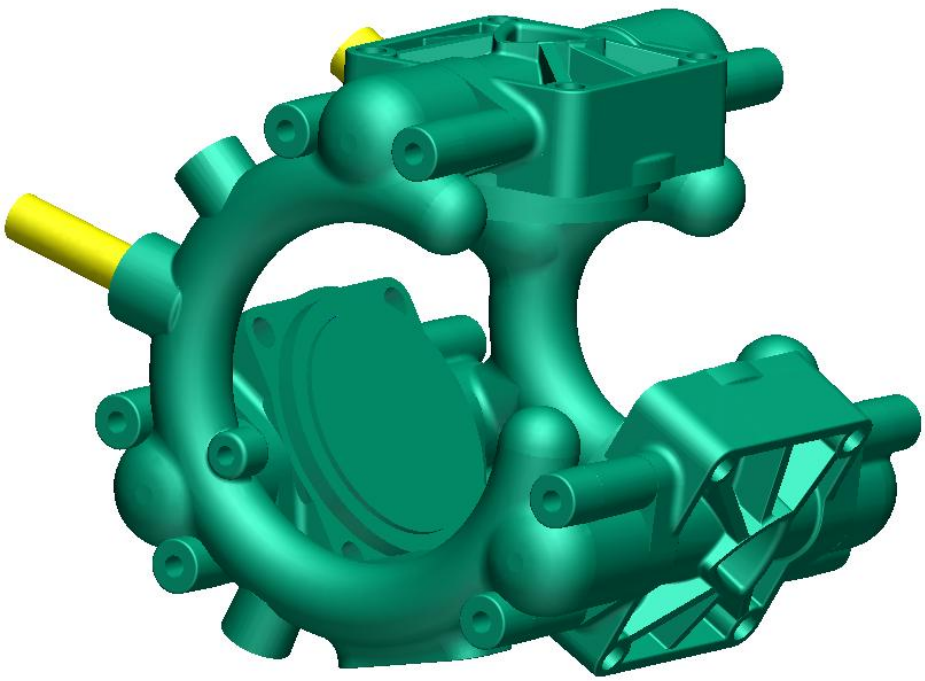

Figure 3.30 Model#15 Which is Used in Experiments

After the mesh independent solution is found, the analysis is run for 1800 iterations (5 strokes) with time step size 0.0003 s until the solution stability is achieved.

Velocity distribution and velocity vectors inside the discharge manifold for different crank angles are given in the following figures.

For θ=90˚;

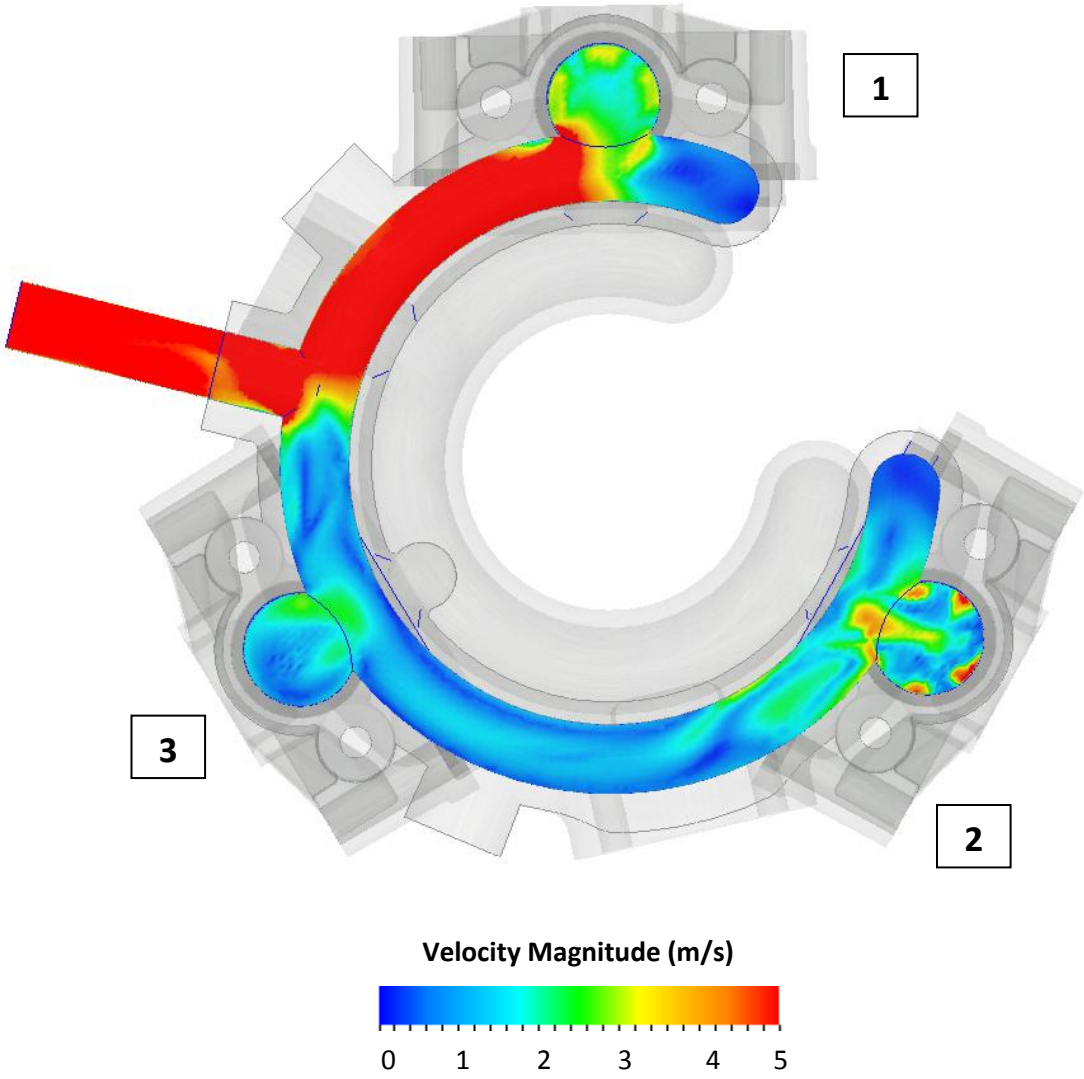

Figure 3.31 Velocity Magnitude in the Discharge Manifold for θ=90˚

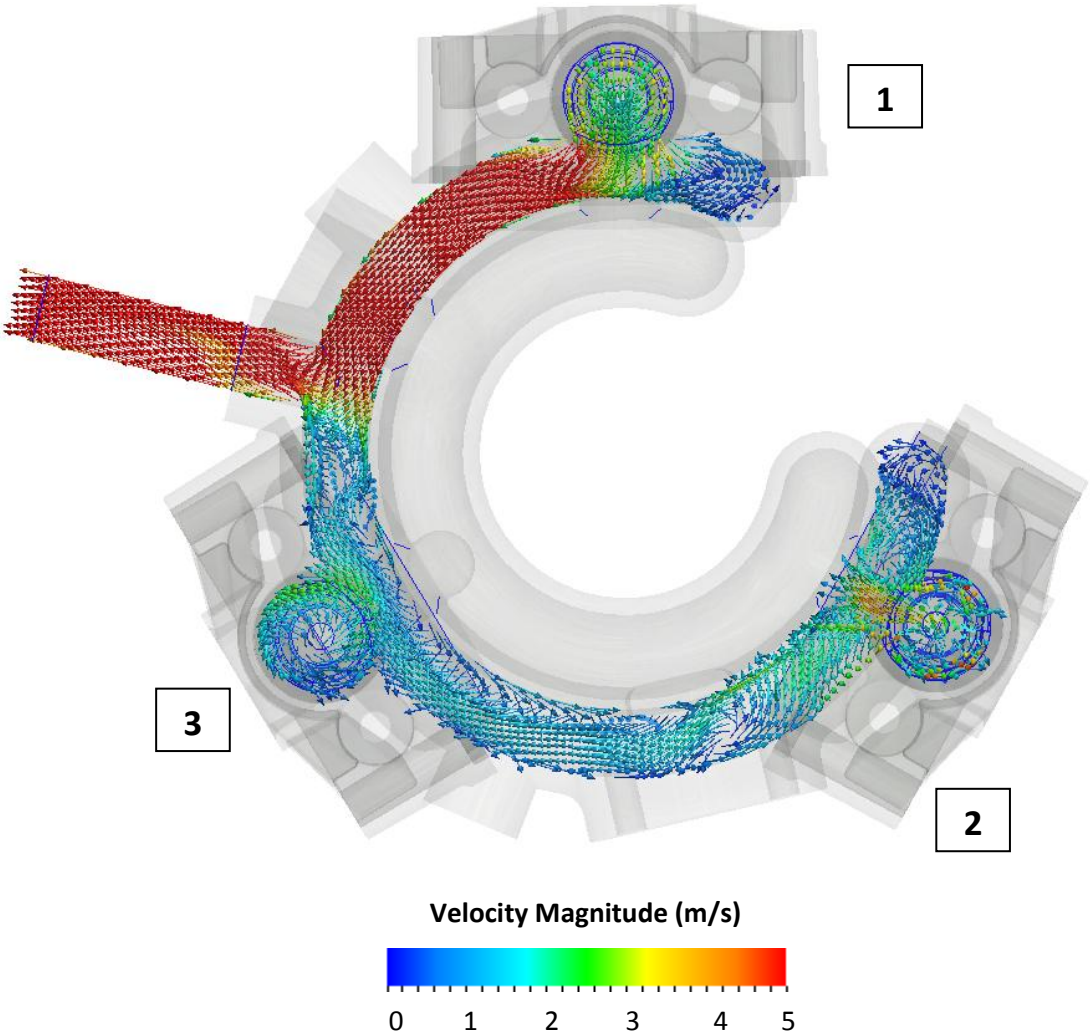

Figure 3.32 Velocity Vectors in the Discharge Manifold for θ=90˚

Since there is a 120˚ time shift between the pistons, piston #2 and piston #3 do not contribute to discharge flow rate at this instant. Velocity magnitude between piston #1 through outlet of the pump increases. Since piston #2 and piston #3 are inactive at this crank angle the velocity magnitude between piston #2 through outlet greatly reduces.

For θ=180˚;

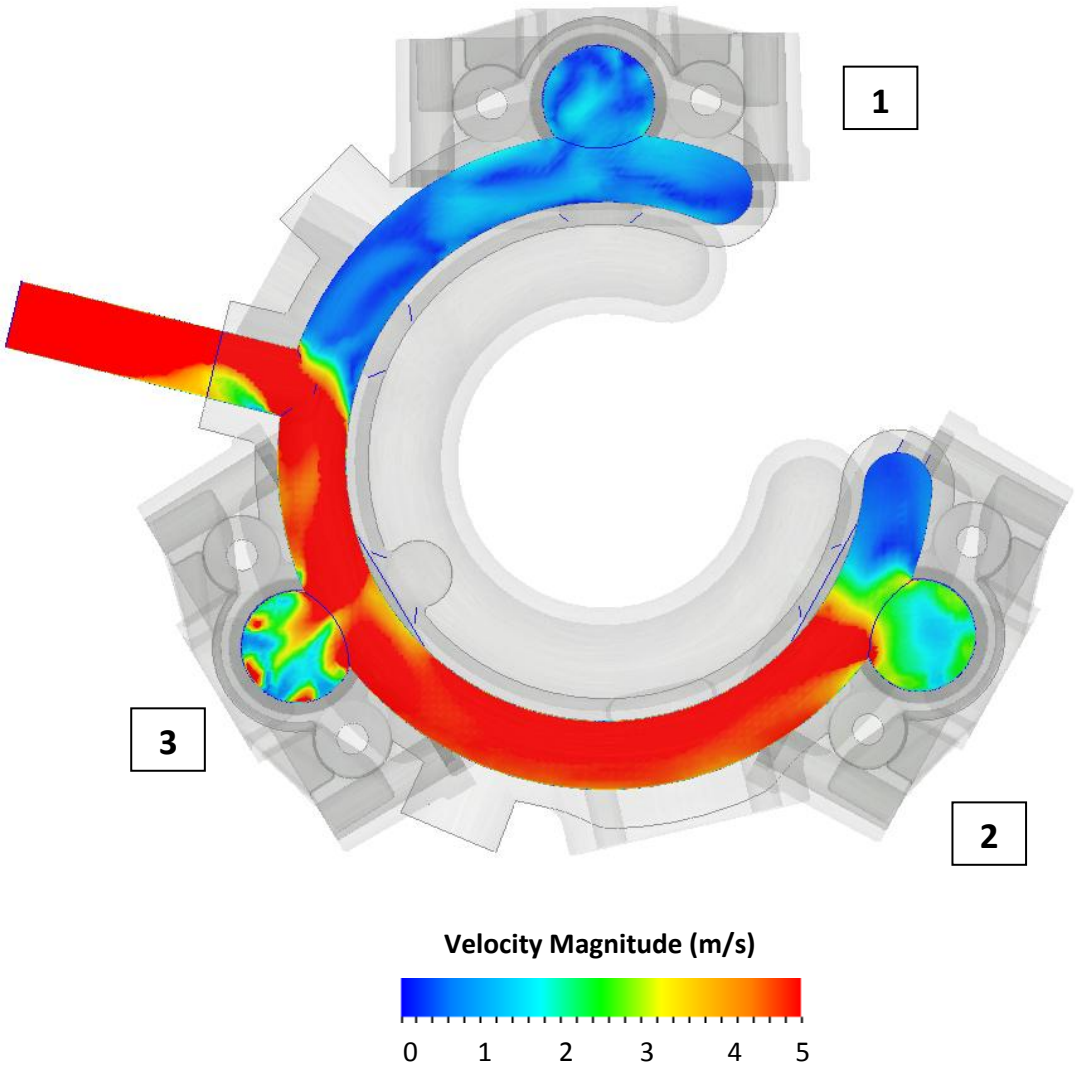

Figure 3.33 Velocity Magnitude in the Discharge Manifold for θ=180˚

Due to the fact that there is a 120˚ time shift between the pistons, piston #1 and piston #3 do not contribute to discharge flow rate at this instant. Velocity magnitude between piston #2 through outlet of the pump increases. Since piston #1 and piston #3 are inactive at this crank angle the velocity magnitude between piston #1 through outlet greatly reduces.

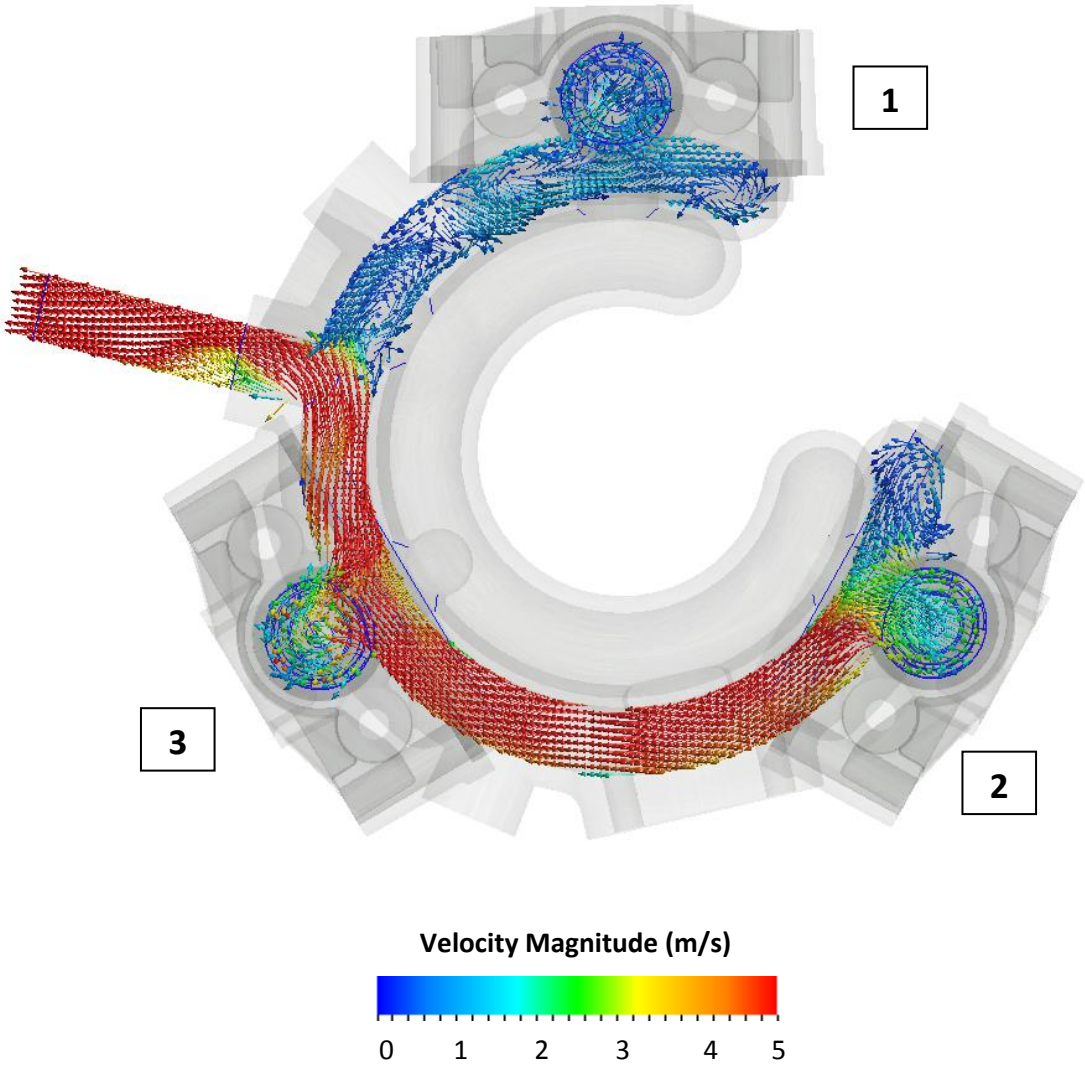

Figure 3.34 Velocity Vectors in the Discharge Manifold for θ=180˚

For θ=270˚;

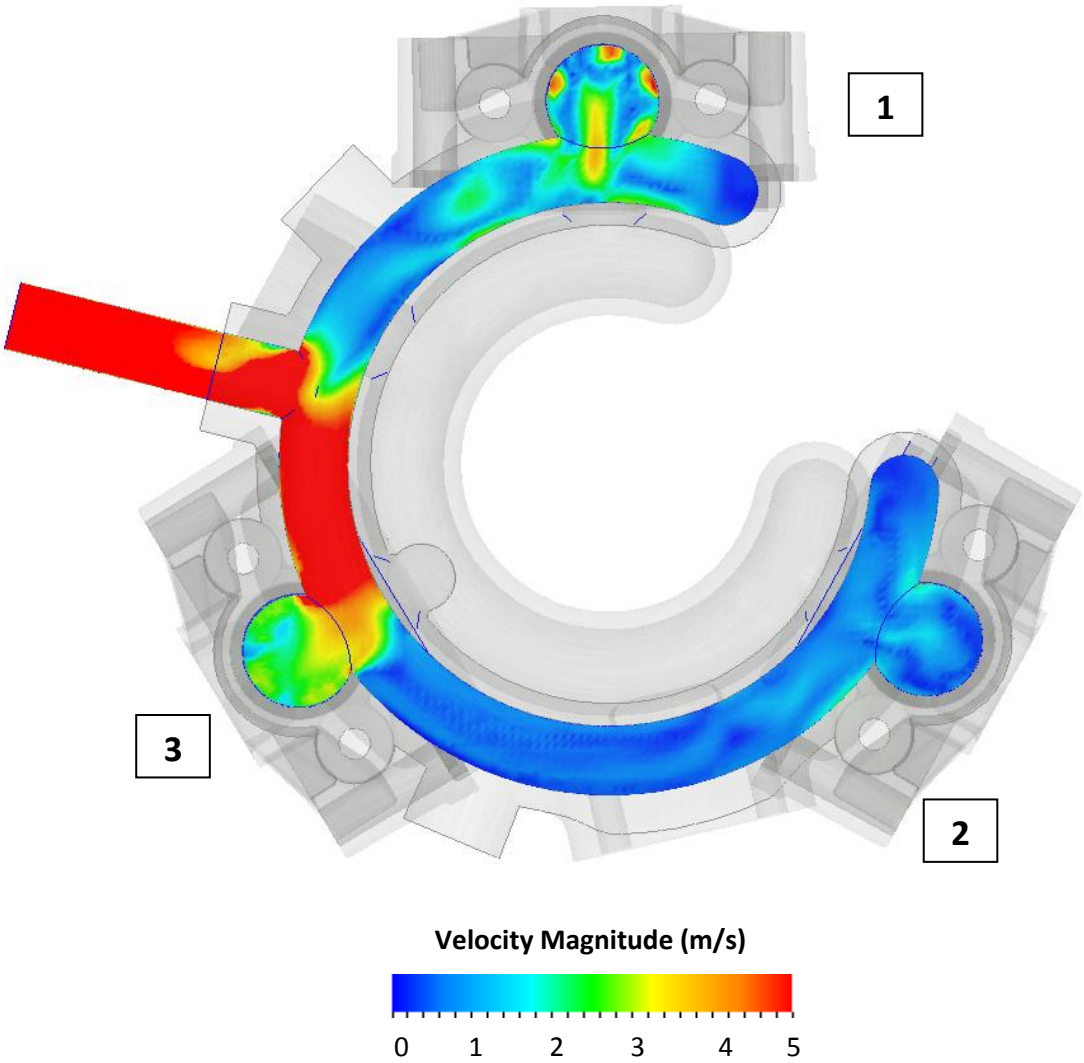

Figure 3.35 Velocity Magnitude in the Discharge Manifold for θ=270˚

Piston #2 and piston #3 are active at this crank angle and piston #1 does not contribute to discharge flow rate. From figure 3.35 it is seen that velocity magnitude between piston #1 through outlet considerably reduces. (piston #2 is active at this crank angle but piston #3 is more dominant therefore, velocity between piston #2 and piston #3 reduces).

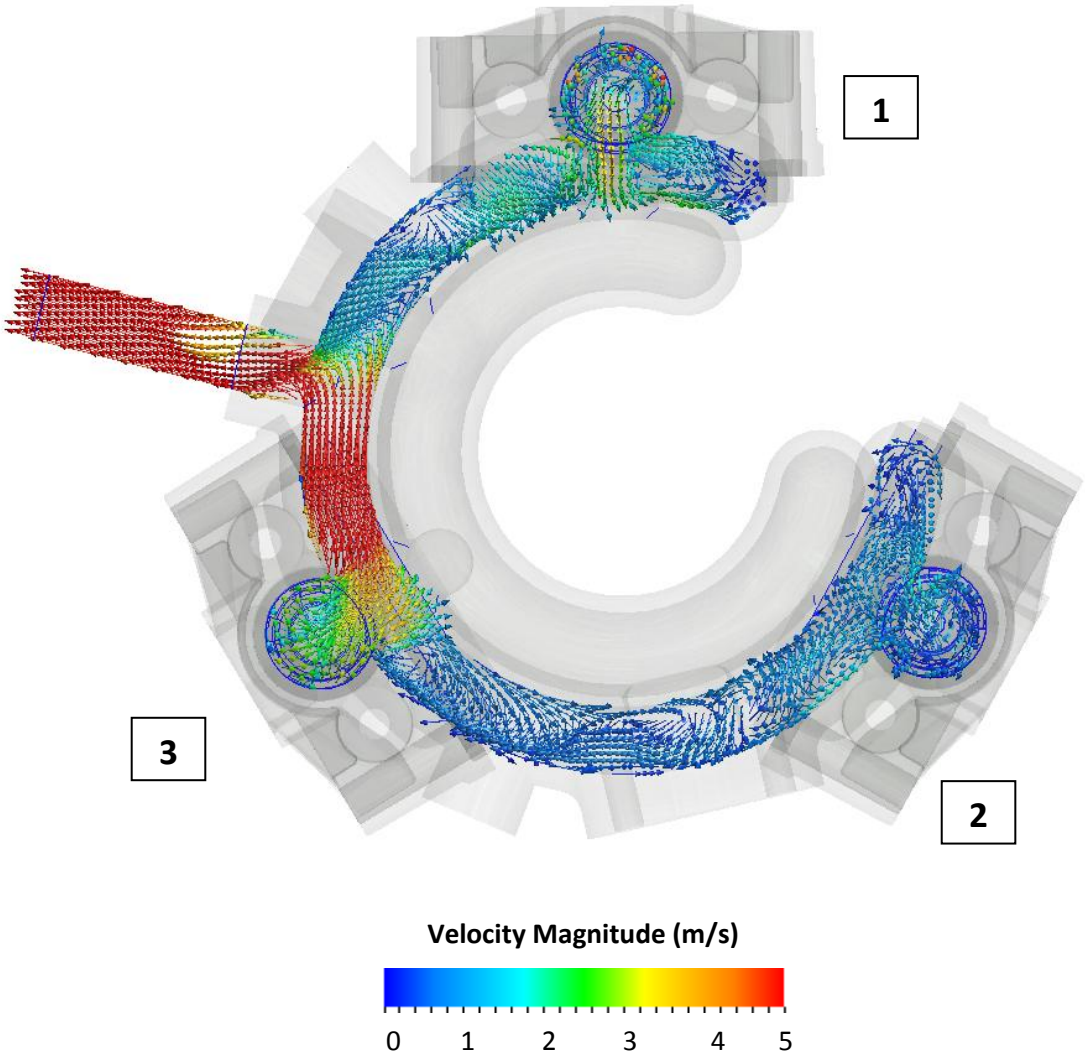

Figure 3.36 Velocity Magnitude on the Discharge Manifold for θ=270°

U type manifold arrangement brings an advantage to a system. The fluid which is discharged from pistons does not reach to outlet of the pump by following different paths unlike in model #1. It is directly head for the pump outlet from one direction. The performance characteristics of the pump are positively influenced from this condition moreover volumetric and hydraulic efficiencies of the pump are greatly increased. The volumetric and hydraulic efficiencies of all models are given in table 3.5.

Table 3.5 Analysis Results

Model	Arrangement	Spring Stiffness	Valve Density	Valve Displacement	Volumetric Efficiency	Hydraulic Efficiency
#1	3-Flat Pistons	3.66 N/cm	8000 kg/m^3	3.1 mm	92 %	84 %
#2	1-Flat Piston	**3.66 N/cm**	8000 kg/m^3	3.1 mm	96 %	91 %
#3	1-Flat Piston	**7.32 N/cm**	8000 kg/m^3	3.1 mm	96.5 %	91 %
#4	1-Flat Piston	**14.64 N/cm**	8000 kg/m^3	3.1 mm	98.5 %	92 %
#5	1-Flat Piston	**29.28 N/cm**	8000 kg/m^3	3.1 mm	99 %	93 %
#6	1-Flat Piston	**58.56 N/cm**	8000 kg/m^3	3.1 mm	94 %	89 %
#7	1-Flat Piston	3.66 N/cm	**16000 kg/m^3**	3.1 mm	93 %	88 %
#8	1-Flat Piston	3.66 N/cm	**32000 kg/m^3**	3.1 mm	92 %	80 %
#9	1-Flat Piston	3.66 N/cm	**6000 kg/m^3**	3.1 mm	96.3 %	91.2 %
#10	1-Flat Piston	3.66 N/cm	**4000 kg/m^3**	3.1 mm	91 %	90.6 %
#11	1-Flat Piston	3.66 N/cm	8000 kg/m^3	**6.1 mm**	91 %	84 %
#12	1-Flat Piston	3.66 N/cm	8000 kg/m^3	**9.1 mm**	89 %	80 %
#13	**1-Round Piston**	3.66 N/cm	8000 kg/m^3	3.1 mm	95 %	88.5 %
#14	3-Flat Pistons	29.28 N/cm	6000 kg/m^3	3.1 mm	91 %	83.5 %
#15	3-Flat Pistons	3.66 N/cm	8000 kg/m^3	3.1 mm	94 %	87 %

CHAPTER 4

COMMENTS ON THE RESULTS

In the previous section, CFD results are given for each model. Now, these results are explained in detail. This section is divided into two main categories as;

First, effects of valve characteristics and piston shape on the pump efficiency are investigated. Second, experimental and CFD results are compared. Following effects are explained in this section:

- Spring stiffness effect on the pump efficiency
- Check valve mass effect on the pump efficiency
- Valve displacement effect on the pump efficiency
- Piston shape effect on the pump efficiency

4.1 The Effect of Valve Characteristics and Piston Shape

Models #3 between #6 are analyzed to investigate spring stiffness effect on the pump efficiency. The results related to spring stiffness analyses are shown in table 4.1.

Table 4.1 Effect of Spring Stiffness on the Pump Efficiency

Model	Arrangement	Spring Stiffness	Volumetric Eff. (%)	Hydraulic Eff. (%)
#2	1-Flat Piston	3.66 N/cm	96	91
#3	1-Flat Piston	7.32 N/cm	96.5	91
#4	1-Flat Piston	14.64 N/cm	98.5	92
#5	1-Flat Piston	29.28 N/cm	99	93
#6	1-Flat Piston	58.56 N/cm	94	89

From table 4.1 it is seen that using stiffer springs causes the volumetric and hydraulic efficiency to increase. In literature some studies stated that using stiffer

valve springs causes the pumps to work more efficiently [8, 20] with the higher suction pressure requirement and higher NPSH. This trend is validated in this thesis, but numerical simulations are conducted with constant suction pressure as a result of this condition pump efficiency reduces with using stiffer springs after the value of 29.28 N/cm.

At first one may think that the ideal valve would be massless and springless one. But this condition is not true. From table 4.1 it can be seen that decreasing spring stiffness tends to reduce efficiency and further reducing stiffness brings valve flutter which contributes to lower volumetric efficiency and increases the pressure pulsations. This condition can also be observed by looking figures 4.1 and 4.2

Using stiffer springs reduces closing time of check valves and this situation tends to increase volumetric efficiency. But stiffer springs contributes pressure drop through check valves and this pressure drop tends to reduce volumetric efficiency. For 29.28 N/cm stiffness value, loss of volumetric efficiency from pressure drop is more dominant than gained volumetric efficiency from fast closing of check valves. As a result of this condition volumetric efficiency reduces with using stiffer springs. This condition can be seen by looking figures 4.1, 4.3, 4.4 and 4.5.

In figure 4.4 it is also observed that closing time of discharge check valve reduces and opening time of discharge check valve increases with using stiffer springs.

Pressure drop through discharge valve at the 5th stoke is given in figure 4.5. It can be seen that using the spring which has 58.56 N/cm stiffness gives the highest pressure drop trough discharge valve and with increasing spring stiffness this pressure drop increases.

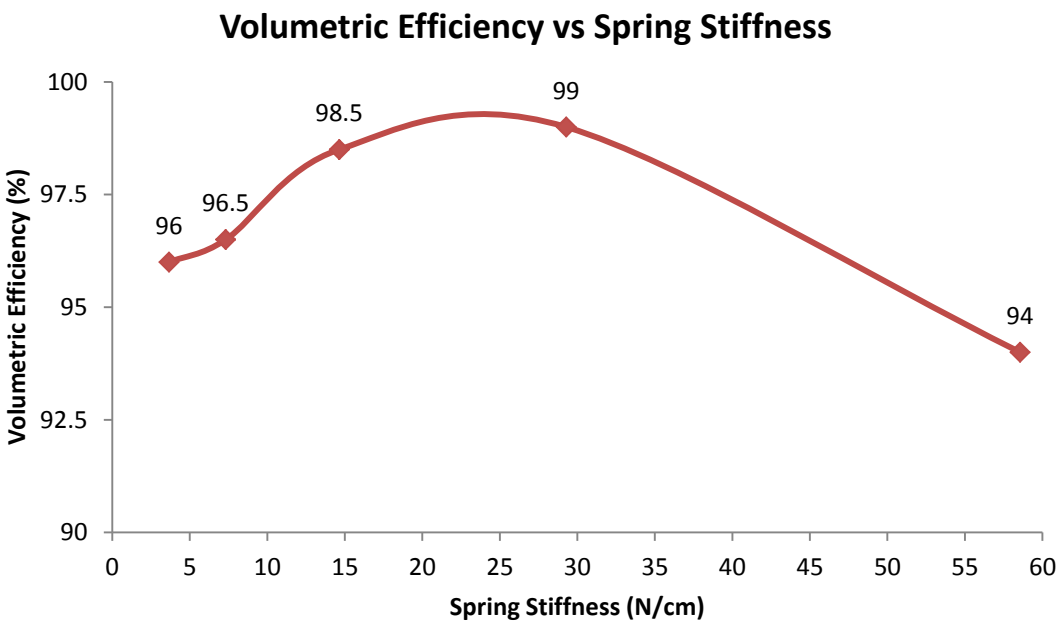

Figure 4.1 Volumetric Efficiency vs. Spring Stiffness

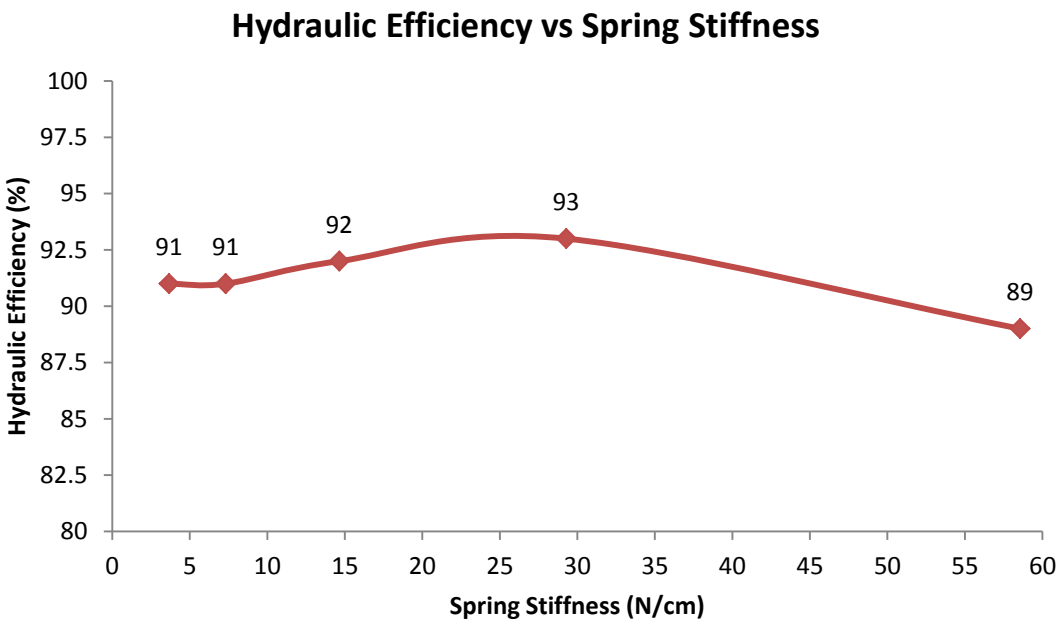

Figure 4.2 Hydraulic Efficiency vs. Spring Stiffness

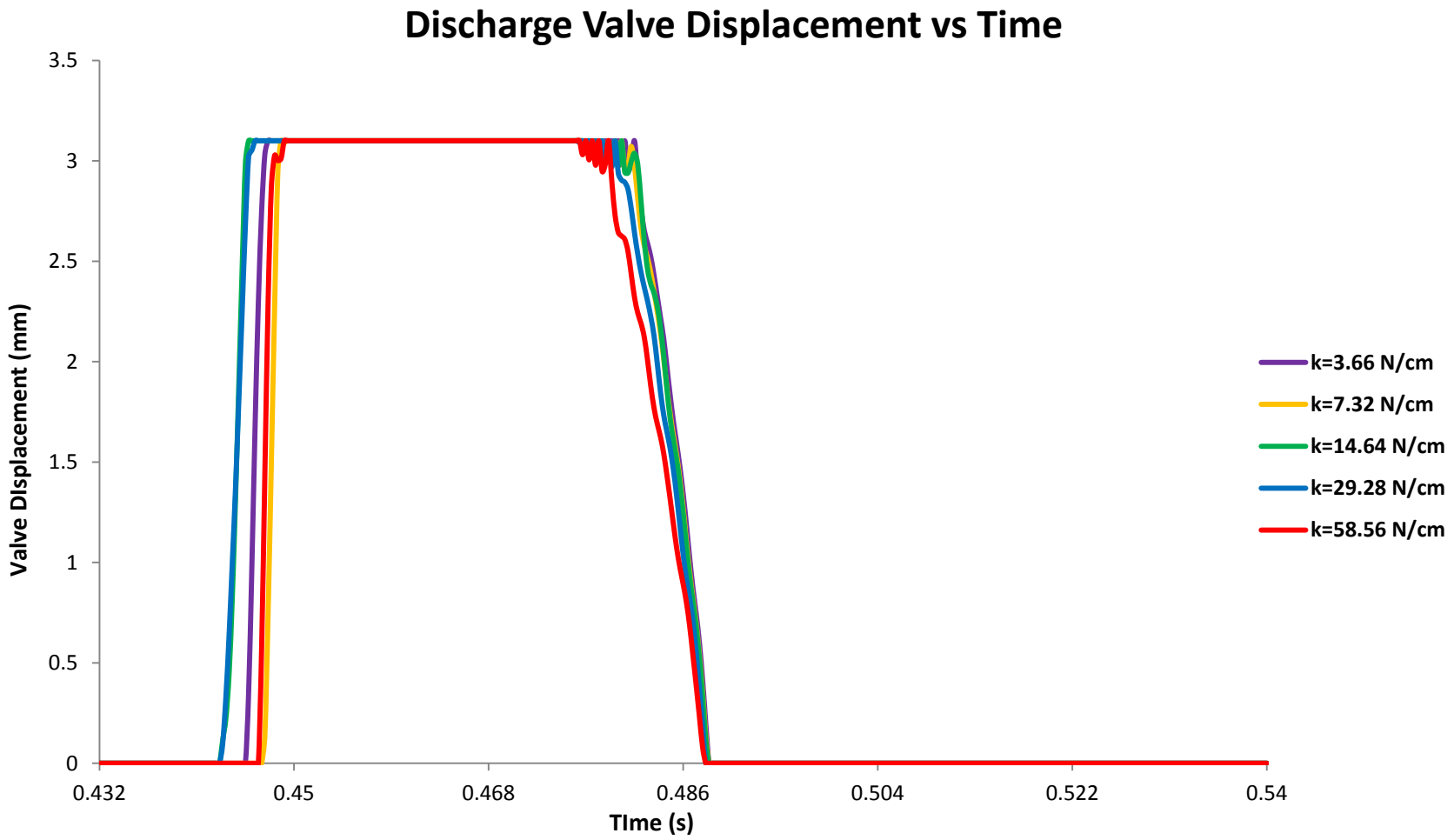

Figure 4.3 Discharge Valve Displacement at the 5th Stroke (0 mm fully closed position, 3.1 mm fully opened position)

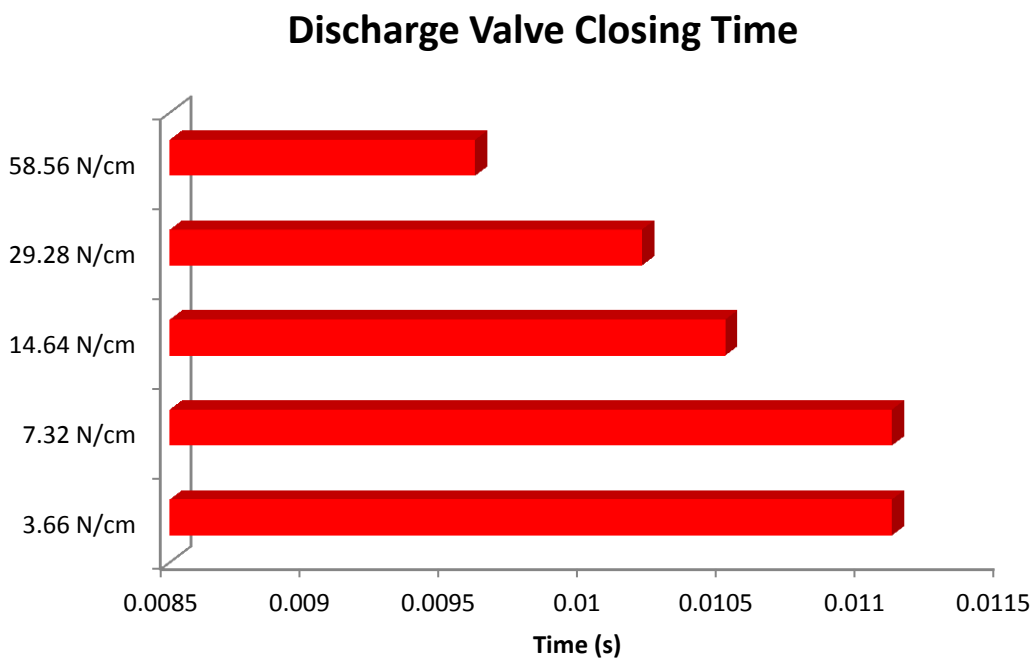

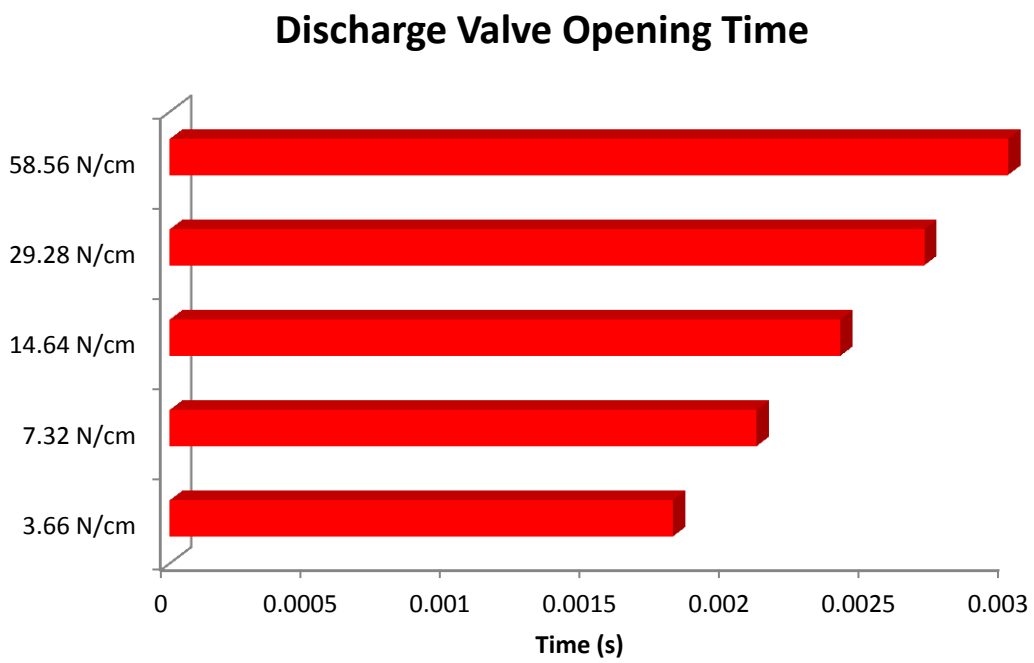

Figure 4.4 Discharge Valve Closing Times and Discharge Valve Opening Times for Different Spring Stiffness

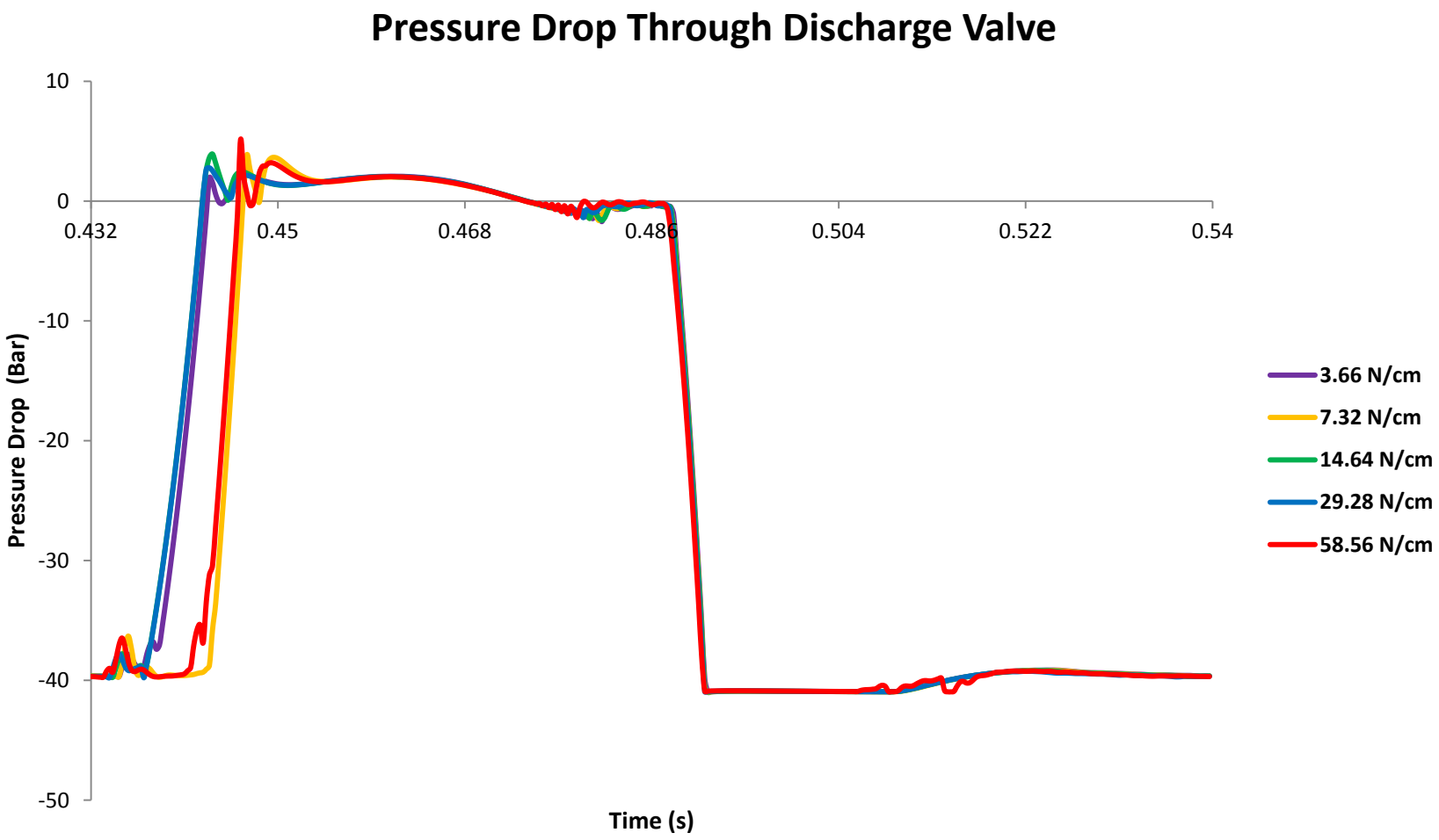

Figure 4.5 Pressure Drop Through Discharge Valve at the 5th Stroke for Different Spring Stiffness

Model #7 through model #9 are analyzed to investigate the check valve mass effect on the pump efficiency. The results of these analyses are shown in table 4.2.

Table 4.2 Effect of Valve Mass on the Pump Efficiency

Model	Arrangement	Valve Density [kg/m^3]	Vol. Eff. (%)	Hydraulic Eff. (%)
#2	1-Flat Piston	8000	96	91
#7	1-Flat Piston	16000	93	88
#8	1-Flat Piston	32000	92	80
#9	1-Flat Piston	6000	96.3	91.2
#10	1-Flat Piston	4000	91	90.6

From table 4.2, it can be seen that using heavier valves (higher density) reduces volumetric and hydraulic efficiency.

From figure 4.6, it is observed that using of lighter valves tends to increase efficiency up to a limit. (For this case 6000 kg/m^3) Further reducing mass of the valves (beyond that limit) brings valve flutter and instability which contributes to lower volumetric efficiency.

In figure 4.9 pressure drop through discharge valve for different valve densities are given. Using heavier valves brings more pressure drop through discharge valve. However, for 4000 kg/m^3 valve density, more pressure drop is obtained than 6000 kg/m^3 valve density.

In figure 4.10, opening and closing times of discharge valve are given. Using heavier valves gives longer closing and opening times. But with using valves which have 4000 kg/m^3 density discharge longer valve closing time is obtained than with using valves which have 6000 kg/m^3. As a result of these conditions after a certain limit of density reducing the mass of the valves give lower volumetric and hydraulic efficiency. This trend results from the valve flutter and increased pressure drop through discharge valve.

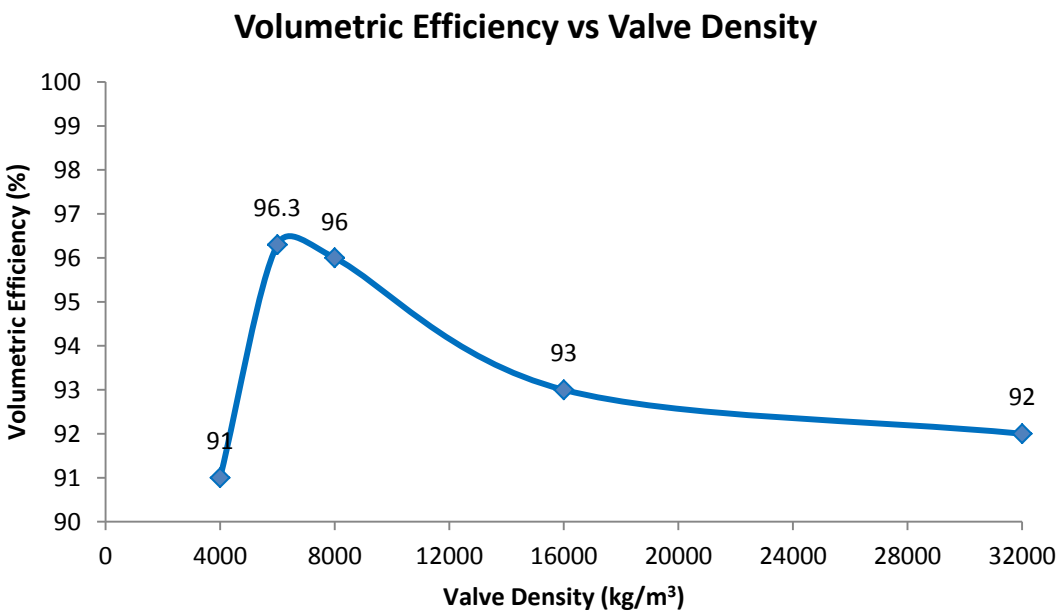

Figure 4.6 Volumetric Efficiency vs. Valve Density

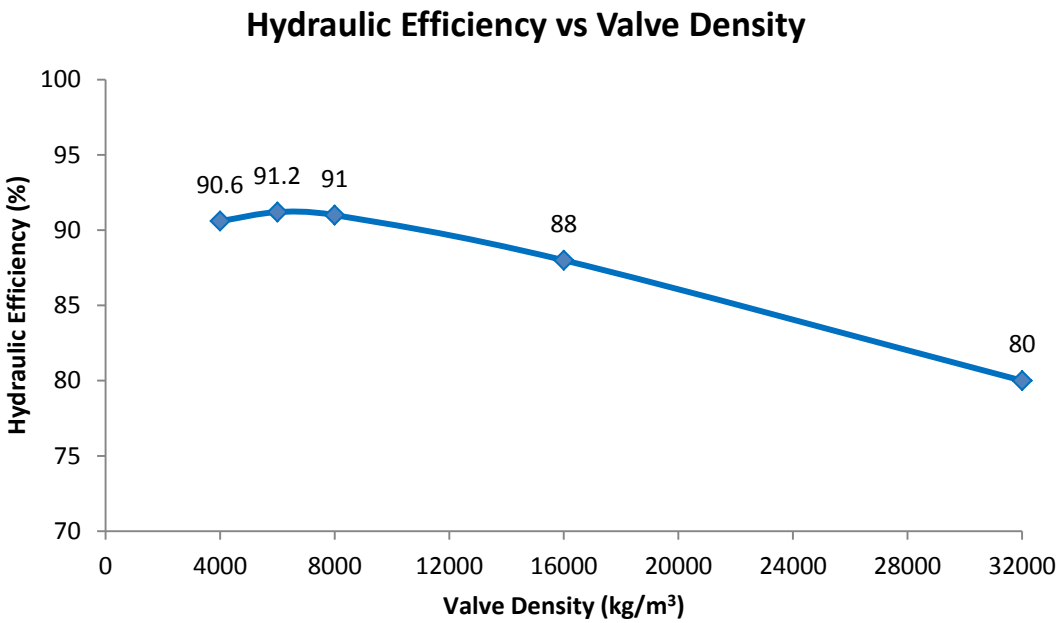

Figure 4.7 Hydraulic Efficiency vs. Valve Density

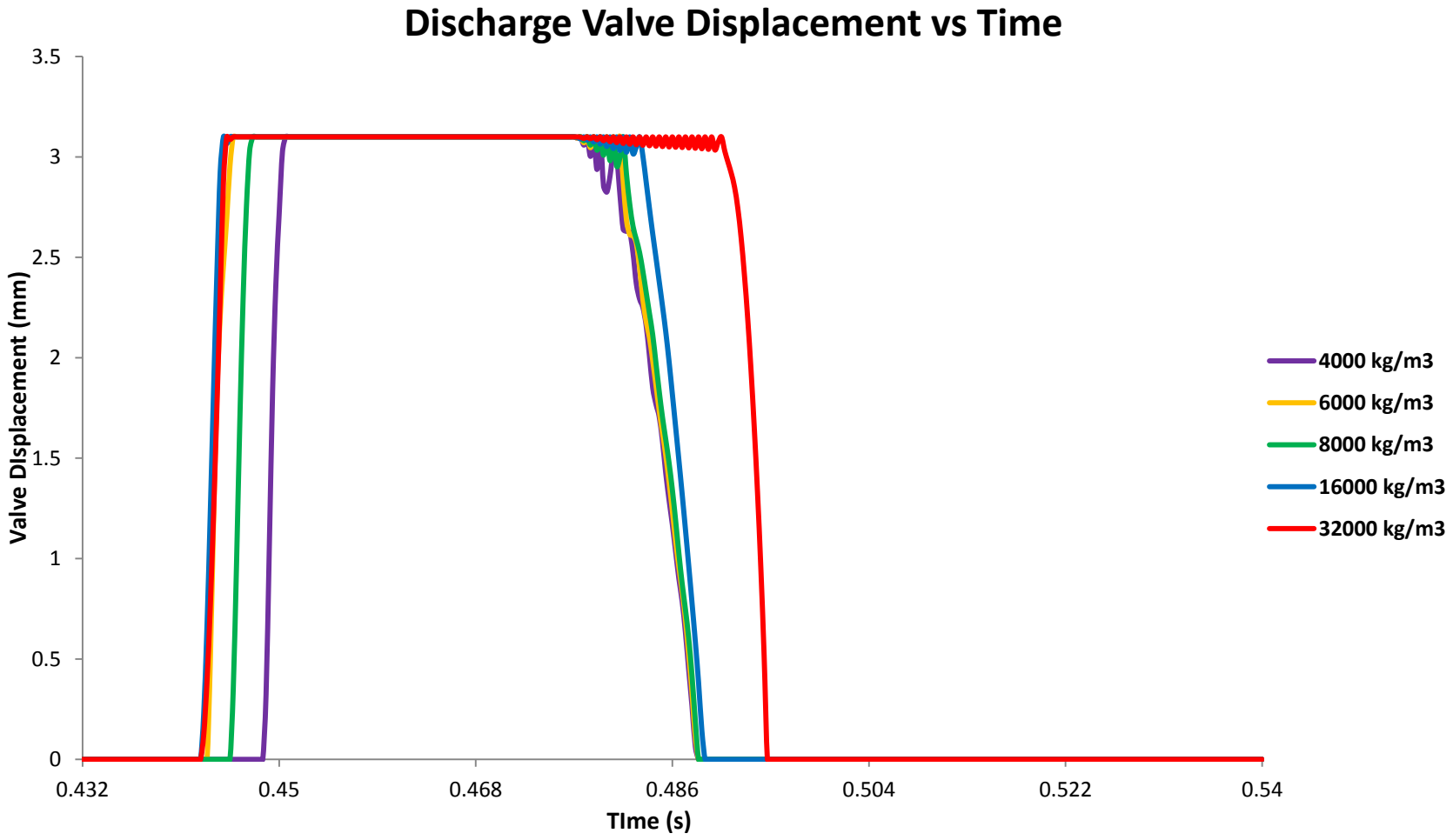

Figure 4.8 Discharge Valve Displacement at the 5th Stroke (0 mm fully closed position, 3.1 mm fully opened position)

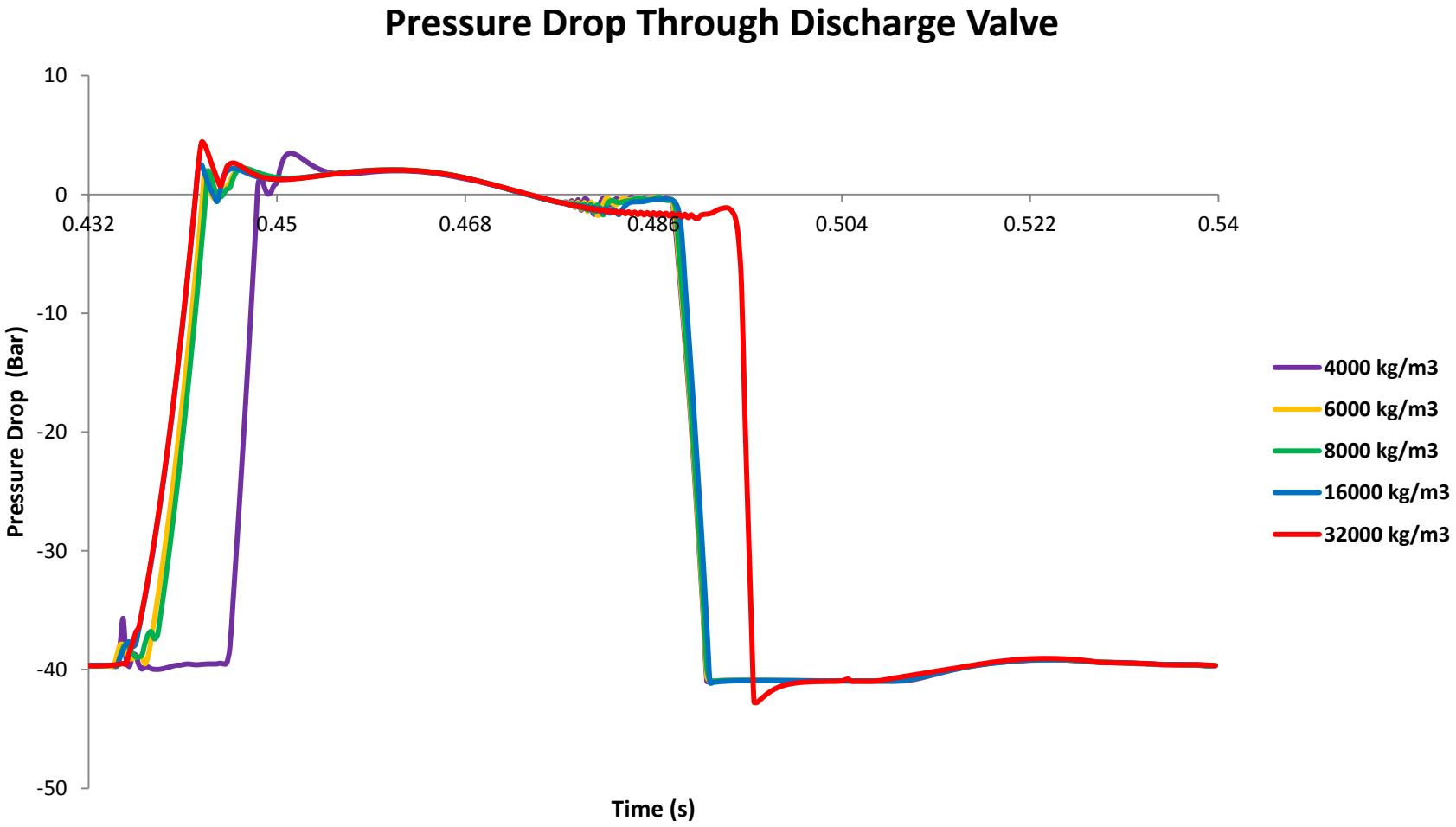

Figure 4.9 Pressure Drop Through Discharge Valve at the 5th Stroke for different valve densities

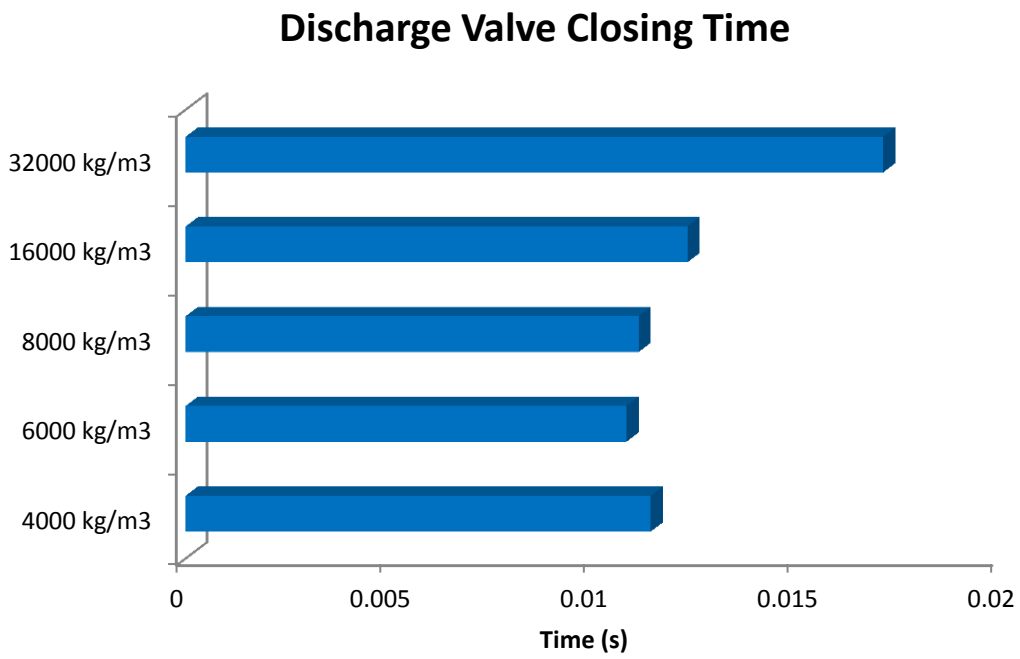

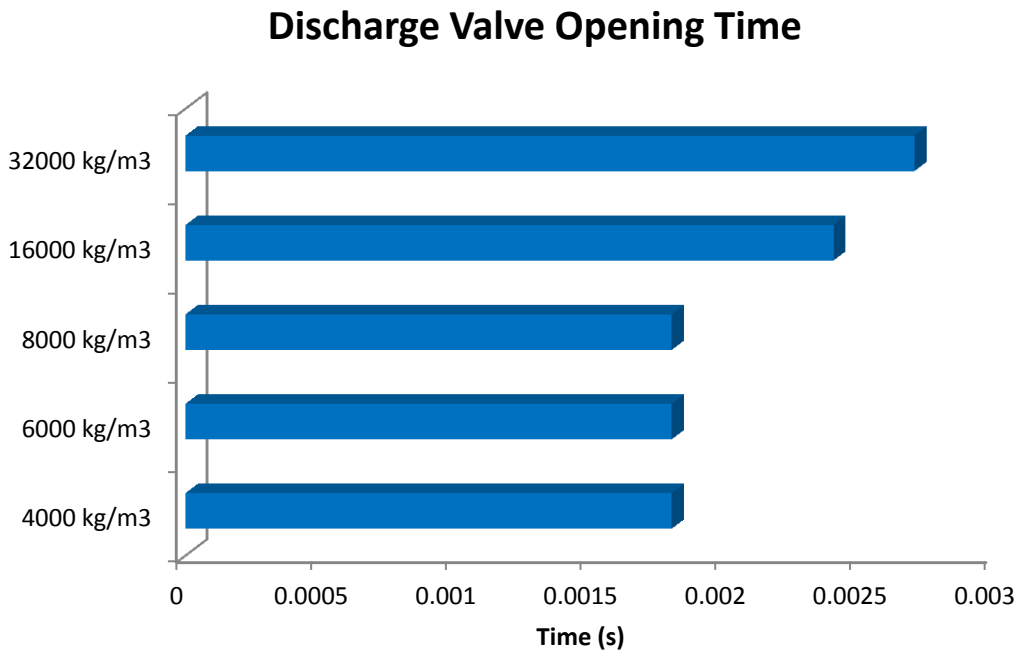

Figure 4.10 Discharge Valve Closing Times and Discharge Valve Opening Times for Different Valve Densities

Model #11 and model #12 are analyzed to investigate the effect of valve displacement on the pump efficiency. The results of these analyses are shown in table 4.3.

Table 4.3 Effect of Valve Displacement on the Pump Efficiency

Model	Arrangement	Valve Disp. (mm)	Volumetric Eff. (%)	Hyd. Eff. (%)
#2	1-Flat Piston	3.1	96	91
#11	1-Flat Piston	6.1	91	84
#12	1-Flat Piston	9.1	89	80

From table 4.3 it can be seen that volumetric and hydraulic efficiencies reduce with increasing valve displacement.

In figures 4.11 and 4.12 effect of valve displacement on the pump efficiency is given. It is observed that if the valve displacement is increased 100%, volumetric efficiency reduces 5.2% and hydraulic efficiency reduces 7.7%. If the valve displacement is increased 200%, volumetric efficiency reduces 7.3% and hydraulic efficiency reduces 12.1%.

Opening and closing times of discharge valve are given in figure 4.14. with using longer valve displacement, discharge valve closing and opening times increase as expected. From figure 4.13 it is also observed that with longer valve displacement, valve flutter increases.

Pressure drop through discharge valve for different valve displacements at the 5th stroke is given in figure 4.15. It is observed that with using longer valve displacement more pressure drop through discharge valve is obtained.

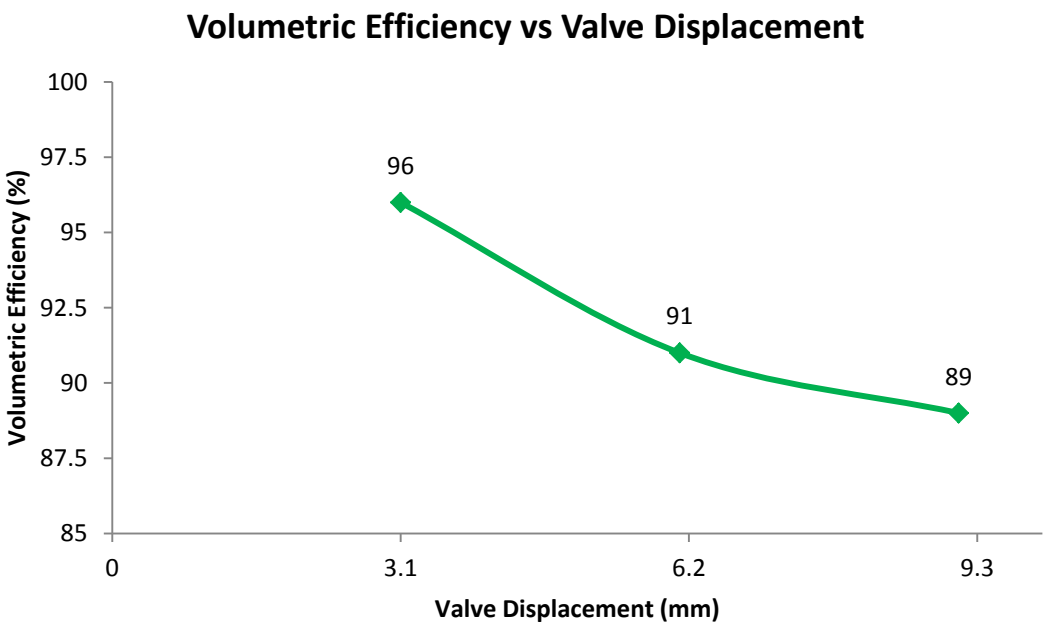

Figure 4.11 Volumetric Efficiency vs. Valve Displacement

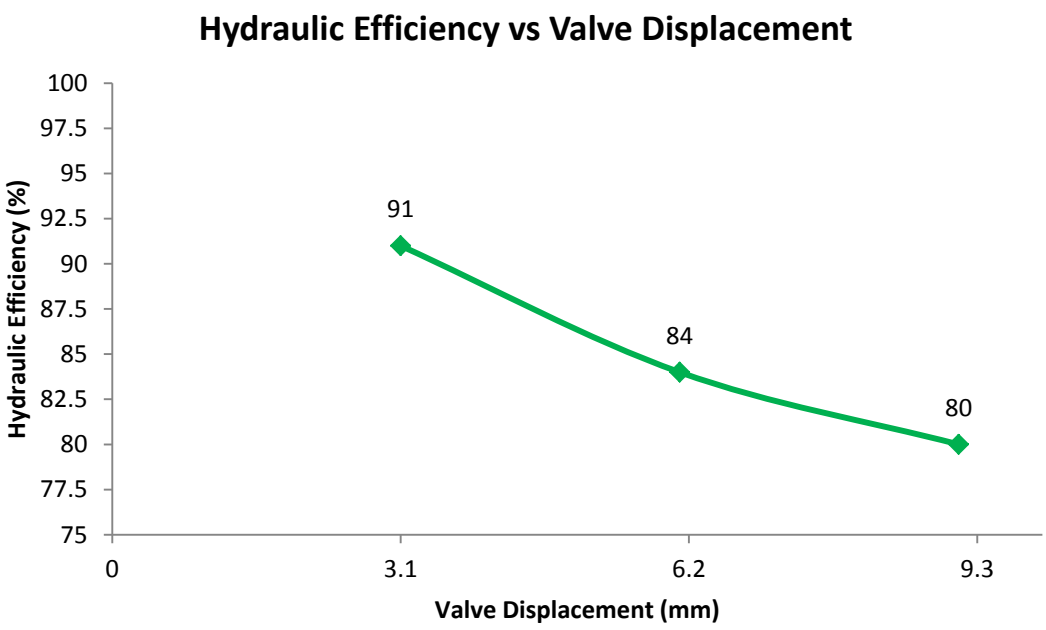

Figure 4.12 Hydraulic Efficiency vs. Valve Displacement

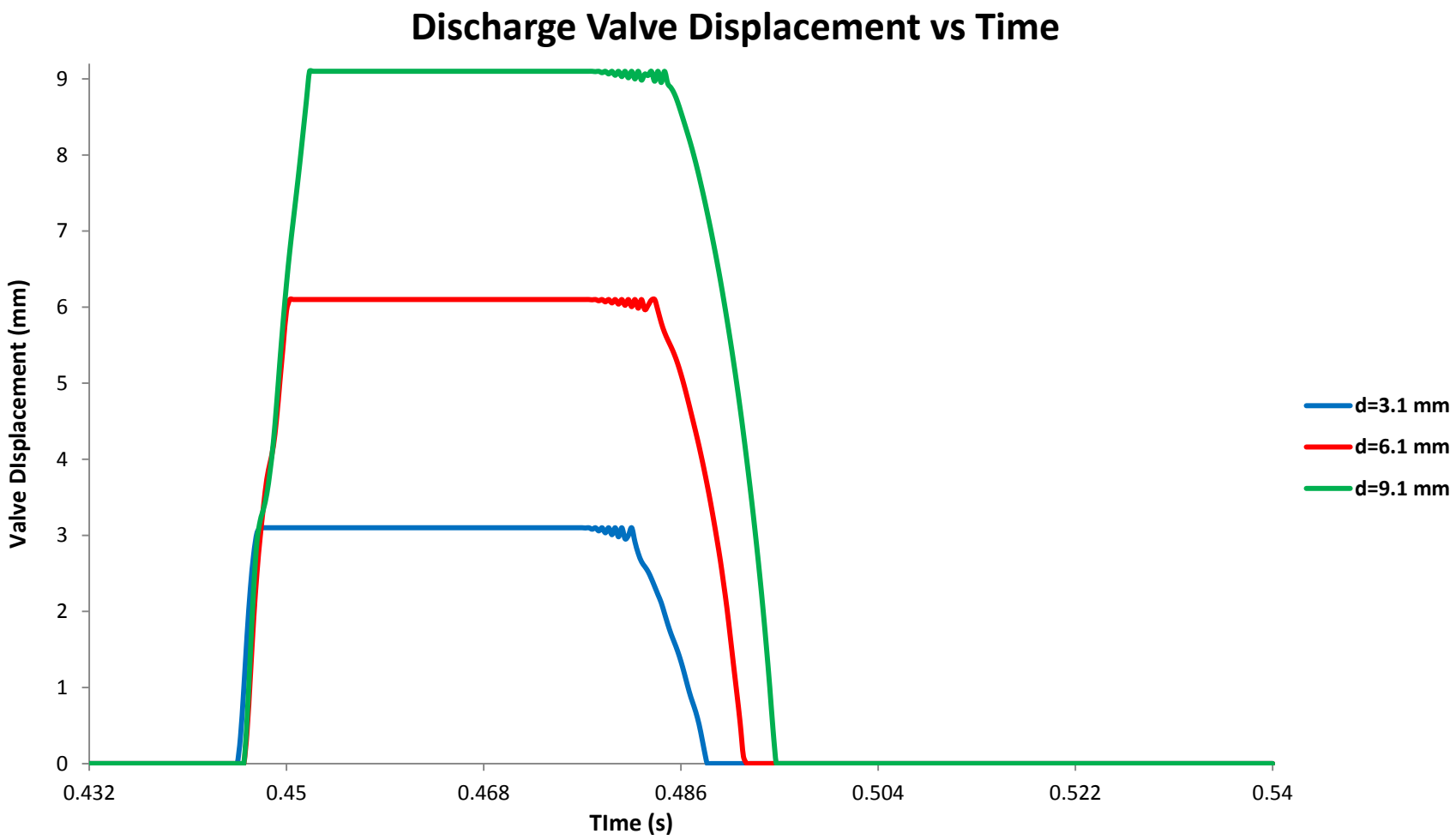

Figure 4.13 Discharge Valve Displacement at the 5th Stroke (0 mm fully closed position, 3.1, 6.1 and 9.1 mm fully opened position)

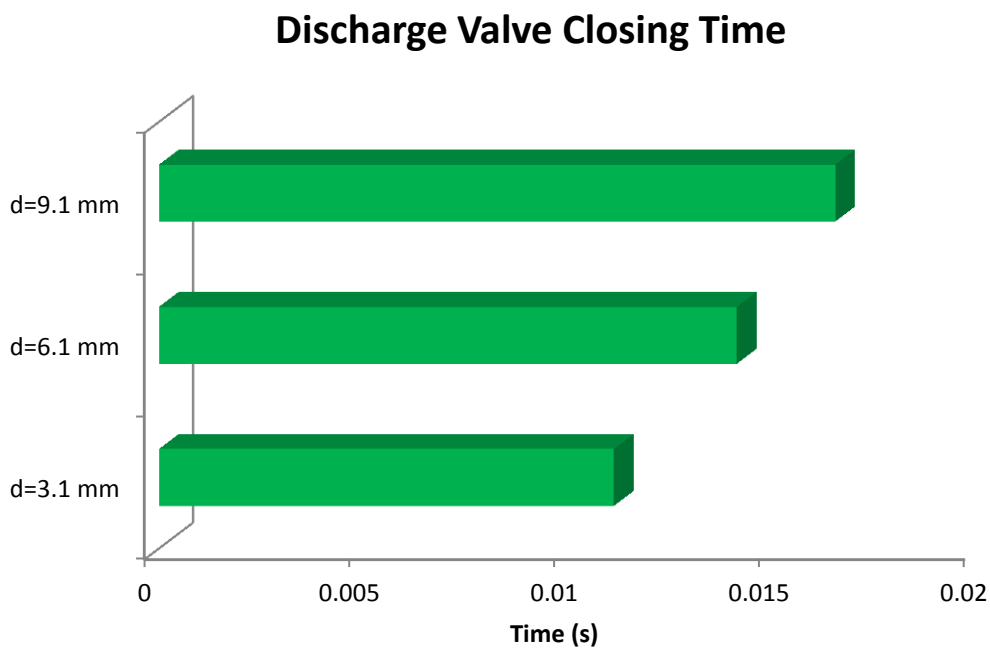

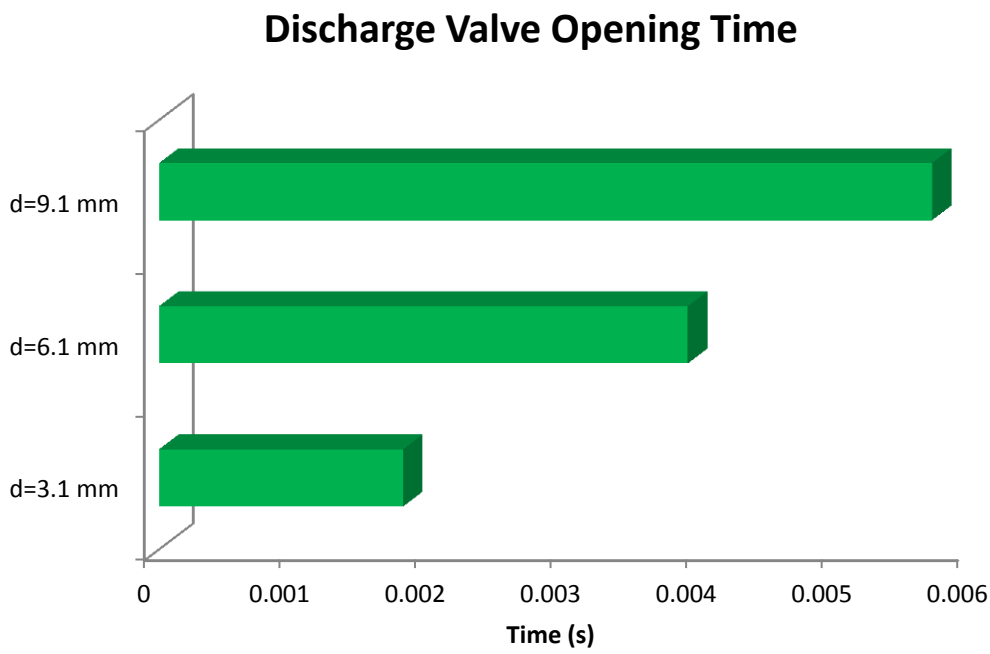

Figure 4.14 Discharge Valve Closing Times and Discharge Valve Opening Times for Different Valve Displacements

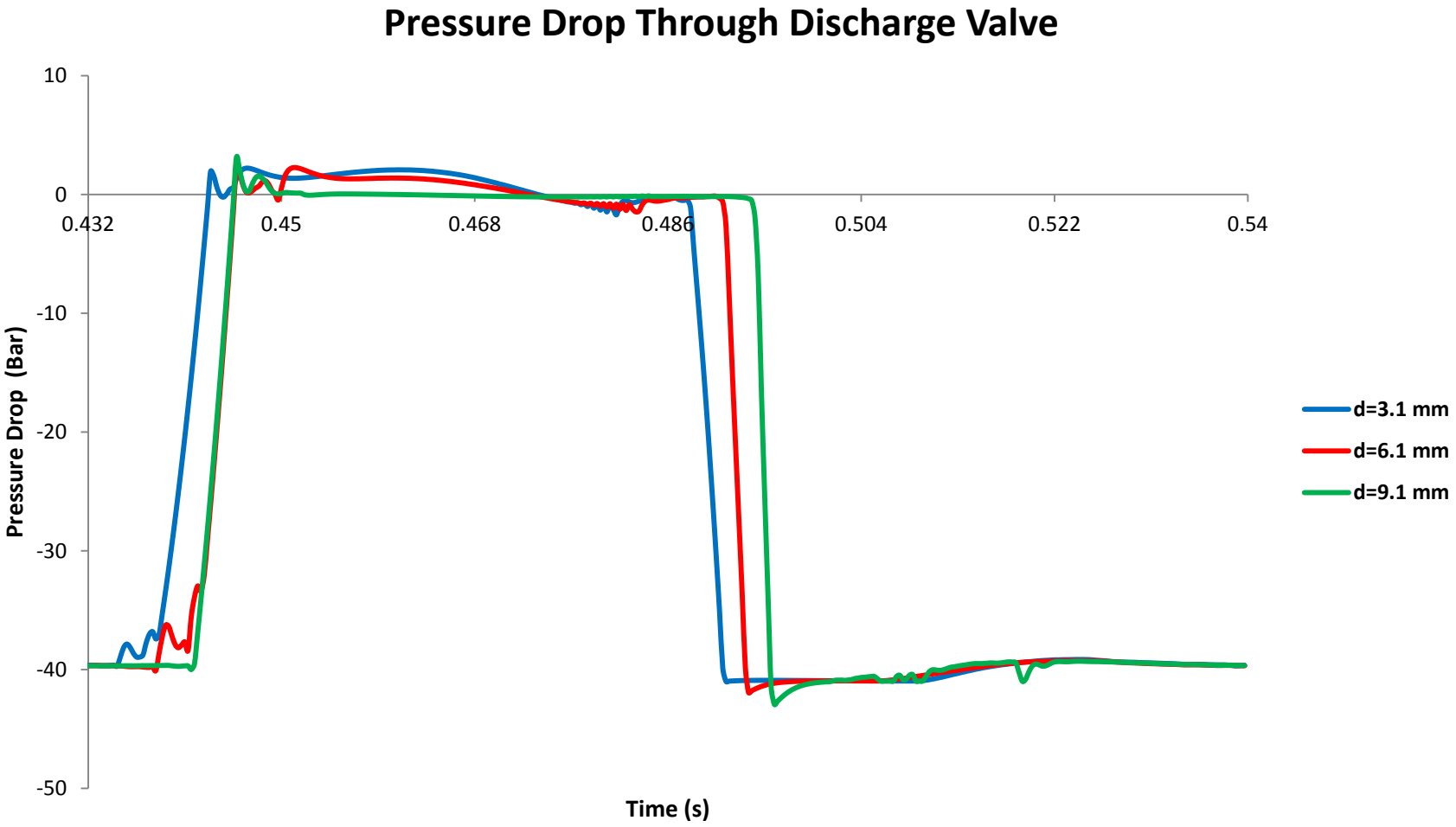

Figure 4.15 Pressure Drop Through Discharge Valve at the 5th Stroke for Different Valve Displacements

Model #12 is analyzed to investigate the effect of piston shape on the pump efficiency. Also the motion of the flexible diaphragm is better represented with this arrangement. The results of these analyses are shown in table 4.4.

Table 4.4 Piston Shape Effect on the Pump Efficiency

Model	Arrangement	Volumetric Eff. (%)	Hydraulic Eff. (%)
#2	Flat Piston	96	91
#12	Round Piston	95	88.5

From table 4.4, it is seen that volumetric and hydraulic efficiencies reduce with using round piston instead of flat piston arrangement. But this reducing trend is not significant. Only 1% of reduction in volumetric efficiency and 2.75% reduction in hydraulic efficiency are obtained. The percentage of reduction in hydraulic efficiency (2.75%) is more dominant than reduction in volumetric efficiency. This trend is obtained from using round piston arrangement. With this arrangement the piston area which exposed to fluid increases. Therefore pressure force on the piston increases accordingly power input to the system increases. The effect of piston shape on the pump efficiency is also shown in figures 4.16 and 4.17.

Opening and closing time of the valves are given in figure 4.19. Using rounded piston arrangement discharge valve opening time increases. There is no difference obtained for the discharge valve closing times. In figure 4.18 the discharge valve displacement vs. time graph is given. From this data with round piston arrangement valve flutter is observed during the opening of discharge valve and valve flutter amplitude increases during the closing of discharge valve.

Pressure drop through discharge valve at the 5th stoke is given in figure 4.20. It is observed that with using round piston arrangement more pressure drop through discharge valve is obtained.

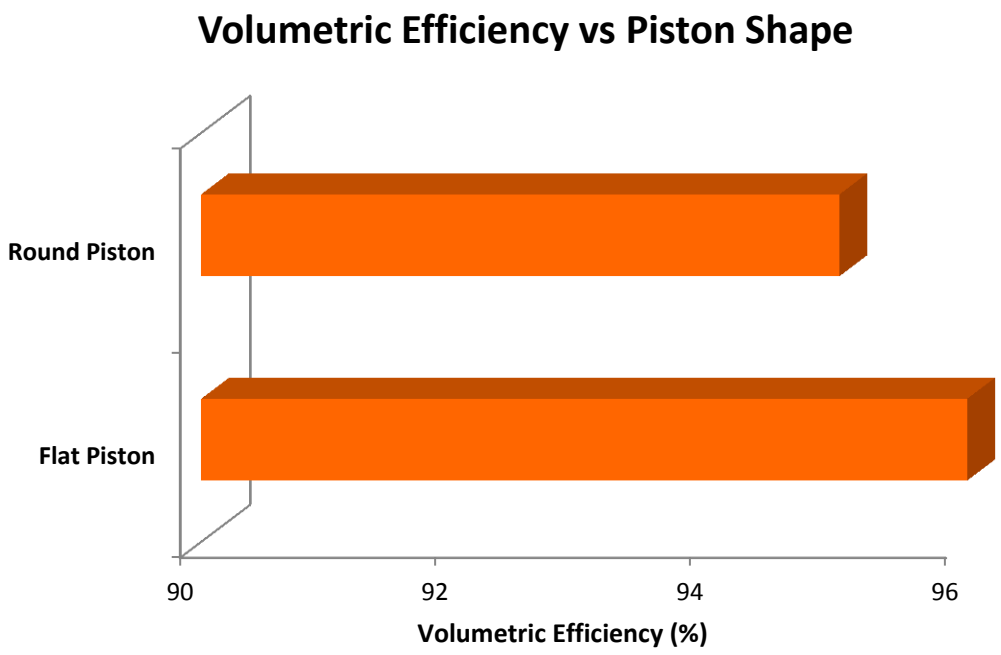

Figure 4.16 Volumetric Efficiency vs. Piston Shape

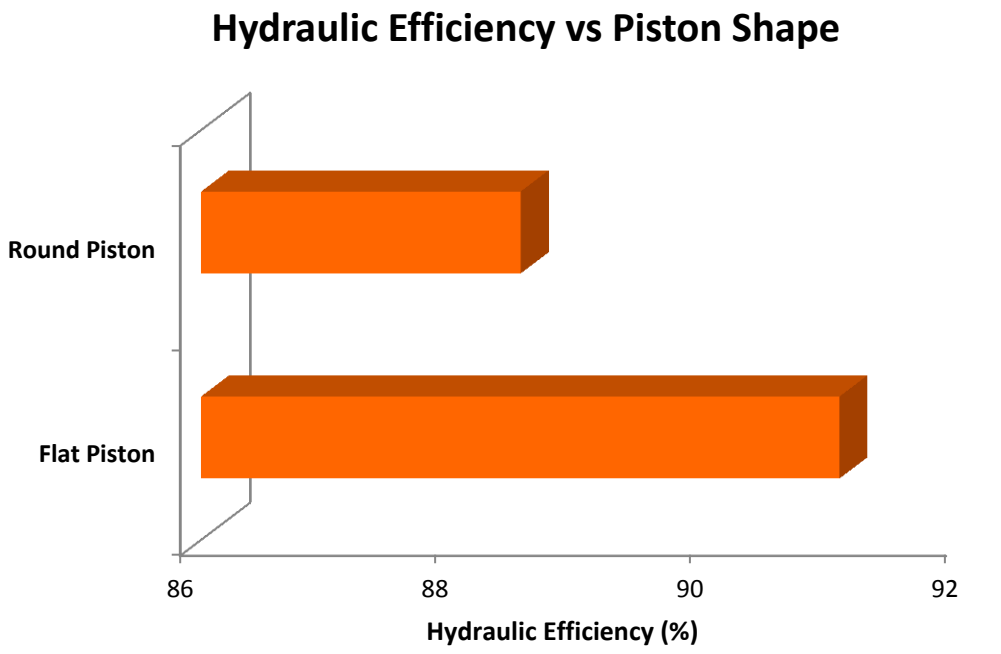

Figure 4.17 Hydraulic Efficiency vs. Piston Shape

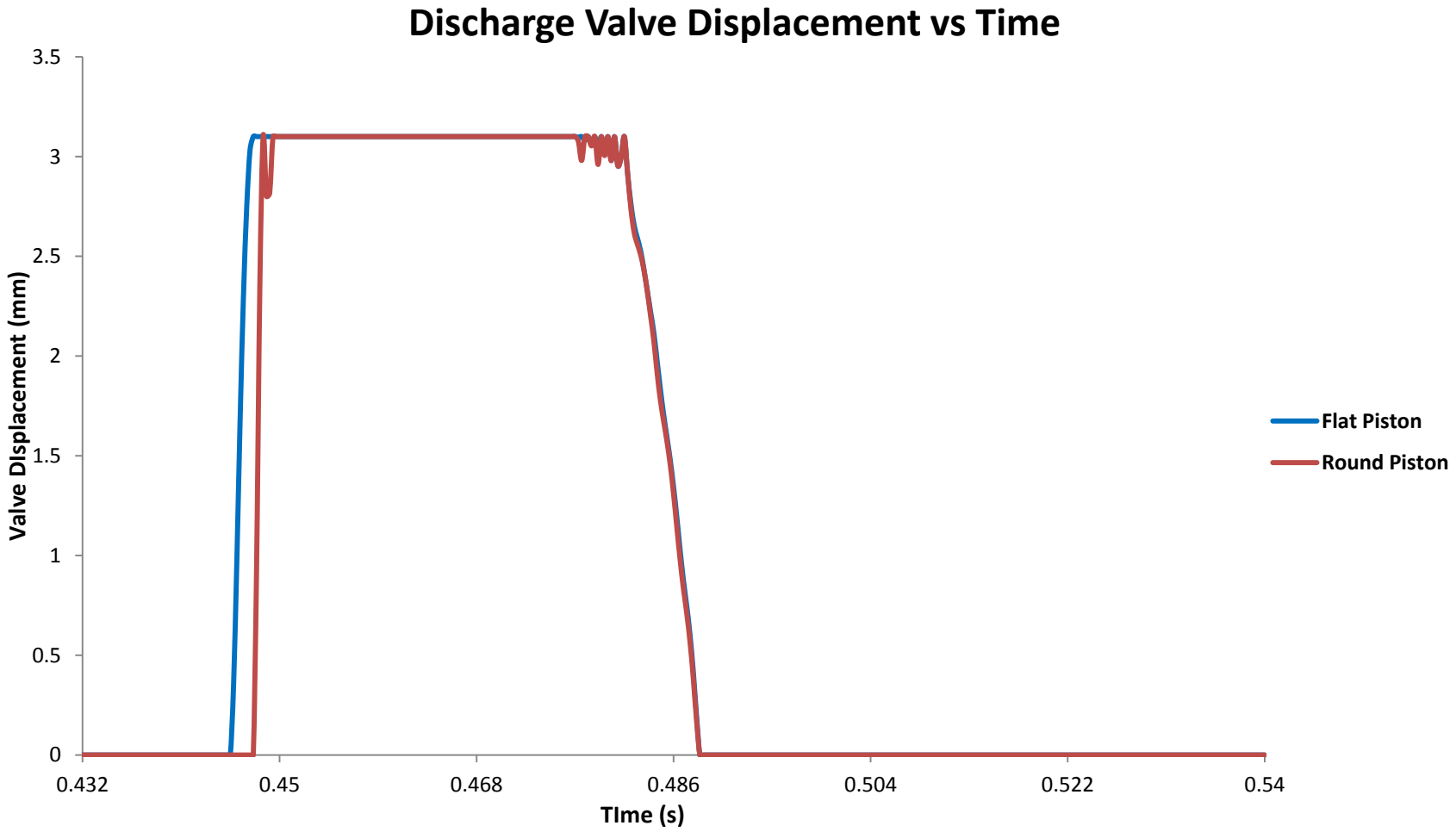

Figure 4.18 Discharge Valve Displacement at the 5th Stroke (0 mm fully closed position, 3.1 mm fully opened position)

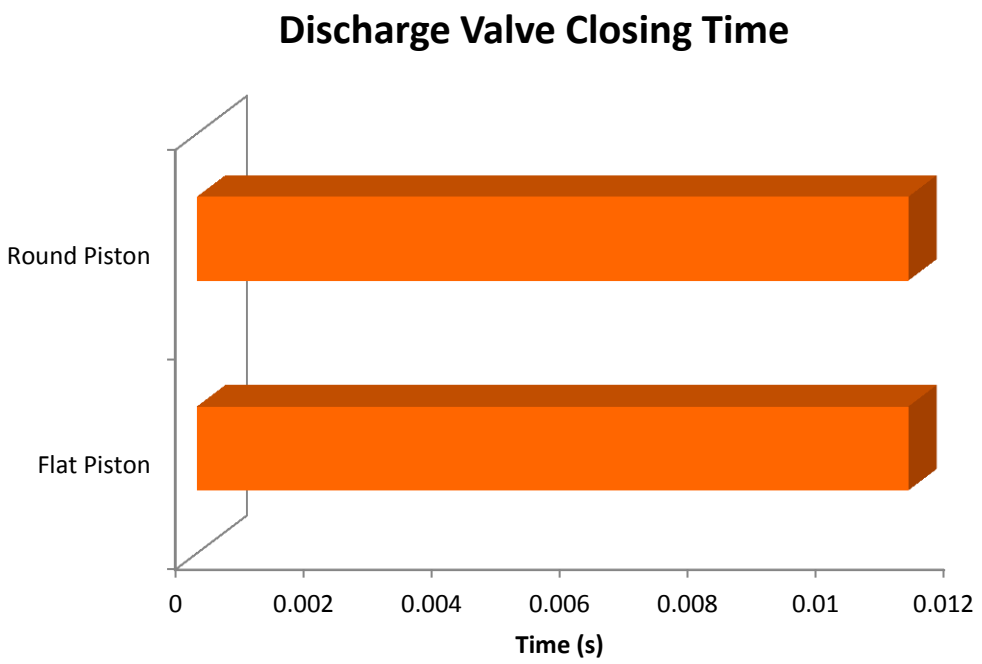

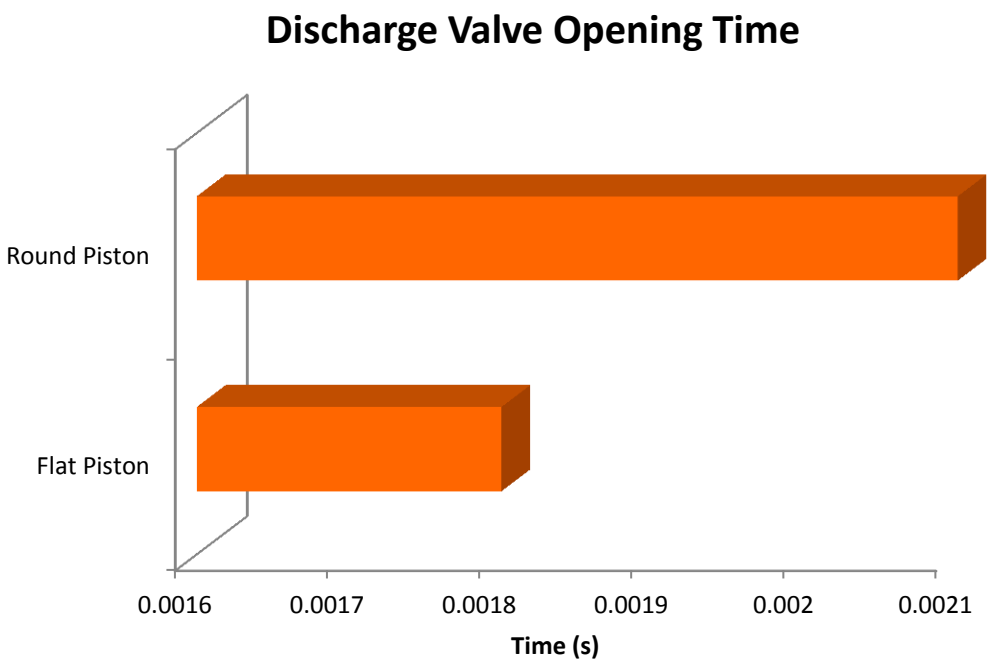

Figure 4.19 Discharge Valve Closing Times and Discharge Valve Opening Times for Different Piston Shapes

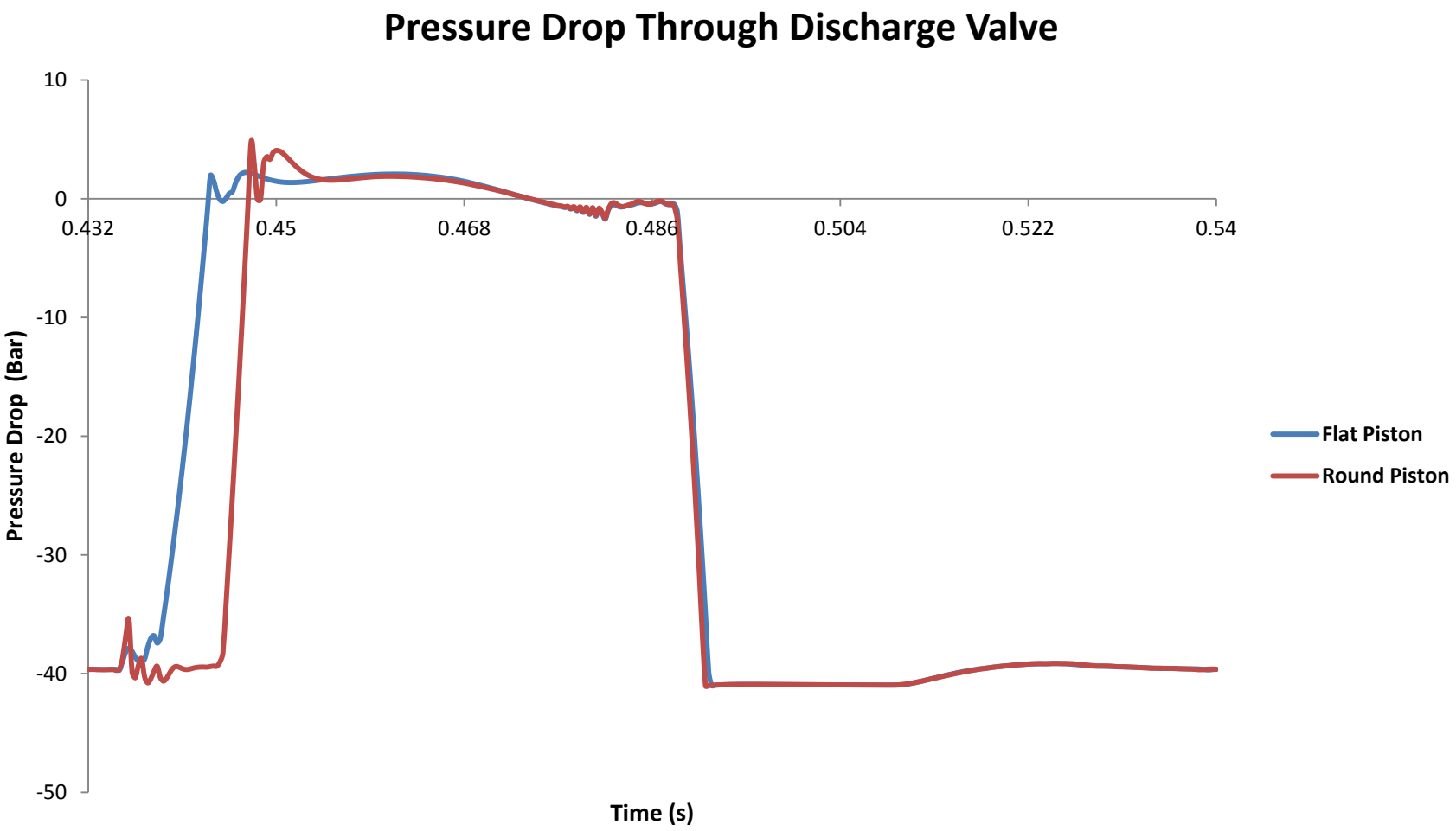

Figure 4.20 Pressure Drop Through Discharge Valve at the 5th Stroke for Different Piston Shapes

4.2 Comparison of CFD Results with Theoretical and Experimental Results

In this section, CFD results of model #15 are compared with the experimental results. First the volumetric flow rates at the pump discharge are compared. Change of theoretical flow rate with crank angle at the pump discharge is given in figure 1.7. This trend is generated for ideal case. Reverse flows at the valves and compressibility of fluid is not taken into account. In figure 4.21 both CFD and theoretical results are given on the same graph.

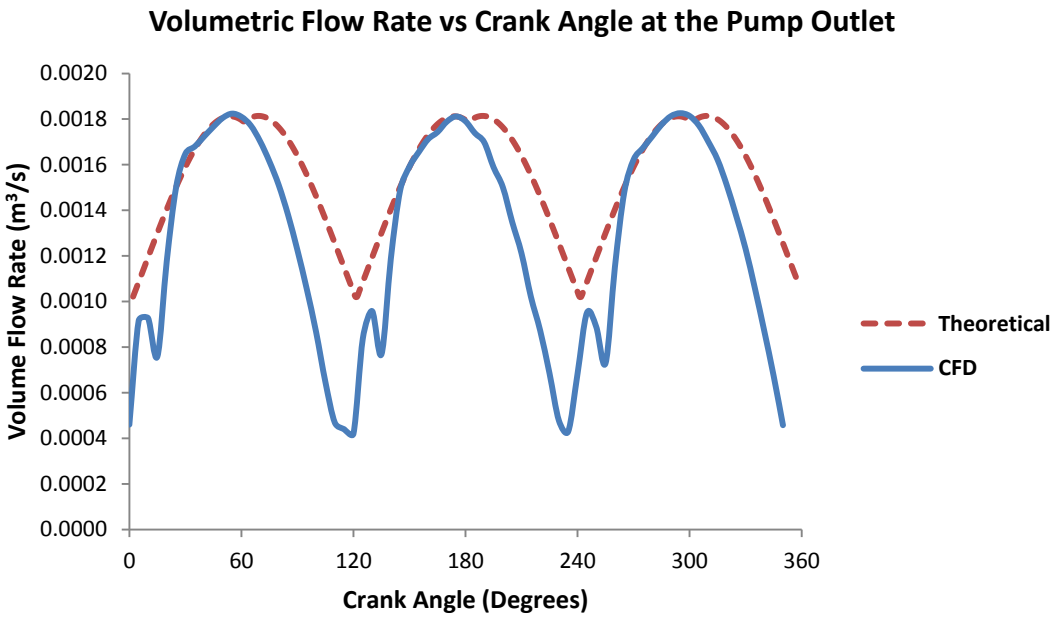

Figure 4.21 Comparison of Volumetric Flow Rates vs. Crank Angles at the Pump Discharge

From Figure 4.21 it can be seen that CFD and theoretical results are in close agreement with each other. The difference may result from the back flows at the valves and compressibility of the liquid. Also in theoretical case the internal leakage inside the pump elements are not taken into account.

Secondly, pressure time histories at the pump discharge and hydraulic efficiencies obtained using CFD method and from experiments are compared in figure 4.22.

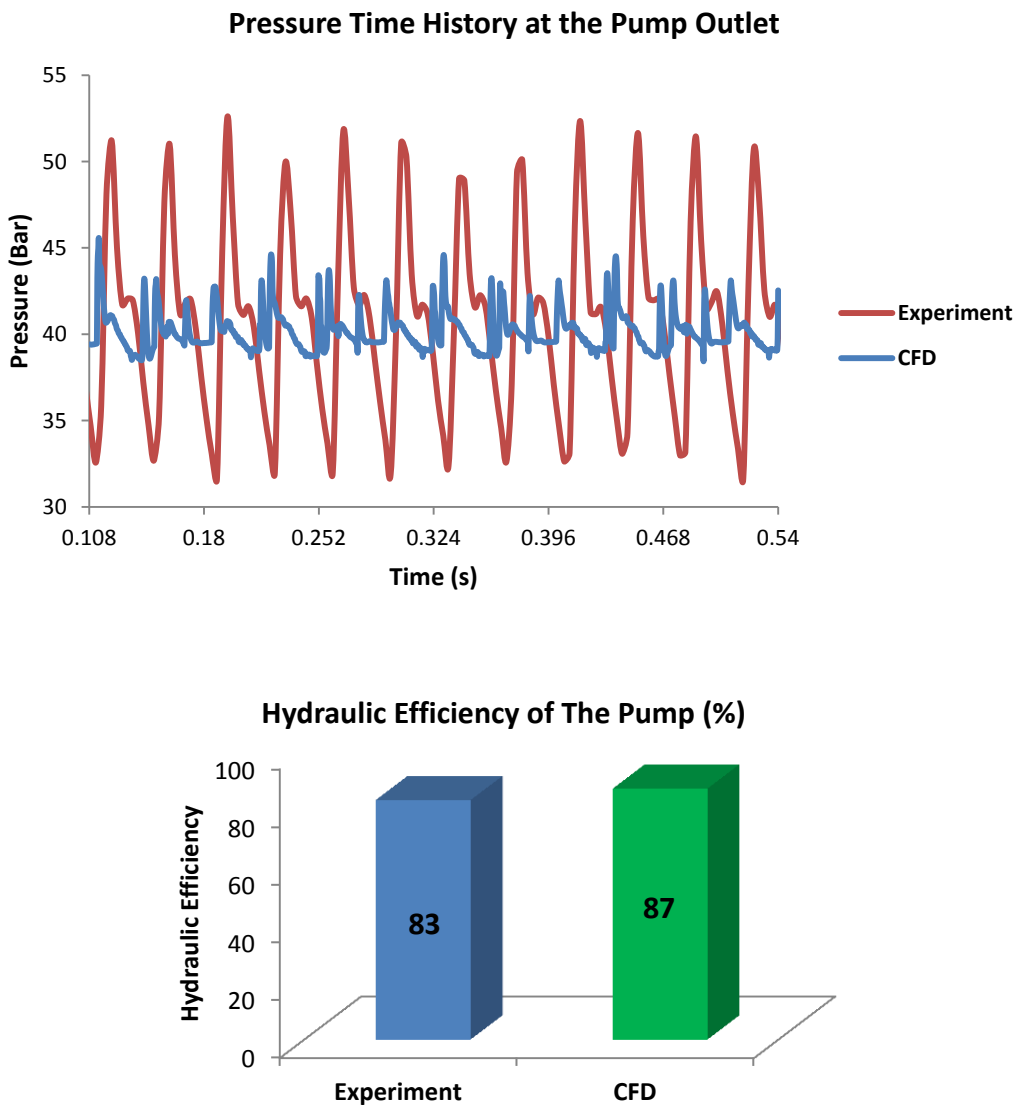

Figure 4.22 Pressure Time History and Hydraulic Efficiency of the Pump

From figure 4.22, it can be stated that hydraulic efficiencies are in close agreement with each other. The difference in the pressure graph may result from the modeling errors in the CFD analysis (instead of flexible diaphragm rigid piston is used) and sampling rate of the pressure transmitter.

CHAPTER 5

CONCLUSION

In previous chapters, general information about diaphragm pumps, their working principle, and literature survey are presented. The aim of the thesis was to find parameters that affect the performance of single-acting triplex diaphragm pump, such as the valve characteristics (valve spring stiffness, mass of valves, valve displacement) and understanding flow field inside the pump in order to achieve maximum volumetric and hydraulic efficiencies. To serve this purpose, CFD models are prepared and subject pump is numerically analyzed. Experiments are conducted to validate numerical approaches are in close agreement with physical behavior of the system. Corresponding results are also explained in detail.

In CFD part, the flow inside positive displacement diaphragm pump is numerically analyzed. The pump mainly consists of very detailed components and it is not possible to analyze the pump exactly. For this reason the components which do not affect the flow field inside the pump are not modeled in this study and some of the components inside the pump are simplified because of the meshing issues.

The system consists of flexible diaphragm and it deforms with time. It is not possible to detect exact diaphragm shape during a stroke. This problem requires solution of fluid-solid interaction with deforming bodies. Due to these difficulties, an equivalent rigid piston is used in analyses instead of flexible diaphragm in such a way that rigid piston delivers the same flow rate with the diaphragm at each stroke.

Unstructured tetrahedral mesh structure is used in analyses. The mesh is refined in the regions where large velocity and pressure gradients occur. The path of check

valves and pistons are drawn as separate parts in CAD program and their meshes are also refined in order to capture flow reversal effect. To ensure the solution is independent from the number of mesh elements used in the computational domain, mesh dependency analyses are conducted until negligible difference is achieved between the cases.

Monotone upwind discretization scheme is used for the solution of pressure velocity coupling and k-e turbulence model is used for the turbulence model. Since the analysis is transient, selecting the time step size plays an important role in analysis. Time step size must be small enough to maintain the solver stability and capture physical behavior of the system. For that reason analyses are conducted to estimate proper time step size. At first time step size is chosen as 0.0003 s ($1/360^{th}$ of one stroke) then the time step size is reduced to 0.00015 s ($1/720^{th}$ of one stroke) and the results are compared. Since there is a minor difference between two cases the bigger time step size (0.0003 s) is used in analyses.

The pump is analyzed for several operating conditions in order to investigate the effect of valve characteristics. Since these analyses are time consuming and require high computational resources the current model is simplified. In simplified model only one piston of the pump is analyzed due to the fact that investigating and improving one part of the model means improving the whole model.

The analyses conducted to investigate valve spring stiffness effect on the pump efficiency showed that using stiffer springs tends to increase efficiency up to a limit. Further increasing stiffness (beyond that limit) contributes to pressure drop through check valves and this pressure drop tends to reduce volumetric efficiency and increases the pressure pulsations. Using stiffer springs reduces closing time of check valves this condition tends to increase volumetric efficiency. For 58.56 N/cm spring stiffness, loss of volumetric efficiency due to pressure drop is more dominant than gained volumetric efficiency from fast closing of check valves. As a result of this condition volumetric efficiency reduces with using heavier springs after a certain point (for this case 29.28 N/cm).

The analyses conducted to investigate the effect of mass of the check valves on the pump efficiency showed that using lighter valves tends to increase efficiency up to a limit. Further reducing mass of the valves (beyond that limit) brings valve flutter and instability which contributes the lower volumetric efficiency. And it is also observed that if heavier valves are used in the system, the stresses on the components of the pump increase and this condition brings the loss of hydraulic efficiency.

It is observed that using longer valve displacement causes discharge valve closing and opening times to increase as expected. It is also stated that using longer valve displacement more pressure drop through discharge valve is obtained.

Using round piston arrangement in the analysis contributes valve flutter. Moreover discharge valve opening time increases. Pressure drop through discharge valve also increases with this arrangement.

After the effect of each parameter is determined on the pump efficiency, best results are taken from each category (spring stiffness, mass of the valves, displacement of the valves) which give the highest pump efficiency and a new combined model is constructed in order to achieve best performance. At first, one may expect that combined model has the best performance characteristics. Unlike expectations the model gives lower efficiencies than the current model due to non-linearity of the system. Since these systems are non-linear one cannot superimpose the improvements linearly.

The CFD results and test results are found to be in close agreement with each other especially volumetric and hydraulic efficiencies. There is little difference in pressure fluctuations graph between CFD and experimental results. This difference may have resulted from modeling errors (for instance instead of flexible diaphragm, rigid piston is used in CFD model) or sampling rate of the pressure transmitter that is used in experiments.

5.1 Recommendations for Future Work

In order to improve design process and produce more efficient positive displacement pumps, several parameters effect on the pump efficiency should be investigated. In this thesis only the valve characteristics like valve spring stiffness, valve density, valve displacement and piston shape effect are investigated. Since it is very hard to model and analyze the fluid-solid interaction with deforming bodies, flat piston model is used instead of flexible diaphragm. One can simulate the real diaphragm motion as a future work. Since these systems are non-linear, the effect of each parameter alone and combined effects should also be investigated.

Although there are many parameters should be investigated to obtain a better positive displacement pump, only the most important ones are listed below.

- The effect of real diaphragm motion
- The effect of rotational speed of the pump
- The effect of valve spring pre-load
- Effect of different inlet and outlet manifold configurations
- Effect of different valve shapes

On the pump efficiency can be studied as a future work.

REFERENCES

[1] "Pump life cycle costs a guide to LCC analysis for pumping systems executive summary" Hydraulic Institute, Europump and US Department of Energy, 2001.

[2] William S. Janna "Design of Fluid Thermal Systems 2nd edition", The University of Memphis, PWS publishing company.

[3] David B. Parker, 1994 "Positive Displacement Pumps Performance and Application", Warren Pumps Incorporated Division of IMO Industries Warren, Massachusetts

[4] Engineers Edge, Page Title: Positive Displacement Pump Characteristic Curve, 2001-2011 last visited 14.08.2011
url:http://www.engineersedge.com/pumps/positive_disp_pump_char.htm

[5] R.W Zappe, 1999 "Valve Selection Handbook 4th edition", Gulf Professional Publishing

[6] Joon-Ho Lee, Xue-Guan Song, San- Mo Kang, Young-Chul Park, 2010 "Optimization of Flow Coefficient for Pan Check Valve by Fluid Dynamic Analysis", Department of Mechanical Engineering, Dong-A University, Busan, Korea

[7] K. Hariri Asli, F.B. Naghiyev, A.K. Haghi, S.A. Aliyev, 2010 "Numerical Modeling of Transients Flow in Water Pipeline", Department of Mathematics and Mechanics, National Academy of Sciences, International Journal of Academic Research

[8] Miller, E. John, 1995, "The Reciprocating Pump-Theory, Design and Use 2nd edition", Krieger Publishing Company, Malabar, Florida

[9] Pumping Designer, page title: Diaphragm Pump, last visited: 14.08.2011
url: http://piping-designer.com/Diaphragm_Pump

[10] Wilden Pump & Engineering Company, page title: the power behind your process, last visited: 14.08.2011
url: http://www.wildenpump.com/

[11] Phil Danielson, 2000, “How to Choose a Diaphragm Pump”, A journal of practical and useful vacuum technology

[12] Wastecorp Pumps, page title: Diaphragm Pumps, last visited: 14.08.2011 url: http://www.wastecorp.com/diaphragm_pumps.html

[13] Pump Users Handbook, 1996, Elsevier Advanced Technology

[14] Brian Nesbitt, 2006, “Handbook of Pumps and Pumping 1st edition”, published by Elsevier in association with Roles & Associates

[15] Brian Nesbitt, 2001, “Guide to European Valves for Control, Isolation and Safety 2nd edition”, Professional Engineering Publishing

[16] Arne Kojolle, 2001, “Hydropower in Norway, Mechanical Equipment”, Norwegian University of Science and Technology, Trondheim 2001

[17] V.L Streeter, 1966, “Hydraulic Transients Caused by Reciprocating Pumps”, University of Michigan

[18] Samson Ag Mess Und Regeltechnik, 2003, “Cavitation in Control Valves”, Frankfurt am Main

[19] Rob Broberg, 2001, “CFD Modeling of an Internal Rotary Pump”, ASME

[20] Terry Henshaw, “Power Pump Valve Dynamics, A Study of the Velocity and Pressure Distribution in Outward Flow Bevel Face and Flat Face Power Pump Valves ”, Magnolia, Texas 2009

[21] Carlisle Power Transmission Products, Inc. “Energy Loss and Efficiency of Power Transmission Belts” Advanced Engineering Research Belt Technical Center, Springfield, Missouri

[22] Siemens Micro Master-and Midi Master Operating Instructions

[23] Abana Motorsan Electric Motors, Abana Motorsan San. Tic. A.S., 2010 last visited: 10.05.2011, url: http://www.motorsan.com.tr/motors

[24] C.T. Shaw, 1992, “Using Computational Fluid Dynamics”, Prentice Hall

[25] T.J Chung, 2002, “Computational Fluid Dynamics”, University of Alabama, Cambridge University Press

[26] WS Atkins Consultants and Members of the NSC, 2009, “Best Practice Guidelines for Marine Applications of Computational Fluid Dynamics”, Imperial College of Science & Technology

[27] H. K. Versteeg & W. Malalasekera, 1995, “An introduction to Computational Fluid Dynamics, The Finite Volume Method”, Longman Scientific & Technical

[28] Uday S. Dixit, 2007, “Lecture Notes, Finite Element Method, An Introduction“, Department of Mechanical Engineering, Indian Institute of Technology

APPENDIX A

TECHNICAL SPECIFICATIONS OF INSTRUMENTS

Table A.1 Test Pump Specifications

TEST PUMP		
Piston Diameter	[mm]	63
Eccentricity	[mm]	10
Discharge	[l/min]	90
Max. Pressure	[kg/cm2]	50
Rotational Speed	[rpm]	540
Power	[hp/kW]	12 / 9
Number of Pistons	-	3
Membrane Dia.	[mm]	120
Useful Membrane Dia.	[mm]	94
Efficiency	[%]	76
Oil Capacity	[l]	1,5
Size	[cm]	35 x 42 x 35
Mass	[kg]	35

Table A.2 Flowmeter Properties

Digital display of rate and total flow
10 point linearization
4-20 mA loop-powered
0-5 or 0-10 V DC outputs

Table A.3 Pressure Transmitter Specifications

Brand	GEMS
Type	2200B G
Pressure Interval	0-60 bars
Current	4-20 mA
Pressure Limit	2 times nominal pressure
Feed	24V DC Rated, 12-36V DC operable
Operating Temperature	-20°C...+80°C compensated
	-40°C...+100°C operable
Connection	G ¼ to BS2779 compatible with ISO228
Shield	IP 65
Response time to pressure	0.5 ms

Table A.4 Datalogger Specifications (LabJack U12)

Command/Response	50 scans/second (up to 4 AI)
Command/Response	25 scans/second (up to 8 AI)
Stream	1200 samples/second (up to 4 AI)
Burst	8192 samples/second (up to 4 AI)

Table A.5 Electric Motor Specifications

Voltage	380 V
Frequency	50 Hz
Current	38 A
Power	18.5 kW
Power Factor	0.87
Speed	1460 rpm

APPENDIX B

SAMPLE CALCULATION OF POWER INPUT AVERAGE

Sample calculation of power input to the system for model #2 is given in this part. Power input (FxV) vs. time graph for the 5th stroke is given in figure B.1 below.

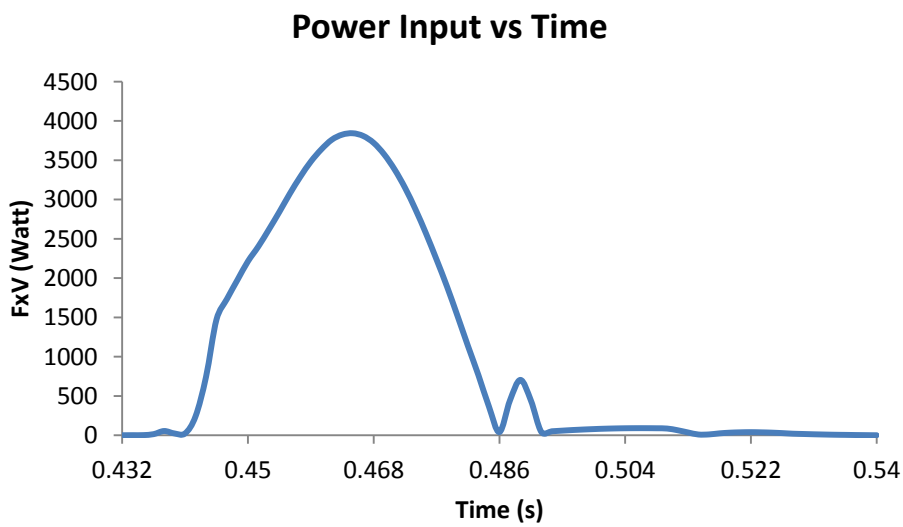

Figure B.1 Power Input vs. Time

The average of power input to the system during the 5th stroke is calculated with trapezoidal rule.

$$P_{input,ave} = \frac{\int_{t_1}^{t_2} (FxV)dt}{(t_2 - t_1)} = \frac{\sum_{n=1}^{N} [(FxV)_{t_{i+1}} - (FxV)_{t_i}](t_{i+1} - t_i)}{2x(t_2 - t_1)}$$

(B.1)

Substituting the variables into equation B.1, the average power input during the 5th stroke is found as; $P_{input,ave} = 2114.4\ W$